MSc. Thesis Report

To determine the effects of propeller ducts on quadrotors in longitudinal forward flight, using flight data and stepwise regression

Max Koster

TU Delft

MSc. Thesis Report

To determine the effects of propeller ducts on quadrotors in longitudinal forward flight, using flight data and stepwise regression

Thesis report

by

Max Koster

to obtain the degree of Master of Science
at the Delft University of Technology
to be defended publicly on December 20, 2022 at 14:00

Thesis committee:	
Chair:	Dr. Ir. C.C. de Visser
Supervisors:	Ir. J.J. van Beers
External examiner:	Dr. E.J.J. Smeur
	Dr. S.J. Hulshoff
Place:	Faculty of Aerospace Engineering, Delft
Project Duration:	May, 2021 - December, 2022
Student number:	4491343

Faculty of Aerospace Engineering · Delft University of Technology

Contents

I Introduction **6**

II Paper **7**

III Preliminary Report **43**
1 Introduction . . . 43
2 Quadrotor dynamics . . . 44
2.1 Reference frames . . . 44
2.2 Reference frame transformations . . . 44
2.3 Quadrotor rigid body dynamics . . . 45
2.4 Modelling Force . . . 46
2.5 Modelling moments . . . 48
2.6 Aerodynamic effects . . . 49
3 Model Identification . . . 54
3.1 Data Collinearity . . . 54
3.2 Stepwise Regression Algorithm . . . 55
3.3 Choosing a regressor pool . . . 57
3.4 Finding the inertia of the Quadrotor . . . 58
4 State Estimation . . . 59
4.1 Sensors . . . 59
4.2 State Estimation methods . . . 60
5 Research Proposal . . . 62
6 Research Plan . . . 63
6.1 Testing the base setup . . . 63
6.2 Flight testing . . . 63
6.3 Modelling . . . 63
6.4 Iteration . . . 63

IV Conclusions and Recommendations **67**

Chapter I

Introduction

Introduction

Quadrotors are widely in use today both for professional and recreational purposes. In order to improve design and controllers of quadrotors more information regarding the dynamics at play are necessary. A lot of the knowledge regarding quadrotors is derived from the already existing knowledge on helicopters, however quadrotors have proven to be more complex systems due to interactions between the multiple rotors. The specific area of interest of this research is propeller ducts used in quadrotors. These ducts are often present on quadrotors mainly to protect the rotors from the environment and also the other way around. Besides the protection it has also been shown that propeller ducts can improve the efficiency of the propellers, however this effect has only been proven for the hover flight condition. Which raises the question how do these propeller ducts affect the quadrotor while it is in forward flight?

To research the effects of propeller ducts different approaches can be taken. A model based approach can be taken where a model of the quadrotor is made which is used to provide insight into the dynamics at play. Other approaches include CFD approaches, or windtunnel experiments using flow visualisation. The downsides of the CFD and windtunnel methods is that they often only describe one specific flight condition, which may not even be a realistic flight condition present in normal flights. Therefore the choice was made to explore model based methods. While they have been proven effective in modelling power, the ability of them being able to identify the difference in configuration has not been tested yet on quadrotors.

Combining these two gaps in literature the following research question came forward:

What are the effects of propeller ducts on quadrotors in forward flight and can the effects be identified and quantified using system identification techniques and flight data?

To answer this question a couple of sub questions have been formed

1. What manoeuvres should be flown to identify the effect of the duct?
   (a) How does the effect differ with flight speed, and when does the effect become unwanted?
   (b) Is there a noticeable difference between manoeuvres?
   (c) How much space is needed to perform the tests?
2. Is it possible to isolate the effect of the ducts on the quadrotor dynamics?
   (a) Can the same model be used between ducted and un-ducted, and does for example a stepwise regression yield the same model terms?
   (b) What regressors dominate the duct related aerodynamics?
3. Which sensors are necessary to gather the data needed?
   (a) Do onboard sensors suffice?
4. How does the duct affect the efficiency or flight time of the quadrotor?

Chapter II

Paper

To determine the effects of propeller ducts on quadrotors in forward flight, using flight data and stepwise regression

M. Koster * and J.J. van Beers †
Delft University of Technology, Delft, Zuid-Holland, 2629HS, The Netherlands

C.C. de Visser‡
Delft University of Technology, Delft, Zuid-Holland, 2629HS, The Netherlands

In order to gain more insight into the effects of propeller ducts on quadrotors in forward flight, this research analyses flight data obtained from free flight tests, performed in the Cyberzoo and the Open Jet Facility of the TU Delft. Using a quadrotor platform with detachable propeller ducts, both trimmed forward flight tests and flights exciting the F_X, F_z forces and the M_y moment, using both ducted and unducted configurations. From the analysis of the steady flight data, the ducted configuration flies at a significantly higher pitch angle compared to the unducted configuration. However, for the power consumption and the rotor speeds, a crossover point is present around an airspeed of 6 ms^{-1}. Before this crossover point the power consumption and total rotor speeds of the ducted configuration are lower than its unducted counterpart. The flights containing the excitations of the forces and the moment are used to identify an aerodynamic model of the quadrotor using stepwise regression. Using this technique a model of the ducts themselves is identified which can be added onto the unducted model in order to predict the response of the ducted quadrotor. The regressors of this model were also used to gain extra insight into the terms at play in the effects of the ducts.

Nomenclature

A	=	polynomial regressor matrix
D	=	Drag, N
F	=	Force, N
M	=	Moment, N m
m	=	mass, kg
p	=	roll rate, rad s^{-1}
q	=	pitch rate, rad s^{-1}
R	=	propeller radius, m
r	=	yaw rate, rad s^{-1}
T	=	Thrust, N
U_p	=	roll control moment, rad^2 s^{-2}
U_q	=	pitch control moment, rad^2 s^{-2}
U_r	=	yaw control moment, rad^2 s^{-2}
u	=	velocity in x-axis of body frame, m s^{-1}
$\underline{V}$	=	vector containing quadrotor body velocities, m s^{-1}
V	=	airspeed, m s^{-1}
v	=	velocity in y-axis of body frame, m s^{-1}
w	=	velocity in z-axis of body frame, m s^{-1}
$\underline{y}$	=	measurement vector
α	=	angle of attack, rad
$\underline{\epsilon}$	=	residual vector

*Student, Faculty of Aerospace Engineering: Control and Simulation
†Ph.D. Candidate, Faculty of Aerospace Engineering: Control and Simulation
‡Assistant professor, Faculty of Aerospace Engineering: Control and Simulation

θ = pitch angle, rad
$\underline{\Theta}$ = parameter vector
$\underline{\lambda}$ = orthogonalized candidate regressor
μ = advance ratio
v_i = induced velocity, $\mathrm{m\,s^{-1}}$
$\underline{\xi}$ = candidate regressor
ρ = air density, $\mathrm{kg\,m^{-3}}$
$\underline{\Omega}$ = vector containing quadrotor body angular rates, $\mathrm{rad\,s^{-1}}$
ω = rotor speed, RPM

Subscripts

x = Body x-axis
y = Body y-axis
z = Body z-axis

Superscripts

E = Earth reference frame
B = body reference frame

I. Introduction

The concept of the quadrotor by itself already dates back to 1907 [1], however quadrotors became popular with the development of smaller and lighter micro electro-mechanical systems (MEMS) [2]. This allowed for the quadrotor as it is now known to be developed. Quadrotors are popular due to their simple design in combination with their agility and their ability to hover. As such, quadrotors have a multitude of applications, mainly to do with observation.

Along with the growing amount of use cases comes the need for quadrotors to perform more efficiently, and for them to be able to perform more specific and extreme manoeuvres [3]. In order to make more effective controllers, and to gain further insight into the driving dynamics, a significant area of research is the modeling of quadrotor dynamics. The basis of most models is the so called hover model [4]. This model is linearised about the hover state of the quadrotor, and performs well near hover, or at near stationary airspeeds of $V < 2\ ms^{-1}$[5]. However, for high speed flight, the hover model starts to deviate from reality as it violates the assumption that the quadrotor operates at a near stationary airspeed [6]. As a result of this, the non-linear effects absent in the hovering model become significant. Therefore, different types of models are researched, for example black box models are used to inform model predictive controllers [7, 8]. Alternatively, gray box and white box models aim to give more insight into the underlying dynamics of the quadrotor. Where white box models are often based on helicopter theory, which includes momentum analysis in combination with the blade element method [9]. Next to this research has been done using wind tunnel tests [10, 11] and CFD simulations, in order to measure or visualise aerodynamic effects [12].

Another trend in quadrotor design is the addition of ducts to the propellers [13], these ducts are mainly added for protective and safety purposes, however when well designed it has also been shown that ducts can improve the performance of the rotors [10, 13, 14]. This advantage is proven for the quadrotor in hover conditions. Ref. [10] shows resulting airflows and vortex interactions of two props, with and without ducts. For the hover case it shows an increase in performance of the rotors equipped with ducts, however for the rotors in forward flight the flow visualisations are shown, but no numerical results are presented. Besides this, the tests are performed with an airflow parallel to the rotor disk, which in normal quadrotor flight is not a state that occurs for a prolonged time.

This leaves a gap in current research where there is knowledge about the effects of ducts on quadrotors in hover, but quadrotor dynamics differ when speeds of $V \geq 2$ are achieved, leading to the belief that the effects of ducts may also change under these circumstances. The contribution of this paper is to provide practical insight into the effects of propeller ducts in forward flight. For this research the same quadrotor was fitted with and without ducts. The effects of the ducts are then analysed based on flight data from free flight experiments gathered at varying flight speeds. Two methods of analysing this data are performed. One based on the raw flight data obtained for a quadrotor flying at increasing airspeeds, which provides insight into the steady state effects of the ducts such as the average rotorspeed necessary to fly per airspeed, and the corresponding power consumption. The second uses the flight data to identify aerodynamic models using stepwise regression [5, 15]. The model regressors are then used as basis for the analysis, and are used to find the state variables that are of the biggest influence for the ducted dynamics. Using this method this work aims to evaluate the claim of efficiency gains due to propeller ducts in practice, with a focus on the unexplored effects of ducts in forward flight.

The paper is structured as follows, first the method of modelling is explained in section II, after which the chosen test platform is presented in section III. Then the tests and the test locations are discussed in section IV, followed by the data processing in section V. Lastly the results obtained from the flight tests and the identified models are discussed in section VI.

II. Method

Here the methods of analysis are discussed, starting at the mathematical description of the stepwise regression algorithm, and ending at the candidate regressor selection.

A. Stepwise Regression

For the model structure and parameter identification the stepwise regression algorithm as described in Ref. [16] was chosen, both because it has already been proven successful for quadrotor flight at slow and high speed conditions in Ref. [5, 15], and because it provides insight into the underlying dynamics due to it using a polynomial structure based on the flight variables. The stepwise regression algorithm is used when the model structure is unknown. The algorithm chooses regressors from a candidate regressor pool based on which regressor reduces the modeling error the most.

The algorithm is initiated with the simplest model possible, often this means the model only contains a bias term, however it can also be a set of fixed regressors. Using this initial model an ordinary least squares problem is set up.

$$\underline{y} = A_k \underline{\Theta}_k + \underline{\epsilon}, \quad A_0 = \begin{bmatrix} 1 \\ \vdots \\ 1 \end{bmatrix}, \quad \text{for } k = 0, 1, \ldots, n \tag{1}$$

Here $\underline{y}$ represents the measurement vector, A_0 the initial regressor matrix, in this example taken as a column vector of ones representing the bias term, $\underline{\Theta}_k$ is the parameter vector containing the parameters corresponding to the regressors, and lastly ϵ which is the vector containing the residuals. The ordinary least squares estimator $\hat{\underline{\Theta}}$ is:

$$\hat{\underline{\Theta}} = (A_k^T A_k)^{-1} A_k^T \underline{y} \tag{2}$$

The residual vector of the current state of the model is:

$$\underline{\epsilon}_k = \underline{y} - A_k \hat{\underline{\Theta}}_k \tag{3}$$

Now it is necessary to orthogonalize the candidate regressors in the pool with respect to the regressors already present in the model. This is done in order to avoid violating the least squares assumption of uncorrelated residuals. The orthogonalization is done according to Equation 4. Here $\underline{\xi}_i$ is the i^{th} candidate regressor, and $\underline{\lambda}_i$ is the orthogonalized version of this regressor.

$$\underline{\lambda}_i = \underline{\xi}_i - A_k \hat{\underline{\Theta}}_k \tag{4}$$

The selected regressor is that which has the highest Pearson correlation coefficient with the residual vector calculated, as shown in Equation 5.

$$j = \underset{i}{\operatorname{argmax}}(\operatorname{corr}(\underline{\lambda}_i, \underline{\epsilon}_k)) \tag{5}$$

The old regressor matrix is then updated by adding the newly selected regressor, which in its turn is then also taken out of the candidate regressor pool.

$$A_{k+1} = \begin{bmatrix} A_k & \underline{\xi}_j \end{bmatrix} \tag{6}$$

This part of the algorithm represents the forward selection part of the stepwise regression, the algorithm also includes a backwards step which re-evaluates the regressors already present in the model, and checks their contribution to the total model and whether its enough to stay in the model. The method described by Ref. [16] uses the F_0 statistic for this as shown in Equation 7. Where the SS_R is the regression sum of squares, and is defined in Equation 8. The s^2 term is the fit error variance and is calculated according to Equation 9. $\hat{\underline{\Theta}}_p$ is the current estimator, and the subscript $p - i$ indicates the parameter vector without the i^{th} parameter which is the parameter which is tested:

$$F_{0,i} = \frac{SS_R(\hat{\underline{\Theta}}_p) - SS_R(\hat{\underline{\Theta}}_{p-i})}{s^2} \tag{7}$$

In the equations below N stands for the total number of data points in the estimation, p for the amount of parameters in the model, $\bar{y}$ indicates the mean of y.

$$SS_R = \hat{\underline{\Theta}}^T A^T \underline{y} - N\bar{y} \tag{8}$$

$$s^2 = \frac{\underline{\epsilon}^T \underline{\epsilon}}{N - p - 1} \tag{9}$$

To test whether a regressor should be removed from the model Equation 10 is applied, here F_{out} is a constant to be set depending on the confidence level required. For models with $N \gg 100$ and $p < 10$ with a confidence level of 95% $F_{out} = 4$ [16].

$$\min_i(F_{0,i}) < F_{out} \tag{10}$$

The main stopping criterion of the algorithm is the Predicted Square Error (PSE) as defined in Equation 11. This error metric takes into account the Mean Square Error (MSE) and a penalty for overfitting which is introduced to limit the amount of parameters in the model. Here σ^2_{max} is taken as the residual error variance of the response with respect to its mean, as shown in Equation 12 [16].

$$PSE = \frac{1}{N}\underline{\epsilon}^T \underline{\epsilon} + \sigma^2_{max}\frac{p}{N} \tag{11}$$

$$\sigma^2_{max} = \frac{1}{N}\sum_{i=1}^{N}[y(i) - \bar{y}]^2 \tag{12}$$

The algorithm then stops when the PSE calculated in the current step becomes bigger than the PSE calculated in the previous iteration. This would indicate that adding a parameter means the over-fitting of the model. In practice however it shows that the modelling performance barely increases after 5 selected regressors, as can be seen in the evolution of R^2 shown in Table 6 from section VI for example. Therefore the limit of selected regressors by the model is set to 5.

In order to compare the models of the two different configurations with each other a method is applied where the stepwise regression algorithm is applied twice. The overall structure of how this is applied is shown in Figure 1. For this method first a model for the unducted configuration is identified. Then the residuals of this model applied to ducted data are calculated, which in turn are used to identify a new model, which models the residuals between the ducted and unducted configurations, meaning that it would describe the effects the ducts have on the quadrotor. The advantage of this method is that it simplifies the comparison of the two configurations, as the residual model itself indicates the differences between the configurations, compared to having two complex model structures which have to be compared with each other. The downside of this method is that it requires clear differences between the data of the two configurations. If the residuals resemble white noise, the method does not work, at the same time however this would indicate there not being a significant difference between the configurations with regards to that variable.

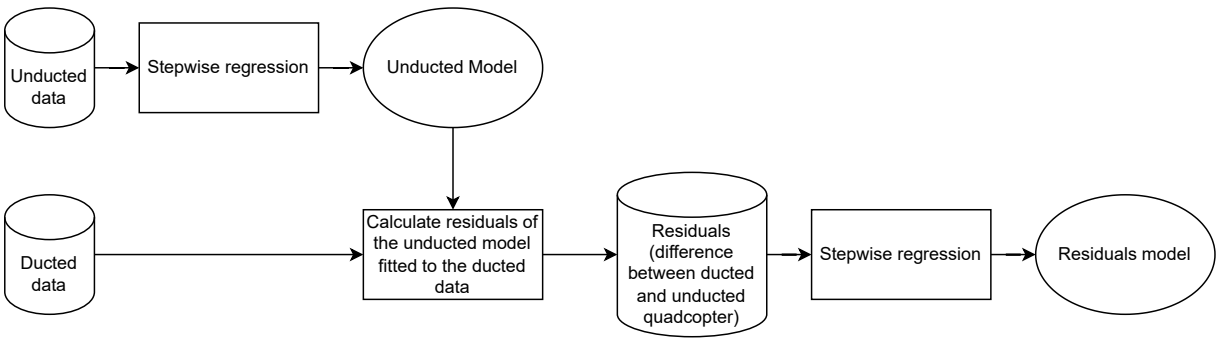

Fig. 1 Flowchart for applying stepwise regression to the residuals

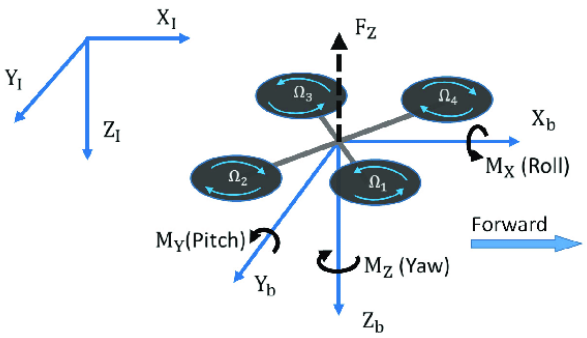

Fig. 2 Body reference frame applied to the quadrotor [17]

B. Reference Frames

In this paper two reference frames are used to describe the dynamics of the quadrotor. The Earth frame and is denoted by an E in the superscript of the vector, and the body reference frame attached to the body of the quadrotor denoted by a B in the superscript of the vector. The inertial Earth reference frame is taken as a point on the ground and is a North East Down (NED) reference frame. It is assumed here that the rotation of the Earth compared to the movement of the quadrotor does not have a noticable effect, and a flat earth approximation is made. The Earth reference frame is therefore considered as an inertial reference frame. The body reference frame is one that is standard in the aerospace industry, depicted in Figure 2 where the X_B axis originates in the center of gravity (c.g.) of the quadrotor and points between the front two rotors, parallel to the propeller plane. The Y_B axis forms a 90 degree angle with the X_B axis and is also parallel to the propeller plane, such that the Z_B axis points downwards opposite of the direction of thrust completing the right handed reference frame.

C. Quadrotor Dynamics

To have an idea of the model structure and what to model first a look is taken into the dynamics of a quadrotor.We start at the rigid body dynamics of the quadrotor which are described by Equation 13.

$$m(\dot{\underline{V}}^B + \underline{\Omega}^B \times \underline{V}^B) = \underline{F}^B \tag{13a}$$

$$I\dot{\underline{\Omega}}^B + \underline{\Omega}^B \times I\underline{\Omega}^B = M^B \tag{13b}$$

In these equations $\underline{V}$ refers to the vector containing the body velocities u, v, and w in their corresponding body axes X_B, Y_B, Z_B respectively. Similar to this $\underline{\Omega}$ is the vector containing the angular rates p, q, and r about their respective body axes X_B, Y_B, Z_B. F^B and M^B are the force and moment vectors acting on the body, and lastly m is the quadrotor mass, and I represents the quadrotor's inertia matrix. The point of interest for the modelling here are the forces and the moments acting on the quadrotor.

1. Thrust on the quadrotor

The force vector can be decomposed into multiple components where there is the component of gravity, the aerodynamic forces, and the thrust generated. This separation is shown in Equation 14 where R_{EB} is the rotation matrix from the Earth frame to the Body frame, $\underline{g}^E$ the gravity vector in the Earth frame, and $\underline{F}^B_{quad}$ the combined aerodynamic and thrust forces acting on the quadrotor. This force vector is also the quantity we are interested in modelling.

$$\underline{F}^B = mR_{EB}\underline{g}^E + \underline{F}^B_{quad} \tag{14}$$

For all three components of the force vector $\underline{F}_{quad}$ a separate model can be made, however for this study the force vector is limited to only two of these models, the F_x model and the F_z model, which are the forces of interest in longitudinal flight. The F_z model is separated into multiple components following the approach of Ref. [15].

$$F_z = -T + D_z \tag{15}$$

Here T is the total thrust generated by the quadrotor, and D_z is the aerodynamic drag acting along the z-axis. The thrust can then be broken up into components as well. Where the basis of the total thrust generated is described by the so called hover model shown in Equation 16 [4]. Here κ_0 represents the thrust coefficient and ω the rotor speed.

$$T_h = \kappa_0 \sum \omega_i^2 \tag{16}$$

As the name of the model suggests the model is only valid near hover conditions, and therefore is supplemented by a model describing the total thrust, Equation 17, taken from Ref. [18, 19]. Equation 17 is the description for one propeller, but by summing the rotor speeds the equation for the total quadrotor can be obtained. Equation 17 does not take into account any inter rotor, or rotor airframe interactions.

$$T = \frac{\rho a b c \omega^2 R^3}{2} \left(\frac{\theta_{prop}}{3} + \frac{V_\infty^2 \cos^2(\alpha) \theta_{prop}}{2\omega^2 R^2} + \frac{V_\infty \sin(\alpha) + \nu_i}{2\omega R} \right) \tag{17}$$

Using the following assumptions shown in Equation 18 the equation can be rewritten into a form containing the body speeds, quadrotor parameters and the induced velocity ν_i, as is shown in Equation 19. The induced velocity is the extra velocity the rotor gives to the air before it enters the rotor. In these equations a, b, c stand for the lift curve slope, number of blades and the blade chord respectively. V_∞ is the freestream airspeed, R is the rotor radius, and ρ is the air density. α represents the angle of attack of the propeller disk with respect to the freestream airspeed, and θ_{prop} is the propeller blade pitch.

$$V_\infty^2 \cos^2(\alpha) = u^2 + v^2 \tag{18a}$$

$$V_\infty \sin(\alpha) = -w \tag{18b}$$

$$T = \frac{\rho a b c \omega^2 R^3}{2} \left(\frac{\theta_{prop}}{3} + \frac{(u^2 + v^2) \theta_{prop}}{2\omega^2 R^2} + \frac{-w + \nu_i}{2\omega R} \right) \tag{19}$$

The induced velocity is defined by Equation 20, which is obtained using momentum theory [19, 20]. Equation 20 is an iterative equation seeing that ν_i is both on the left and right side of the equation. The equation can be solved by either solving the fourth order equation that appears when rewriting the equation, or by applying a Newton-Raphson iterative solver with as initial guess $\nu_i = \nu_h$ [20].

$$\nu_i = \frac{\nu_h^2}{\sqrt{(V_\infty \cos\alpha)^2 + (V_\infty \sin\alpha + \nu_i)^2}} \tag{20}$$

Here ν_h is the induced velocity produced in hover, calculated according to Equation 21, where A is the area of the rotor disk.

$$\nu_h = \sqrt{\frac{T}{2\rho A}} \tag{21}$$

It should be noted here that this equation is only valid in a certain range of conditions. Especially in descending flight, when there is a point where the airflow through the rotor disk is not defined anymore by the momentum theory, which is the range where $-2\nu_i \leq -w \leq 0$. This raises a problem for the flight manoeuvres effective in the system identification process. For the identification of C_x quick stops and changes in direction are effective for the system identification process, but cause the quadrotor to enter the invalid range of w. An example of such a flight is shown in Figure 3.

Another problem with the induced velocity is that if one were to calculate it according to Equation 20 and take into account the four rotors either the airspeed at each rotor needs to be known, or a fictive ν_i for the combined rotors can be calculated. Because of these reasons the decision has been made to not include this term in the models, even though it is a vital term in rotor dynamics.

Before continuing on to the candidate regressors extra terms used in the identification are introduced. First the average and total rotor speeds as defined in Equation 22 and Equation 23 respectively.

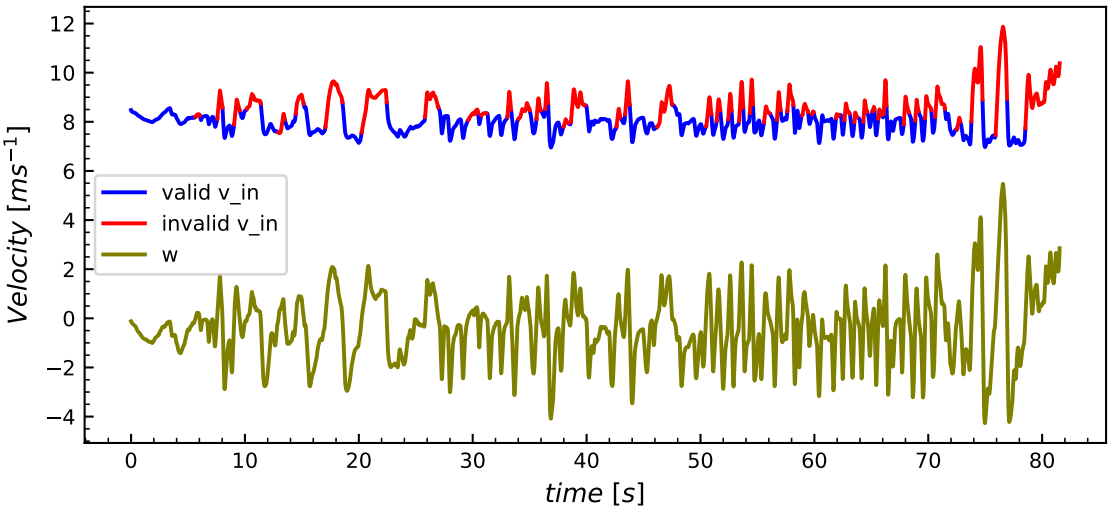

Fig. 3 Validity check for v_i in a test flight

$$\bar{\omega} = \sqrt{\frac{\sum_{i=1}^{N_{rot}} \omega_i}{N_{rot}}} \tag{22}$$

$$\omega_{tot} = \sum_{i=1}^{N_{rot}} \omega_i \tag{23}$$

Using the average rotor speeds the advance ratio for for the quadrotor can be calculated using Equation 24, here it is assumed that there is one average advance ratio for the entire quadrotor, instead of one advance ratio per rotor.

$$\mu_x = \frac{u}{\bar{\omega}R}, \qquad \mu_y = \frac{v}{\bar{\omega}R}, \qquad \mu_z = \frac{w}{\bar{\omega}R} \tag{24}$$

Finally the control moments are introduced. The control moments are the variables representing the resulting moment coming from the difference in rotor speeds about the axes of the quadrotor frame.

$$U_p = (\omega_1^2 + \omega_4^2) - (\omega_2^2 + \omega_3^2) \tag{25}$$

$$U_q = (\omega_1^2 + \omega_2^2) - (\omega_3^2 + \omega_4^2) \tag{26}$$

$$U_r = (\omega_1^2 + \omega_3^2) - (\omega_2^2 + \omega_4^2) \tag{27}$$

D. Candidate Regressor Structures

The candidate model structures are based on creating polynomials using model terms. The polynomials are written as $P^n(x, y)\{1\}$ where n is the order of the polynomial, x and y are the polynomial variables, and $\{\bullet\}$ forms the set with which the entries in the polynomial are multiplied, where the set consists out of a 1 and state variables. Below an example is given:

$$\begin{aligned} &P^2(x, y)\{1, a\} = P^2(x, y) + P^2(x, y)a \\ &\text{Where:} \\ &P^2(x, y) = x + y + x^2 + y^2 + xy \end{aligned} \tag{28}$$

The candidate regressor polynomials all have been based on Ref. [5]. The F_x candidate regressor polynomial is shown in Equation 29 here terms corresponding to X_0 and X_1 are considered fixed in the regression, meaning that they

are initialized as A_0 Equation 1. The other polynomials are there to model potential effects related to body speeds, control moments, rotor speeds and pitch rate. The selected terms for the polynomials are limited to the longitudinal flight data.

$$\begin{aligned} F_x = X_0 + X_1\mu_x + P^4(|u|, w)\{1\ \omega_{tot}, |q|, |U_q|, \sin(\theta), \cos(\theta)\} \\ + P^4(|\mu_x|, \mu_z)\{1, \omega_{tot}, |q|, |U_q|, \sin(\theta), \cos(\theta)\} + P^4(|U_q|)\{1, \omega_{tot}\} \\ + P^4(\omega_{tot})\{1, \sin(\theta), \cos(\theta)\} + P^4(|q|)\{1, \omega_{tot}\} \end{aligned} \tag{29}$$

For the candidate regressors of F_z first F_z is split into separate parts, as shown in Equation 30. Here T_h is calculated using Equation 16, the κ_0 is determined based on flight data of the quadrotor in hover. $F_{a,T}$ is then to be identified by the stepwise regression [15].

$$F_z = T_h + F_{a,T}, \qquad F_{a,T} = T_a + D_z \tag{30}$$

Given that T_h is estimated separately and taking the fact that for the collected test data the calculations of ν_i are invalid, the candidate regressors for F_z can be represented as in Equation 31, here the terms preceded by Z_i are the fixed regressors derived from Equation 17. The other polynomials are selected like for the F_x candidate models.

$$\begin{aligned} F_z = -T_h + Z_0 + Z_1\mu_z + Z_2(\mu_x^2 + \mu_y^2) + P^4(|u|, w)\{1\ \omega_{tot}, |q|, |U_q|, \sin(\theta), \cos(\theta)\} \\ + P^4(|\mu_x|, \mu_z)\{1, \omega_{tot}, |q|, |U_q|, \sin(\theta), \cos(\theta)\} + P^4(|U_q|)\{1, \omega_{tot}\} \\ + P^4(\omega_{tot})\{1, \sin(\theta), \cos(\theta)\} + P^4(|q|)\{1, \omega_{tot}\} \end{aligned} \tag{31}$$

The last standard candidate polynomial to be defined is M_y for this two fixed regressor terms are selected, U_q which is a logical regressor seeing as this term directly controls the pitching moment created, and q is believed to be a dampening term for the aerodynamic moment [21].

$$\begin{aligned} M_y = M_0 + M_1 q + M_2 U_q + P^4(u, w)\{1, \omega_{tot}, q, U_q, \sin(\theta), \cos(\theta)\} \\ + P^4(\mu_x, \mu_z)\{1, \omega_{tot}, q, U_q, \sin(\theta), \cos(\theta)\} + P^4(q)\{1, \omega_{tot}\} \\ + P^4(U_q)\{1, \sin(\theta), \cos(\theta), \omega_{tot}\} + P^4(\omega_{tot})\{1, \sin(\theta), \cos(\theta)\} \end{aligned} \tag{32}$$

Due to the unknown effects of the ducts, the candidate polynomials for the residual models do not contain fixed regressors, besides this the choice has been made to put the variables inside one polynomial, allowing for more combinations, but also introducing less consistency in the selected regressors as there may be more correlation between the candidate regressors. The variables were mainly selected based on their correlation with the residuals.

$$F_{x_{res}} = P^4(\omega_{tot}, \mu_x, \mu_z, \sin(\theta), q, u, w)\{1\} \tag{33}$$

$$F_{z_{res}} = P^4(\omega_{tot}, \mu_x, \mu_z, \sin(\theta), u, w)\{1\} \tag{34}$$

$$M_{y_{res}} = P^4(U_q, \mu_x, \mu_z, \sin(\theta), q, u, w)\{1\} \tag{35}$$

III. Test platform

As test platform a quadrotor was built using the CineGo HD frame produced by GEPRC, the frame has as advantage that the ducts are removable, making it ideal for testing ducted (Figure 4) versus unducted (Figure 5) configurations. To compensate for the mass and inertia of the ducts when removed, tungsten putty was added to the frame when flying without the ducts, placed in such a way to keep the mass and Moment of Inertia (MoI) constant between configurations, the physical properties of the quadrotor are shown in Table 1. The application of the tungsten putty is shown in Figure 6

On board of the MATEK F722 MINI flight computer a dual IMU setup is used, with the MPU-6000 and ICM-20602 IMUs. The RPM of the propellers is measured using the bidirectional digital shot (DShot) protocol. All the data is logged by the flight controller at 250 Hz. For the propellers, the quadrotor is fitted with the HQProp 3x3x3, which is a 3 inch propeller with 3 blades and 3 inches of pitch.

Fig. 4 Quadrotor in its ducted configuration

Fig. 5 Quadrotor in its unducted configuration

Fig. 6 Thungsten putty placed near the propellers in order to keep the same mass and inertia between configurations

The firmware installed on the flight computer is Betaflight, which was chosen due to it being compatible with the selected flight computer and the bidirectional DShot protocol, which allows for measuring the motor rotational rate instead of the motor commands, and it providing the possibility to do First Person View (FPV) flights. The downside of Betaflight is that it does not allow for autonomous or pre-programmed flights, meaning that all flights have to be done by hand. The PX4 firmware does allow this, but does not support bidirectional DShot, meaning that the essential RPM data cannot be recorded using the onboard sensors, and would require extra sensors.

For the acquisition of the positions, attitude, and velocity of the quadrotor an Optitrack system is used which tracks the quadrotor using an array of infra red cameras tracking reflective surfaces on the quadrotor, at 120 Hz with a spatial accuracy of 1mm RMS.

While the same test platform has been used throughout all the tests, there are some things that changed between test flights. The batteries used for the flights were 4S Lithium-Polymer (LiPo) batteries from the same brand, however there was a slight difference in mass between the different batteries used. Next to this the batteries do not have mounting point that locks them in the same position every flight. The batteries were placed on a sticky surface on the quadrotor and strapped down by a band. While the batteries are relatively securely attached, it does not assure the exact same placement every time, and small displacements still occur during flight. The other parameter that changes slightly between different flights is the tungsten putty and its placement, while the attempt was made to keep the position the

same, exact placement cannot be guaranteed. These two changes mainly affect the c.g. and MoI of the quadrotor. While the changes are likely small, they have quite the impact on the U_q variable. This is because a shift of c.g. along the x-axis of the quadrotor requires a U_q to account for this change.

Table 1 Physical properties of the ducted and unducted CineGo including battery

	mass kg	I_{xx} kg m^3	I_{yy} kg m^3	I_{zz} kg m^3
CineGo Ducted	0.3659	$7.77{\cdot}10^{-4}$	$7.32{\cdot}10^{-4}$	$1.23{\cdot}10^{-3}$
CineGo Unducted	0.3629	$5.49{\cdot}10^{-4}$	$6.92{\cdot}10^{-4}$	$9.53{\cdot}10^{-4}$

IV. Flight Tests

To gather data, flight tests were performed in two different environments. The first environment is the so called Cyberzoo at the faculty of Aerospace engineering at the TU Delft, which is a space dedicated for flying inside, fitted with an Optitrack system. The space itself is about 7 meters tall, and about 10 meters in width and depth. Due to the constraints of this space, the employed quadrotor cannot reach speeds $\geq 5\ ms^{-1}$ when flying in purely longitudinal flight. Higher speeds can be achieved when for example a circular flight pattern is used, however these flights stray away from the purely forward flight test case proposed for this research and introduce more variables in the flight analysis such as the new rolling and yawing motions. Therefore a second test facility was used, the Open Jet Facility (OJF) at the TU Delft, which is as the name suggests an open nozzle wind tunnel. The OJF supports wind speeds of up to 35 ms^{-1} with a test section of 2.5x2.5x5 meters in which the airspeed can be assumed relatively constant, and like the Cyberzoo is also fitted with an optitrack system.

All flights were flown manually, which has both its advantages and disadvantages. The advantageous part of flying manually is that the optimal flight paths for system identification are unknown. Flying manually results in the pilot introducing some extra variation into the flight meaning that most likely more states are reached in the flight, where it should be noted that the pilot may also have a bias for a certain type of flight taking away from this advantage. A downside of manual flight is that the flights are not reproducible, which has as result that a model identification may turn out different depending on the data set used, in an attempt to keep the flight data similar the types of manoeuvres performed throughout the testing are kept similar.

A. Cyberzoo Flight Tests

In the Cyberzoo two different types of tests were performed. The quadrotor was flown in hover to evaluate its base performance, and active flights were performed to gather data for the system identification process. Active here means that the quadrotor was flown to excite three of its six degrees of freedom. This was done by performing punch-outs, high acceleration and braking manoeuvres, and quick oscillations of the pitch angle. The aim was to gather data for accelerations in the body axes x and z, and rotational rates about the y axis. These degrees of freedom were chosen due to the fact that they are replicable in the OJF making for better comparison of the test data, and also making it possible to combine the data for the modelling.

B. OJF Flight Tests

The OJF flights are also divided into two different types of flights. The first set of flights consists of flights where the aim is to keep the quadrotor in the flow of the jet as steady as possible. These tests were performed at different speeds ranging between 2 - 15 ms^{-1}, where for each flight the airspeed of the jet was kept constant for the entire flight. The specific airspeeds flown at are 2, 3, 4, 5, 6.5, 8, 10, 12, 15 ms^{-1}. A higher density of speeds in the lower speed regime was selected due to the fact that during first analysis of the results, the quadrotor configurations showed small differences in the variables of interest, especially the w_{tot} and the power use. The flights were flown using (FPV) goggles as this configuration seemed to yield results closest to steady flight without the use of an autonomous controller. The aim of these tests was to gather data for the steady forward flight and compare the data between the configurations directly.

The second set of flights aims to excite F_x, F_z and M_y. These tests were performed at three different speeds, 5, 8, and 10 ms^{-1}. A lower top speed than for the other type of flight in the wind tunnel was chosen here due to the fact that the tests take up more space and ask more of the quadrotor. Speeds higher than 10 ms^{-1} resulted in the pilot not feeling in control anymore, and therefore was capped at this number. The control of the quadrotor is important for multiple

reasons. First of all, crashes are to be avoided of course in order to limit damage to the test platform. Moreover, when losing control the quadrotor leaves the laminar flow of the windtunnel where the airspeeds are unknown, and lastly the quadrotor needs some room for performing manoeuvres necessary to excite the dynamics. If the propellers are saturated by purely flying at high speed there is less room to also fly aggressive manoeuvres. These tests were flown in what is called line of sight (LOS) flight, meaning that the quadrotor was in direct sight of the pilot.

V. Data Processing

The recorded data comes from two or three different sources, depending on if there is wind data from the windtunnel, with different time clocks and therefore also different timings. Furthermore, there is noise present in the data and there may be data points missing, for example when the optitrack system loses its tracking of the quadrotor. Therefore, it is necessary to first process the data before it can be used for the analysis.

It was found that the onboard clock of the quadrotor has a slight drift, causing problems in the synchronization of the data sources with the onboard IMU data. Using the OptiTrack host computer's clock as a reference, a linear scaling correction was identified to align the onboard clock with the optitrack clock. This correction is found to be consistent across all flights. This correction was achieved by multiplying every time measurement by a constant found to be 1.00196.

Before merging the onboard data, optitrack data, and potentially the wind tunnel data, the optitrack data is filtered to remove any outliers, and any points where tracking was lost are filled using linear interpolation. When all this is done the data has to be resampled due to the fact that the clock times can be inconsistent and that the data from different sources was not recorded at the same sampling rate. All new data is resampled to 250 Hz. If wind data is present from the wind tunnel, the wind speed data is transformed from the earth frame to the quadrotor body frame and added to the optitrack data. Now there are two data sources, the quadrotor data, and the optitrack data, which now also includes the wind data when present. To align these two data sources the Euler angles measured by both are cross-correlated. This method was used instead of the timestamps of the data, due to the time stamps differing between systems. The time shift for which the correlation is maximal is taken as the shift necessary to align the data sources and merge them in to one.

After all data is merged, the data is subsequently filtered by an Extended Kalman Filter (EKF) based on Ref. [22]. The EKF both filters the data, and removes potential biases present in the IMU measurements. One difference from the work of Ref. [22] is that instead of continuously estimating the biases in flight the biases are estimated in a stationary period before the flight. This is due to the fact that the highly non-linear flight of the quadrotor does not allow the filter to estimate the biases in flight. After the EKF, the IMU and motor data is low-pass filtered by a fourth order butterworth filter with a cut-off frequency of 80 Hz. The frequency was selected based on the Power Spectral Densities (PSD) of the data of interest. In both the PSD of the accelerations Figure 7a, and the PSD of the pitch rate Figure 7b, a small bump can be seen around 90 Hz which most likely resembles some sort of structural resonance which was chosen to be filtered out.

After filtering, the gravity component contained in the acceleration measurements of the IMU is removed, and the body angular rates $\underline{\Omega}$ are numerically differentiated in order to obtain the body angular accelerations $\dot{\underline{\Omega}}$ necessary for calculating the moments acting upon the quadrotor as seen in Equation 13.

VI. Results

A. Steady flight results

Figure 8 shows the relation between the airspeed and the pitch angle required to maintain steady flight at a given airspeed. In the plot the distribution of the dependent variable (pitch angle) is shown, however note that there is also variability in the in the independent variable (airspeed). This is not plotted for visual clarity. Also shown are the 2σ confidence bounds of the mean pitch angle as shown in the inset. Two linear trendlines fitted to these means are also included. Note that the shown airspeeds are the true windtunnel airspeed which differ slightly from the set airspeeds mentioned in subsection IV.B, the differences are most likely to be due to the control system of the wind tunnel fan. It can clearly be seen that the required pitch angle for the ducted quadrotor configuration is considerably higher than the unducted. To visualize this difference, Figure 9 shows both configurations of the quadrotor inside the windtunnel while flying at approximately 12 ms^{-1}. Indeed, the ducted configuration in Figure 9a is flying at a higher pitch angle compared to the unducted configuration in Figure 9b. Considering that the mass of the two configurations is approximately the same this would indicate that the drag coefficient of the ducted configuration is higher than the unducted configuration.

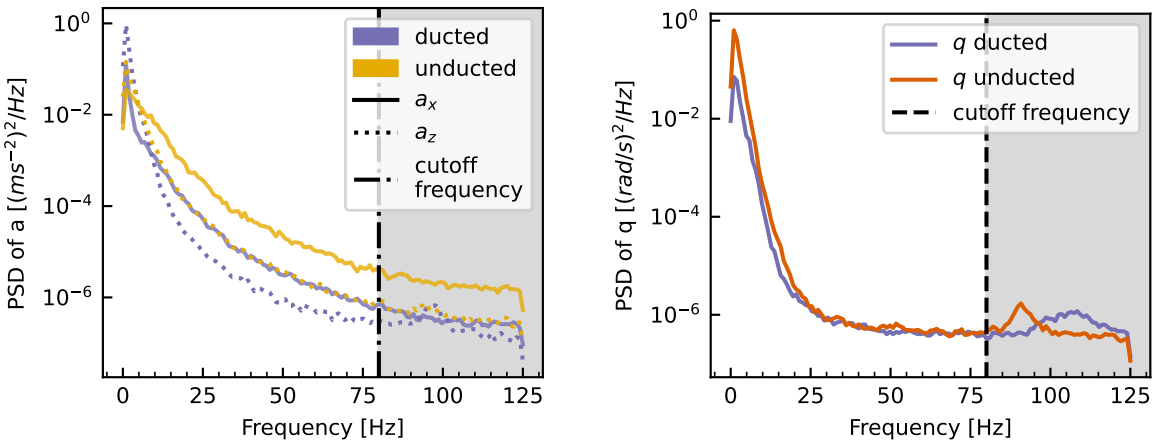

(a) Power spectral densities of the accelerations of interest **(b) Power spectral density of the pitch rate q**

Fig. 7 Power spectral densities of 5 ms^{-1} flight of the to be filtered data

A linear trend line provides a good fit in Figure 8 for both configurations (supported also by the high R^2 values). This relation is in line with the results presented in [23] where a linear relation between the pitch and airspeed is found. Noteworthy here is that the unducted configuration does not seem to start off linear. The higher drag present in the ducted configuration does however not tell the complete story as it does not take into account the potential efficiency gain due to the ducts.

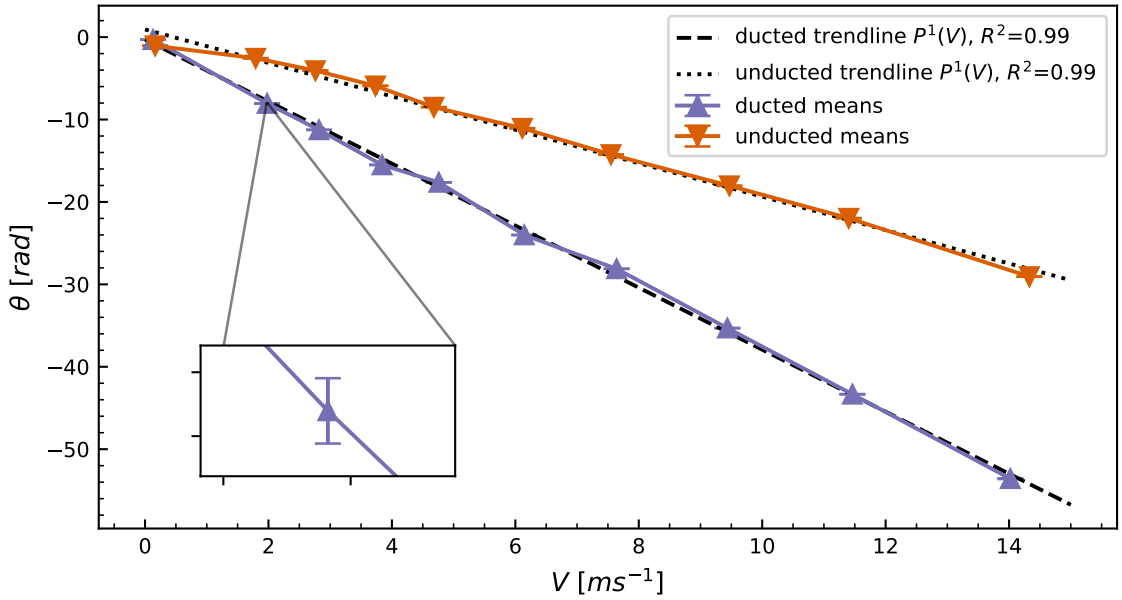

Fig. 8 Comparison of the pitch angles between ducted and unducted configurations during steady flight conditions at different speeds

To see how these pitch angles translate to required rotor speeds, Figure 10 depicts the relation between airspeed and the total rotor speed, for which a quadratic trendline is fitted to the data. A quadratic trend is selected to reflect the quadratic relation between rotor thrust and velocity [20]. The R^2 values of the trendlines seem to indicate a good fit.

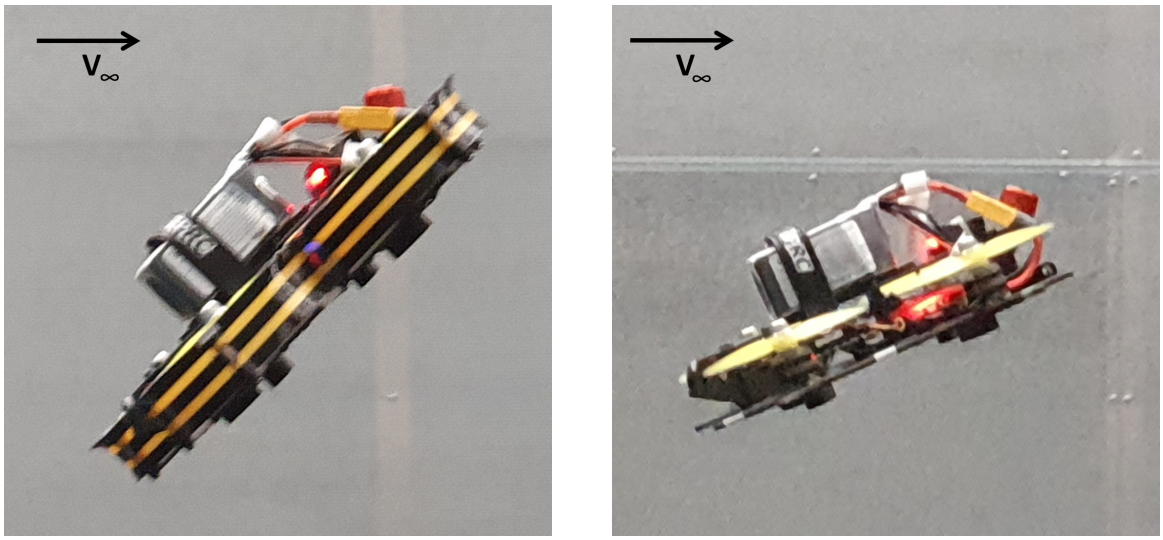

(a) Ducted flight in the windtunnel at approximately 12 ms^{-1} (b) Unducted flight in the windtunnel at approximately 12 ms^{-1}

Fig. 9 Comparing the ducted and unducted pitch angles at 12 ms^{-1}

However, looking at the ducted configuration for airspeeds up to 5 ms^{-1}, there seems to be more of a linear relation between the airspeed and the total rotorspeeds. Comparing the two trends, the data seems to indicate that there is some crossover point where the total rotor speed for the unducted configuration becomes lower than that of the ducted configuration at the same airspeed. Two sample t-tests show a significant difference between ducted and unducted rotor speed means for all airspeeds. With the criterion that the null hypothesis, equivalent means, is rejected for $\alpha < 0.05$, all airspeeds show a significant ($p < 0.001$) difference in mean rotor speed between configurations. These results show that the ducts do both positively and negatively affect the total rotor speeds necessary in forward flight for this quadrotor configuration. However, before claiming a gain in efficiency one should also look at the power used at the different airspeeds. While the average rotor speed is a good indication of the power used, it is possible that more power is required to achieve similar rotor speeds in different configurations.

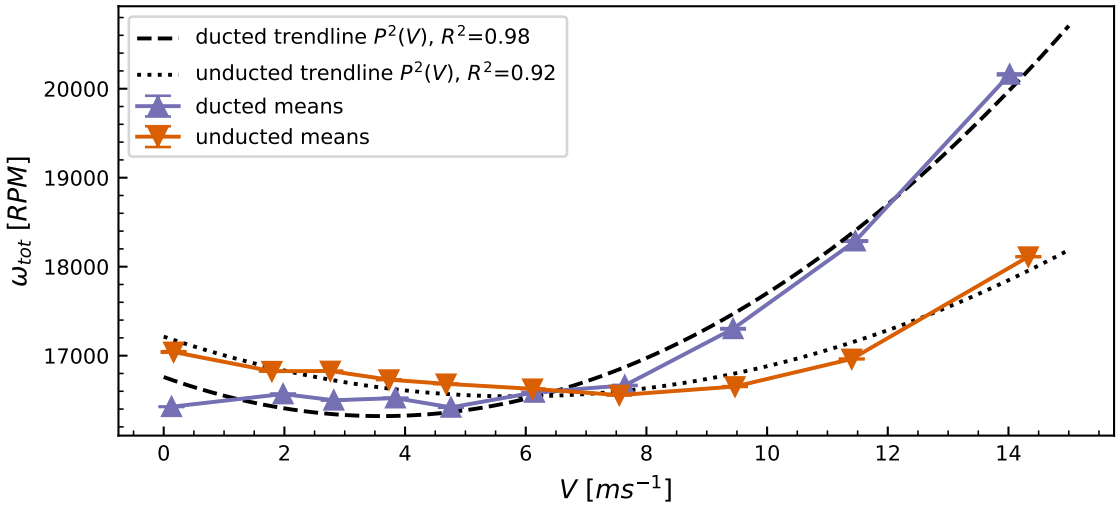

Fig. 10 Comparison of the average rotor speeds between ducted and unducted configurations during steady flight conditions at different speeds

Figure 11 presents the power versus the airspeed, and is fitted with a cubic trendline. A cubic trendline is selected a the power required by a rotor in ideal hover conditions scales with the V^3. Again here the two sample t-tests are performed with the null hypothesis that the means are the same, which is rejected for $\alpha < 0.05$. Similarly to the previous tests, at all airspeeds the null hypothesis is rejected with $p < 0.001$. For the power a similar trend is present as in Figure 10 and with a similar crossover point, at about 6 ms^{-1}. This is where the unducted configuration becomes more efficient in forward flight, compared to the ducted configuration. Additionally, there appears to be a minimum of power consumption that occurs for $V > 0$ for the unducted configuration, this is in line with theory described in Ref. [6, 20] which also finds such power minima for $V > 0$. Interestingly, this does not seem to hold for the quadrotor in its ducted configuration, where the lowest power consumption seems to be at hover.

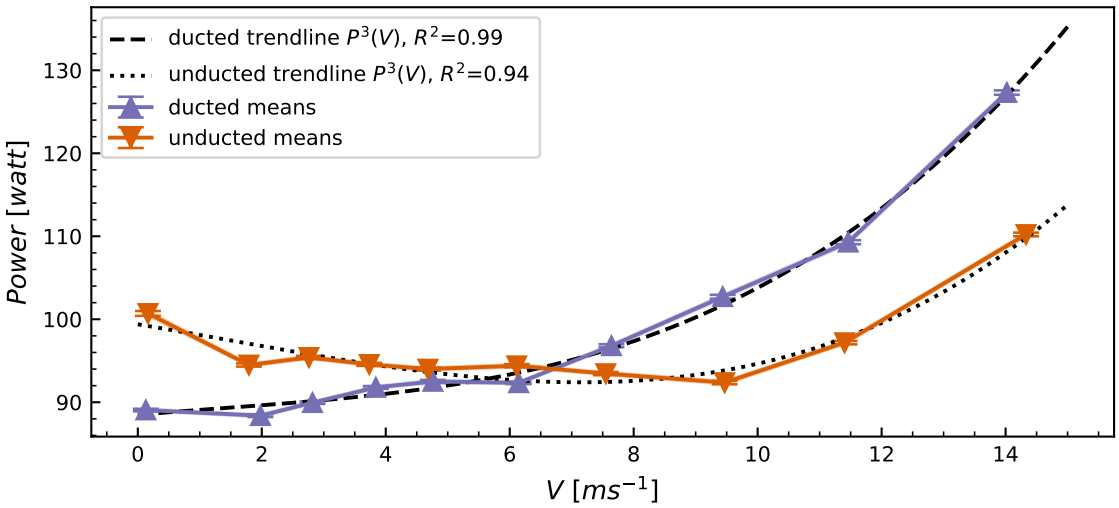

Fig. 11 Comparison of the power used between ducted and unducted configurations during steady flight conditions at different speeds

In comparison to the linear trends observed for the pitch angle, the total rotor speed and power rise upwards for airspeeds above 8 ms^{-1}. This can be explained by the relation between the pitch angle and generated thrust. Assuming the thrust is generated purely along the z-axis of the quadrotor, and that the quadrotor operates purely in pitch (no roll angle is present), the thrust necessary to maintain altitude is given by Equation 36. Due to the division by $\cos(\theta)$, the thrust increases exponentially as the pitch angle increases towards 90 degrees. As seen in Equation 16 the thrust model is heavily reliant on the rotorspeed which therefore explains the difference in trend between the pitch angle and the total rotor speed. Seeing that the majority of the power usage of the quadrotor is used to power the rotors, it is logical that the power consumption follows this trend.

$$T = \frac{-mg}{\cos(\theta)} \tag{36}$$

B. Models

The active flights were used to identify polynomial models using the stepwise regression algorithm, these models are then in turn used to analyse the performance of the quadrotor in forward flight. For the model based analysis first the general model performance is analysed. After which the residual models are used to have a look at the effects of the ducts.

1. Model performance

Models were identified for two forces F_x, and F_z, and one moment M_y in the body frame. These models were identified for 4 different average airspeeds: 0, 5, 8, 10 ms^{-1}. Finally, a model was identified by combining all the airspeeds, with the aim to identify a more generally applicable model. The statistical model performance of the ducted

and unducted configuration models are shown in Table 2 and Table 3 respectively. It can be seen that overall the global models for both the ducted and unducted configurations, have the worst performance or close to the worst performance of all models. However, the global model serves its purpose in being a generally applicable model of the quadrotor over a bigger range of airspeeds, as the other models would be extrapolating when estimating behaviour away from their trim position. Therefore the global model can be considered as the general model describing the CineGo quadrotor platform. Where the models for each airspeed serve their use in closer analysis into the regressors, and possible dynamics at play. It is also clear that the model for M_y is performing considerably less than the force models. A couple of reasons can be considered for this. The first being that for the calculation of the applied moment M_y a numerical differentiation has to be performed on the rotational rate q, which amplifies noise in the signal. The second being that due to the nature of the controls of the quadrotor, the excitation of the moment is only happening for short bursts of time. To mitigate this the training data is isolated to these manoeuvres.

Table 4 shows a more detailed look into the unducted model for F_x at 5 ms^{-1}. The info on the other models is included in Appendix A. Here the regressors and their parameter coefficients $\hat{\Theta}$, in combination with the standard deviation ($s(\hat{\Theta})$) on the parameter estimate are shown. The low values for the ratio $s(\hat{\Theta})/|\hat{\Theta}|$ shows that the model is certain about the estimated parameter coefficients. Figure 12 shows a heatmap of the parameter correlations, notable is that $\sin(\theta)\omega_{tot}$, $\sin(\theta)\omega_{tot}^2$, and $\sin(\theta)\omega_{tot}^3$ have near 1 or -1 parameter correlations with each other, but as shown in Table 4 this does not affect the parameter estimation performance.

Table 2 Statistical model performance for the ducted configuration models

Ducted Configuration	F_x		F_z		M_y	
	R^2	RMSE	R^2	RMSE	R^2	RMSE
$0ms^{-1}$	0.993	0.160	0.965	0.403	0.802	$6.62{\cdot}10^{-3}$
$5ms^{-1}$	0.974	0.182	0.938	0.267	0.802	$4.93{\cdot}10^{-3}$
$8ms^{-1}$	0.958	0.196	0.940	0.248	0.828	$4.59{\cdot}10^{-3}$
$10ms^{-1}$	0.959	0.165	0.935	0.195	0.864	$4.55{\cdot}10^{-3}$
Global	0.916	0.361	0.937	0.351	0.758	$6.03{\cdot}10^{-3}$

Table 3 Statistical model performance for the unducted configuration models

Unducted Configuration	F_x		F_z		M_y	
	R^2	RMSE	R^2	RMSE	R^2	RMSE
$0ms^{-1}$	0.988	0.180	0.954	0.355	0.764	$4.98{\cdot}10^{-3}$
$5ms^{-1}$	0.962	0.220	0.922	0.301	0.884	$4.95{\cdot}10^{-3}$
$8ms^{-1}$	0.940	0.252	0.922	0.202	0.830	$4.50{\cdot}10^{-3}$
$10ms^{-1}$	0.952	0.217	0.932	0.237	0.846	$4.93{\cdot}10^{-3}$
Global	0.946	0.276	0.918	0.325	0.805	$5.33{\cdot}10^{-3}$

2. Residual Models

To isolate the effects due to the propeller ducts the method shown in Figure 1 from section II is included in the analysis. Through this, three different models are identified (ducted, unducted and combined) that can be compared to each other. How these models are obtained is shown in Figure 13. The residual stepwise regression block in this diagram represents the flow diagram shown in Figure 1. For the analysis all three models are used to predict data gathered by a quadrotor in ducted configuration.

Figure 14 shows the three models predicting F_x for a flight recorded at a wind tunnel setting of 5 ms^{-1}, the regressors corresponding to the models can be found in Table 6. From the zoomed inset it can be seen that the unducted model has a clear bias from the reference data as is also present in the mean residual $\bar{\epsilon}$ shown in Table 5. Looking at the peaks present in the reference data it also shows that the unducted model does not dip down as far as the reference data would. This lack in tracking is also reflected in its R^2 value being only 0.665. The combined model then shows improvement to

where it visually performs nearly identical to the ducted model. Which is reflected in the model fit statistics shown in Table 5 which are nearly identical between the ducted and combined model.

Table 4 Estimated parameter values and their standard deviations ($s(\hat{\Theta})$), for the unducted F_x model at 5 ms^{-1}

	Ducted F_x		
Regressor	$\hat{\Theta}$	$s(\hat{\Theta})$	$s(\hat{\Theta})/\lvert\hat{\Theta}\rvert$
$bias$	$-2.63\cdot10^{-1}$	$2.29\cdot10^{-3}$	0.009
μ_x	$1.76\cdot10^{-1}$	$2.00\cdot10^{-3}$	0.011
$\sin(\theta)\omega_{tot}$	$-1.46\cdot10^{-4}$	$6.79\cdot10^{-7}$	0.005
$\omega_{tot}u$	$-4.49\cdot10^{-6}$	$9.19\cdot10^{-9}$	0.002
$\sin(\theta)\omega_{tot}^2$	$1.84\cdot10^{-9}$	$1.67\cdot10^{-11}$	0.009
$\omega_{tot}u^2w^2$	$1.89\cdot10^{-8}$	$1.45\cdot10^{-10}$	0.008
$\sin(\theta)\omega_{tot}^3$	$-7.46\cdot10^{-15}$	$1.02\cdot10^{-16}$	0.014

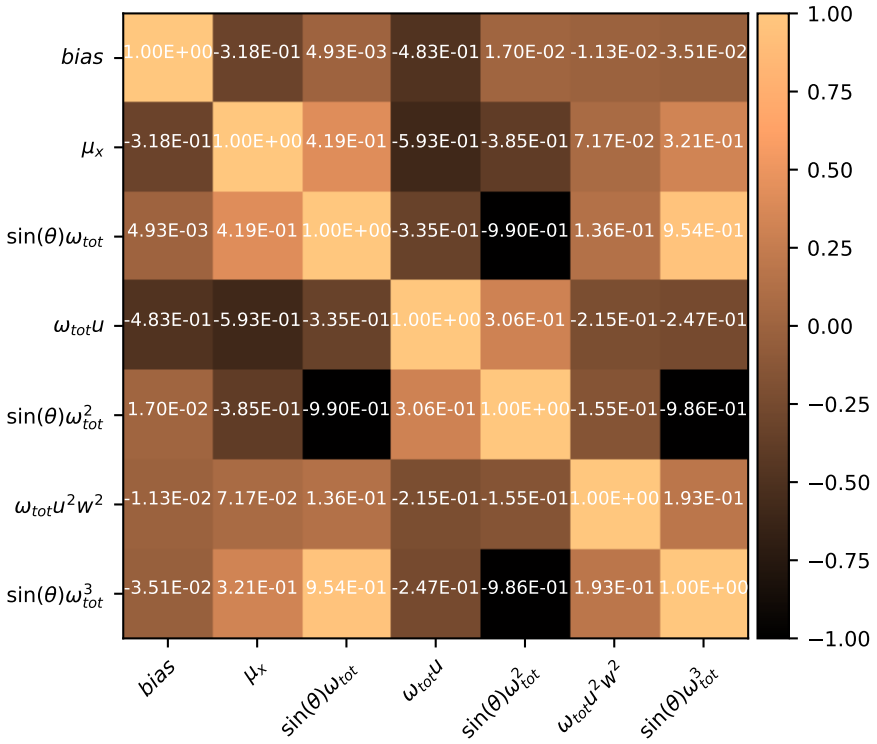

Fig. 12 Heatmap of the parameter correlation matrix for the ducted F_x model at 5 ms^{-1}

Table 5 Model fit statistics of different model types applied to one 5 ms^{-1} dataset

	F_x			F_z			M_y		
	R^2	RMSE	$\bar{\epsilon}$	R^2	RMSE	$\bar{\epsilon}$	R^2	RMSE	$\bar{\epsilon}$
Unducted Model	0.665	0.609	-0.534	0.910	0.504	0.122	0.702	$6.13\cdot10^{-3}$	$1.75\cdot10^{-3}$
Ducted Model	0.958	0.216	0.102	0.943	0.400	0.084	0.771	$5.38\cdot10^{-3}$	$-1.88\cdot10^{-3}$
Combined Model	0.955	0.222	0.109	0.944	0.398	0.107	0.777	$5.31\cdot10^{-3}$	$-1.81\cdot10^{-3}$

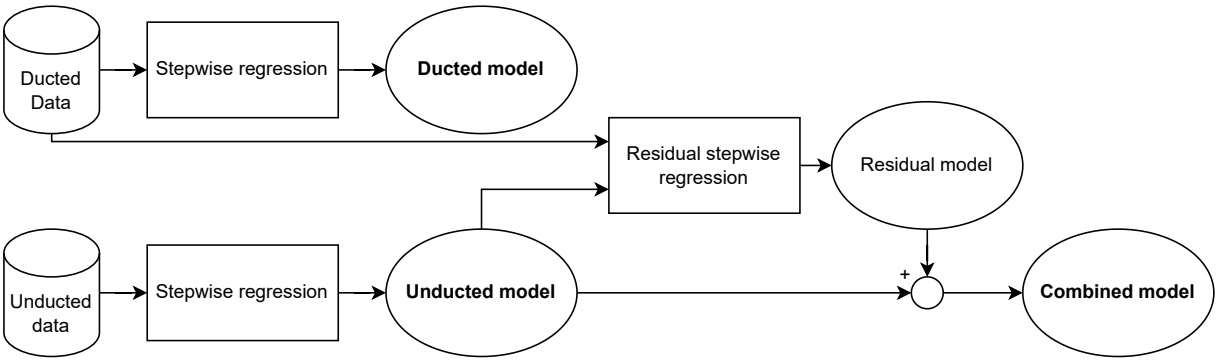

Fig. 13 Definition of the three different models used for analysis are identified

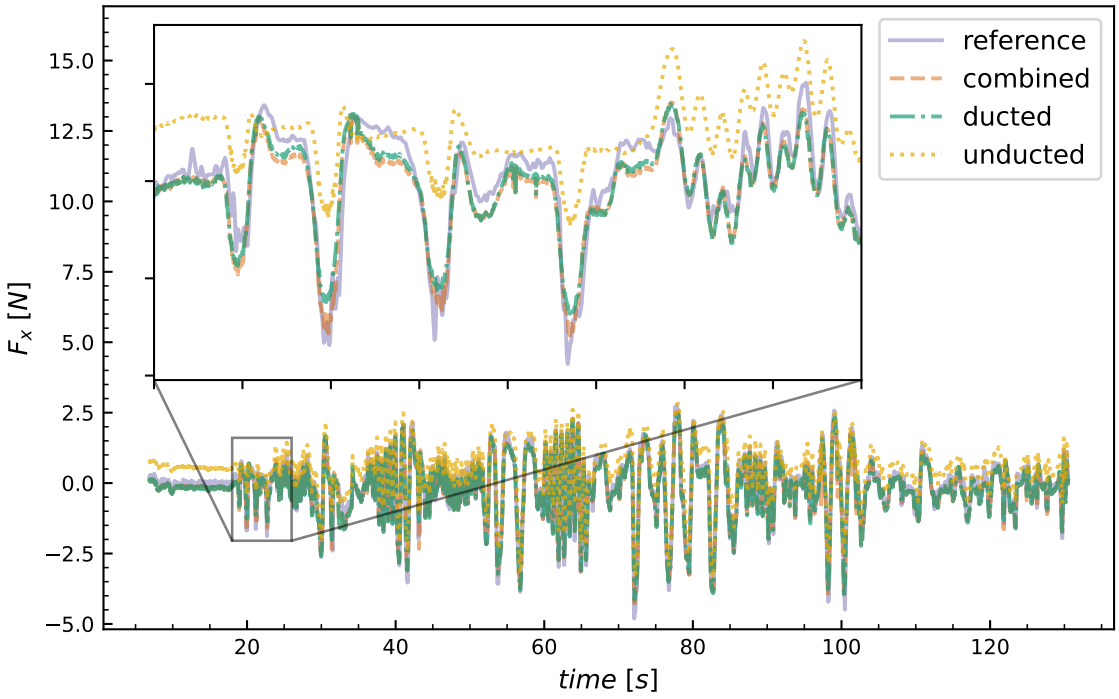

Fig. 14 Model predictions on ducted data of F_x at 5 ms^{-1}

The predictions for F_z are plotted in Figure 15, again for a flight with the wind tunnel set to 5 ms^{-1}. The regressors selected by the stepwise regression are presented in Table 7, note that these are the regressors for $F_{z_{a,T}}$ and that in the plot the hover thrust is added. In contrast to the predictions for F_x, visually not a big difference between models can be seen. Nonetheless, the model fit statistics in Table 5 show an improvement for the combined model, but the improvement is significantly lower.

Lastly the pitching moment coefficient M_y at 5 ms^{-1} is plotted in Figure 16 with the corresponding regressors summarized in Table 8. Visually the difference between the model responses of the three different models is not clear. The model fit statistics from Table 5, again shows a small increase for the combined model compared to the unducted model, but again not as significant as for F_x

Given that the biggest performance gains are obtained for the F_x combined model, this model is also expected to contain most information regarding the effects of ducts. Therefore further analysis starts with the F_x residual model. Table 9 shows the selected regressors for the residual models at different airspeeds. $\omega_{tot}u$ is the regressor selected first

Table 6 Regressors for the C_x models at 5 ms^{-1}

F_x	Ducted		Unducted		Residual	
	Regressor	R^2	Regressor	R^2	Regressor	R^2
Fixed regressors	$bias$	-	$bias$	-	-	-
	μ_x	0.009	μ_x	0.015	-	-
Selected regressors	$\sin(\theta)\omega_{tot}$	0.778	$\sin(\theta)\omega_{tot}$	0.921	$\omega_{tot}u$	0.450
	$\omega_{tot}u$	0.948	$\omega_{tot}u$	0.949	$\mu_z \sin(\theta)uw$	0.511
	$\sin(\theta)\omega_{tot}^2$	0.963	$\sin(\theta)\omega_{tot}^2$	0.960	μ_x	0.547
	$\omega_{tot}u^2w^2$	0.972	q^2	0.961	$\omega_{tot}uw^2$	0.564
	$\sin(\theta)\omega_{tot}^3$	0.974	$\omega_{tot}u^2w^2$	0.962	$\omega_{tot}^3 \sin(\theta)$	0.580

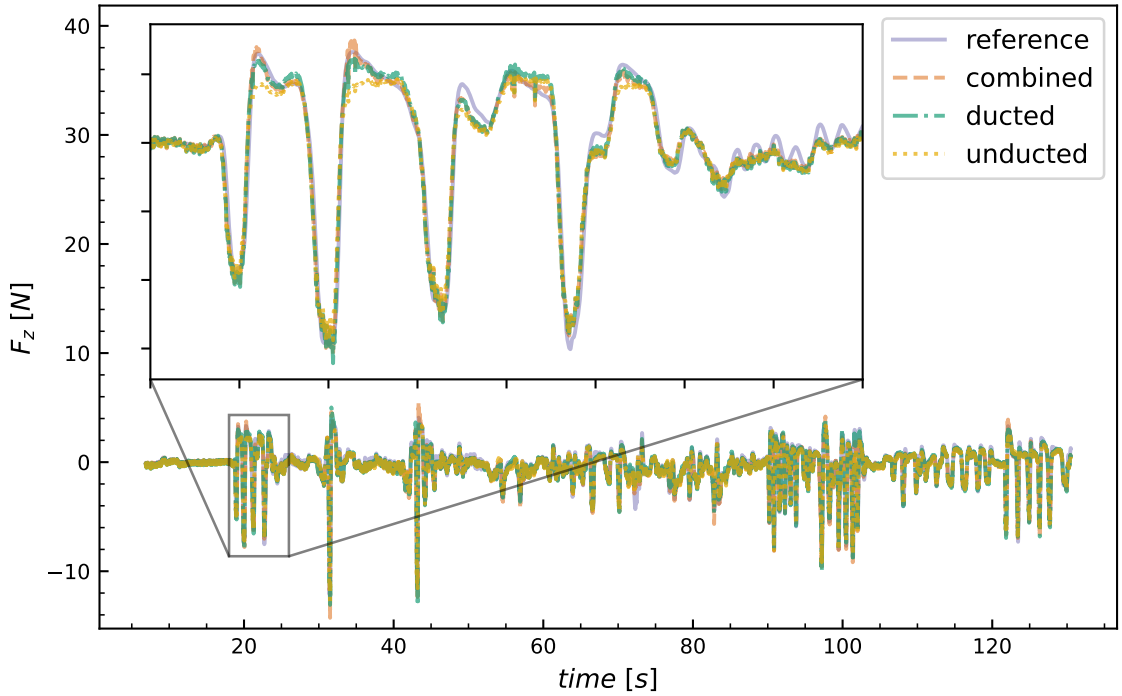

Fig. 15 Model predictions on ducted data of F_z at 5 ms^{-1}

for every airspeed. Indicating that this term seems to play an important role for the dynamics introduced by the ducts. Since the regressor portrays a relation between the rotor speed and the body velocity parallel to the rotor plane, this could indicate a link to blade flapping. Another possibility could be the effect presented in Ref. [10], where it is shown that for a airspeed parallel to the propeller plane the ducts shed extra vortices which interact with the rotor wakes. $\omega_{tot}u$ and its parameters can also be used to compare the effect over different airspeeds. For this comparison a residual model has been identified using only the $\omega_{tot}u$ regressor such that the parameters are not adjusted by any other regressors selected. The parameters at each airspeed are shown in Table 10. First thing that catches the eye is that the sign of the parameter switches between 0 and 5 ms^{-1}. Which would mean that the ducts actually reduce the drag at lower airspeeds. Looking back at Ref. [10] it is shown there that for hovering flight the ducts clean up the flow downstream of the propellers and prevent interactions between the propellers. These coefficients could be related to this effect, however there is no proof of this, seeing that no Stereo Particle Image Velocimetry (SPIV) visuals or alike are available in the tests performed for this research.

Table 7 Regressors for the $F_{z_{a,T}}$ model at 5 ms^-1

$F_{z_{a,T}}$	Ducted		Unducted		Residual	
	Regressor	R^2	Regressor	R^2	Regressor	R^2
Fixed regressors	*bias*	-	*bias*	-	-	-
	$\mu_x^2 + \mu_y^2$	-	$\mu_x^2 + \mu_y^2$	-	-	-
	μ_z	0.015	μ_z	0.005	-	-
Selected regressors	$\sin(\theta)\mu_z$	0.333	$\sin(\theta)\mu_z$	0.234	$\lvert\mu_x\rvert^2 \sin(\theta)$	0.187
	ω_{tot}^3	0.411	$\sin(\theta)\lvert\mu_x\rvert^2$	0.322	μ_z	0.224
	$\sin(\theta)\lvert\mu_x\rvert$	0.464	$\cos(\theta)\lvert\mu_x\rvert^2$	0.372	w^2	0.285
	$\omega_{tot}\lvert u\rvert^2 w^2$	0.485	$\cos(\theta)\omega_{tot}$	0.395	$w\mu_z$	0.324
	$\omega_{tot}\mu_z^2$	0.499	$\sin(\theta)\omega_{tot}$	0.413	$\lvert\mu_x\rvert^2 \sin(\theta)^2$	0.346

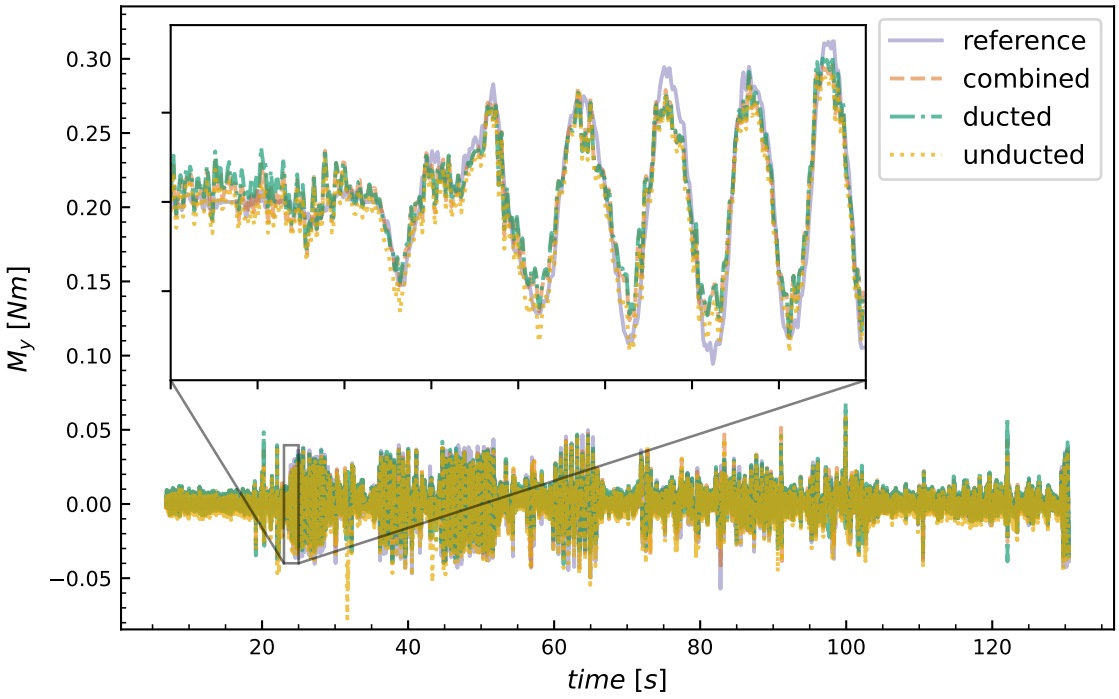

Fig. 16 Model predictions on ducted data of M_y at 5 ms^{-1}

The regressors of the residual model of F_z and M_y however do not show this big of a similarity between the regressors where there is one form of regressor that sticks out as can be seen in Table 11 and Table 12. This also shows the weakness of the stepwise regression method. While its modelling power has shown to be high, it does not always provide actual physical insights. The inconsistency in the modelling terms shows the phenomenological nature of the stepwise regression model. Leading to the fact that these terms cannot be taken as a representation for the actual physics behind the quadrotor dynamics.

VII. Conclusions

From the analysis of steady flights and residual model identification more insights into the effects of propeller ducts on quadrotor in forward flight are obtained. The steady flight tests seem to indicate that there is a transition from where

Table 8 Regressors for the C_m model at 5 ms^{-1}

M_y	Ducted		Unducted		Residual	
	Regressor	R^2	Regressor	R^2	Regressor	R^2
Fixed regressors	$bias$	-	$bias$	-	-	-
	q	-	q	-	-	-
	U_q	0.733	U_q	0.867	-	-
Selected regressors	$U_q uw$	0.768	$\cos(\theta)\mu_z^2$	0.872	$\sin(\theta)$	0.118
	$\omega_{tot} u$	0.780	$\cos(\theta)u_q$	0.876	μ_z^3	0.182
	$\sin(\theta)\mu_x^2$	0.794	$U_q\mu_x$	0.879	U_q	0.208
	w^4	0.798	$\sin(\theta)U_q$	0.881	$U_q\mu_z$	0.243
	$\cos(\theta)U_q$	0.802	$\cos(\theta)\omega_{tot}$	0.884	$U_q w^3$	0.264

Table 9 $F_{x_{res}}$ regressors at different airspeeds, and the evolution in R^2

0 ms^{-1}		5 ms^{-1}		8 ms^{-1}		10 ms^{-1}	
Regressor:	R^2	Regressor:	R^2	Regressor:	R^2	Regressor:	R^2
$\omega_{tot} u$	0.539	$\omega_{tot} u$	0.450	$\omega_{tot} u$	0.531	$\omega_{tot} u$	0.594
$\sin(\theta)$	0.869	$\mu_z \sin(\theta) uw$	0.511	$u^2 w^2$	0.556	$\mu_z w^3$	0.631
μ_x^2	0.874	μ_x	0.547	$\mu_x^2 \omega_{tot}^2 \sin(\theta)$	0.584	$\sin(\theta)$	0.653
uw^2	0.878	$\omega_{tot} uw^2$	0.564	$qu^2 w$	0.599	quw	0.675
uw^3	0.884	$\omega_{tot}^3 \sin(\theta)$	0.580	$\omega_{tot}^2 \mu_x$	0.612	$\omega_{tot}^2 uw$	0.697

Table 10 Coefficients corresponding to the $\omega_{tot} u$ regressor for residual models at different airspeeds

Model	Coefficient
$0ms^{-1}$	$2.32 \cdot 10^{-6}$
$5ms^{-1}$	$-1.89 \cdot 10^{-6}$
$8ms^{-1}$	$-1.88 \cdot 10^{-6}$
$10ms^{-1}$	$-1.98 \cdot 10^{-6}$

Table 11 $F_{z_{res}}$ regressors at different airspeeds, and their evolution in R^2

0 ms^{-1}		5 ms^{-1}		8 ms^{-1}		10 ms^{-1}	
Regressor:	R^2	Regressor:	R^2	Regressor:	R^2	Regressor:	R^2
$\sin(\theta)^2$	0.079	$\lvert\mu_x\rvert^2 \sin(\theta)$	0.187	$\lvert\mu_x\rvert \sin(\theta)$	0.149	$u^2 \sin(\theta)^2$	0.332
$uw \sin(\theta)$	0.135	μ_z	0.224	uw^2	0.181	$u^3\mu_x$	0.363
$w^2\mu_z\lvert\mu_x\rvert$	0.185	w^2	0.285	$w\lvert\mu_x\rvert \sin(\theta)$	0.211	$\sin(\theta)^4$	0.393
$\sin(\theta)$	0.227	$w\mu_z$	0.324	uw	0.259	$u^2 w$	0.404
$u \sin(\theta)$	0.242	$\lvert\mu_x\rvert^2 \sin(\theta)^2$	0.346	$w^3\mu_z$	0.267	$\mu_z \sin(\theta)^3$	0.417

the effect of the ducts is beneficial, around hover conditions, to where the ducts are actually detrimental to performance, forward flights of about 6 ms^{-1} and up, given equal weight and inertia.

To expand on these results, tests with a set airspeed and varying angles of attack, or vice versa, could be performed to obtain more insight into the effects at play. Next to this the measurements can be refined by using an autonomous controller to keep the quadrotor steady at its position, and to reduce the effect of the human variations in the data.

The identified models also give a first insight into the differences between configurations. Here for the F_x models the biggest difference was present, and the $\omega_{tot} u$ regressor plays an important role in the modelling of the propeller ducts.

Table 12 $M_{y_{res}}$ **regressors at different airspeeds, and their evolution in** R^2

$0\ ms^{-1}$		$5\ ms^{-1}$		$8\ ms^{-1}$		$10\ ms^{-1}$	
Regressor:	R^2	Regressor:	R^2	Regressor:	R^2	Regressor:	R^2
$\sin(\theta)^2 q$	0.086	$\sin(\theta)$	0.118	μ_z^4	0.101	$U_q \sin(\theta)^2$	0.062
$U_q \mu_z$	0.165	μ_z^3	0.182	w	0.155	$\sin(\theta)^4$	0.103
$w \sin(\theta)$	0.200	U_q	0.208	U_q^4	0.171	w^2	0.149
$U_q w^2$	0.220	$U_q \mu_z$	0.243	$U_q^3 \sin(\theta)$	0.184	$\sin(\theta)$	0.169
$\sin(\theta) q^2$	0.236	$U_q w^3$	0.264	U_q^2	0.200	$\sin(\theta)^3$	0.194

However, the model identification is still heavily influenced by the available data. Furthermore, the data collection could be improved by finding the best manoeuvres to excite the system, and automating these giving more repeatable data, which hopefully results in more consistent models. Next to this when more information is obtained regarding the effects at play, the candidate polynomials can also be improved resulting in better models as well.

While there are definitely some improvements to be done, this paper makes a good start on the modelling of ducts and obtains some interesting phenomenological insights on how they affect the quadrotor in flight. To continue this research several steps can be taken. Currently the research methods applied are unable to distinguish the added performance of the ducts from the drag added because of the ducts. So further research can look into methods able to isolate the positive and negative contributions of the ducts. Additionally, this research is performed using only one quadrotor platform, further research can look into if these effects are present for different configurations as well, and if they can be generalised.

References

[1] AbuAssi, L., "The breguet-richet quad-rotor helicopter of 1907," *Vertiflite*, 2002. URL `https://www.academia.edu/815361/The_breguet_richet_quad_rotor_helicopter_of_1907`.

[2] Bouabdallah, S., Murrieri, P., and Siegwart, R., "Design and control of an Indoor micro quadrotor," Institute of Electrical and Electronics Engineers Inc., 2004, pp. 4393–4398. https://doi.org/10.1109/robot.2004.1302409.

[3] Bauersfeld, L., Kaufmann, E., Foehn, P., Sun, S., and Scaramuzza, D., "NeuroBEM: Hybrid Aerodynamic Quadrotor Model," 2021. URL https://arxiv.org/abs/2106.08015v1.

[4] Six, D., Briot, S., Erskine, J., and Chriette, A., "Identification of the Propeller Coefficients and Dynamic Parameters of a Hovering Quadrotor from Flight Data," *IEEE Robotics and Automation Letters*, Vol. 5, 2020, pp. 1063–1070. https://doi.org/10.1109/LRA.2020.2966393.

[5] Sun, S., de Visser, C. C., and Chu, Q., "Quadrotor Gray-Box Model Identification from High-Speed Flight Data," *Journal of Aircraft*, Vol. 56, 2019, pp. 645–661. https://doi.org/10.2514/1.C035135, URL https://arc.aiaa.org/doi/10.2514/1.C035135.

[6] Hoffmann, G. M., Huang, H., Waslander, S. L., and Tomlin, C. J., "Precision flight control for a multi-vehicle quadrotor helicopter testbed," *Control Engineering Practice*, Vol. 19, 2011, pp. 1023–1036. https://doi.org/10.1016/J.CONENGPRAC.2011.04.005.

[7] Torrente, G., Kaufmann, E., Fohn, P., and Scaramuzza, D., "Data-Driven MPC for Quadrotors," *IEEE Robotics and Automation Letters*, Vol. 6, 2021, pp. 3769–3776. https://doi.org/10.1109/LRA.2021.3061307.

[8] Ferdaus, M. M., Pratama, M., Anavatti, S. G., and Garratt, M. A., "Online identification of a rotary wing Unmanned Aerial Vehicle from data streams," *Applied Soft Computing Journal*, Vol. 76, 2019, pp. 313–325. https://doi.org/10.1016/j.asoc.2018.12.013.

[9] Barcelos, D., Kolaei, A., and Bramesfeld, G., "Aerodynamic interactions of quadrotor configurations," *Journal of Aircraft*, Vol. 57, 2020, pp. 1074–1090. https://doi.org/10.2514/1.C035614, URL https://doi.org/10.2514/1.C035614.

[10] Shukla, D., Hiremath, N., and Komerath, N., "Low reynolds number aerodynamics study on coaxial and quadrotor," American Institute of Aeronautics and Astronautics Inc, AIAA, 2018. https://doi.org/10.2514/6.2018-4118.

[11] Shukla, D., and Komerath, N., "Multirotor Drone Aerodynamic Interaction Investigation," *Drones 2018, Vol. 2, Page 43*, Vol. 2, 2018, p. 43. https://doi.org/10.3390/DRONES2040043, URL https://www.mdpi.com/2504-446X/2/4/43/htmhttps://www.mdpi.com/2504-446X/2/4/43.

[12] Hwang, J. Y., Jung, M. K., and Kwon, O. J., "Numerical study of aerodynamic performance of a multirotor unmanned-aerial-vehicle configuration," *Journal of Aircraft*, Vol. 52, 2015, pp. 839–846. https://doi.org/10.2514/1.C032828/ASSET/IMAGES/LARGE/FIGURE13.JPEG, URL https://arc.aiaa.org/doi/10.2514/1.C032828.

[13] Throneberry, G., Hocut, C. M., and Abdelkefi, A., "Multi-rotor wake propagation and flow development modeling: A review," *Progress in Aerospace Sciences*, Vol. 127, 2021, p. 100762. https://doi.org/10.1016/J.PAEROSCI.2021.100762.

[14] Li, Y., Yonezawa, K., Liu, H., Li, Y. ., Yonezawa, K. ., Liu, H., and Armanini, S., "Effect of Ducted Multi-Propeller Configuration on Aerodynamic Performance in Quadrotor Drone," *Drones 2021, Vol. 5, Page 101*, Vol. 5, 2021, p. 101. https://doi.org/10.3390/DRONES5030101, URL https://www.mdpi.com/2504-446X/5/3/101/htmhttps://www.mdpi.com/2504-446X/5/3/101.

[15] Sun, S., Schilder, R., and de Visser, C. C., "Identification of Quadrotor Aerodynamic Model from High Speed Flight Data," American Institute of Aeronautics and Astronautics, 2018. https://doi.org/10.2514/6.2018-0523, URL https://arc.aiaa.org/doi/10.2514/6.2018-0523.

[16] Klein, V., and Morelli, E. A., *Aircraft system identification: theory and practice*, American Institute of Aeronautics and Astronautics, 2006.

[17] He, X., Guo, D., and Leang, K., "Repetitive Control Design and Implementation for Periodic Motion Tracking in Aerial Vehicles," 2017. https://doi.org/10.23919/ACC.2017.7963746.

[18] Powers, C., Mellinger, D., Kushleyev, A., Kothmann, B., and Kumar, V., *Influence of Aerodynamics and Proximity Effects in Quadrotor Flight*, Springer International Publishing, Heidelberg, 2013, pp. 289–302. https://doi.org/10.1007/978-3-319-00065-7_21, URL https://doi.org/10.1007/978-3-319-00065-7_21.

[19] Johnson, W., *Helicopter theory*, Princeton, N.J.: Princeton University Press, 1980. Includes index.

[20] Leishman, J. G., *Principles of helicopter aerodynamics*, 2nd ed., Camebridge University Press, 2005.

[21] Pounds, P., Mahony, R., and Corke, P., "Modelling and control of a large quadrotor robot," *Control Engineering Practice*, Vol. 18, 2010, pp. 691–699. https://doi.org/10.1016/J.CONENGPRAC.2010.02.008.

[22] Armanini, S. F., Karasek, M., Croon, G. C. D., and Visser, C. C. D., "Onboard/Offboard Sensor Fusion for High-Fidelity Flapping-Wing Robot Flight Data," *Journal of Guidance, Control, and Dynamics: devoted to the technology of dynamics and control*, Vol. 40, 2017, pp. 2116–2127. https://doi.org/10.2514/1.G002527, URL https://repository.tudelft.nl/islandora/object/uuid%3Abf93134a-1b2b-4ab8-878f-69a9130e0522.

[23] Meier, K., Hann, R., Skaloud, J., and Garreau, A., "Wind Estimation with Multirotor UAVs," *Atmosphere*, Vol. 13, 2022. https://doi.org/10.3390/atmos13040551.

Appendix A: Quadrotor Models

The tables in this appendix show the identified models at every airspeed.

Table 13 F_x **models for 8** ms^{-1}

F_x models 8 ms^{-1}												
Unducted Model				Ducted Model				Residual Model			
Regressor	$\hat{\Theta}$	$s(\hat{\Theta})/\lvert\hat{\Theta}\rvert$	RMSE	Regressor	$\hat{\Theta}$	$s(\hat{\Theta})/\lvert\hat{\Theta}\rvert$	RMSE	Regressor	$\hat{\Theta}$	$s(\hat{\Theta})/\lvert\hat{\Theta}\rvert$	RMSE
$bias$	$-9.79\cdot10^{-2}$	0.052	-	$bias$	$7.58\cdot10^{-1}$	0.011	-				
μ_x	$1.71\cdot10^{-2}$	0.101	1.017	μ_x	$-1.40\cdot10^{-1}$	0.021	0.925	$bias$	$-1.52\cdot10^{-1}$	0.017	0.288
$\sin(\theta)\omega_{tot}$	$-7.70\cdot10^{-5}$	0.007	0.400	μ_z	$-4.84\cdot10^{-1}$	0.006	0.409	$\omega_{tot}u$	$-9.35\cdot10^{-6}$	0.014	0.197
$\omega_{tot}u$	$-1.97\cdot10^{-6}$	0.004	0.288	$\cos(\theta)\omega_{tot}$	$-1.64\cdot10^{-5}$	0.010	0.317	u^2w^2	$3.35\cdot10^{-4}$	0.008	0.192
$\sin(\theta)\omega_{tot}^2$	$4.87\cdot10^{-10}$	0.012	0.258	$\sin(\theta)\omega_{tot}$	$-2.67\cdot10^{-5}$	0.005	0.236	$\mu_x^2\omega_{tot}^2\sin(\theta)$	$3.60\cdot10^{-11}$	0.009	0.186
$\sin(\theta)\mu_x$	$-3.56\cdot10^{-1}$	0.017	0.254	$\omega_{tot}u$	$-3.02\cdot10^{-6}$	0.005	0.203	qu^2w	$-2.69\cdot10^{-4}$	0.017	0.182
$\omega_{tot}w^2$	$7.49\cdot10^{-8}$	0.025	0.252	$\sin(\theta)u$	$-1.06\cdot10^{-1}$	0.013	0.196	$\omega_{tot}^2\mu_x$	$4.66\cdot10^{-10}$	0.018	0.179
R^2: 0.940				R^2: 0.958				R^2: 0.612			

Table 14 F_x **models for 10** ms^{-1}

F_x models 10 ms^{-1}												
Unducted Model				Ducted Model				Residual Model			
Regressor	$\hat{\Theta}$	$s(\hat{\Theta})/\lvert\hat{\Theta}\rvert$	RMSE	Regressor	$\hat{\Theta}$	$s(\hat{\Theta})/\lvert\hat{\Theta}\rvert$	RMSE	Regressor	$\hat{\Theta}$	$s(\hat{\Theta})/\lvert\hat{\Theta}\rvert$	RMSE
$bias$	$-1.74\cdot10^{-3}$	3.236	-	$bias$	1.29	0.007	-				
μ_x	$-2.75\cdot10^{-2}$	0.056	0.974	μ_x	$5.86\cdot10^{-2}$	0.044	0.764	$bias$	$2.11\cdot10^{-1}$	0.026	0.305
$\sin(\theta)\omega_{tot}$	$-6.34\cdot10^{-5}$	0.006	0.449	$\sin(\theta)\mu_z$	$-3.42\cdot10^{-1}$	0.015	0.345	$\omega_{tot}u$	$-2.39\cdot10^{-6}$	0.004	0.195
$\omega_{tot}u$	$-2.00\cdot10^{-6}$	0.003	0.292	$\cos(\theta)\omega_{tot}$	$-3.95\cdot10^{-5}$	0.003	0.285	$\mu_z w^3$	$3.21\cdot10^{-4}$	0.009	0.186
$\sin(\theta)\mu_x$	$-4.24\cdot10^{-1}$	0.010	0.229	$\omega_{tot}\mu_z$	$-1.89\cdot10^{-5}$	0.003	0.208	$\sin(\theta)$	$6.57\cdot10^{-1}$	0.009	0.180
$\sin(\theta)\omega_{tot}^2$	$3.62\cdot10^{-10}$	0.011	0.222	$\cos(\theta)u^2$	$-1.52\cdot10^{-2}$	0.005	0.180	quw	$-1.48\cdot10^{-3}$	0.011	0.174
$\omega_{tot}uw^2$	$1.01\cdot10^{-8}$	0.017	0.217	qu^2w	$-2.49\cdot10^{-4}$	0.008	0.165	ω_{tot}^2uw	$-1.10\cdot10^{-12}$	0.013	0.168
R^2: 0.952				R^2: 0.959				R^2: 0.697			

Table 15 Global models for F_x

Global F_x models											
Unducted Model				Ducted Model				Residual Model			
Regressor	$\hat{\Theta}$	$s(\hat{\Theta})/\lvert\hat{\Theta}\rvert$	RMSE	Regressor	$\hat{\Theta}$	$s(\hat{\Theta})/\lvert\hat{\Theta}\rvert$	RMSE	Regressor	$\hat{\Theta}$	$s(\hat{\Theta})/\lvert\hat{\Theta}\rvert$	RMSE
$bias$	$-8.28\cdot10^{-2}$	0.014	-	$bias$	$-1.07\cdot10^{-1}$	0.013	-				
μ_x	$3.04\cdot10^{-2}$	0.025	1.186	μ_x	$1.76\cdot10^{-1}$	0.007	1.248	$bias$	$-6.65\cdot10^{-2}$	0.019	0.553
$\sin(\theta)\omega_{tot}$	$-9.03\cdot10^{-5}$	0.002	0.481	$\sin(\theta)\omega_{tot}$	$-6.85\cdot10^{-5}$	0.002	0.748	$\omega_{tot}u^2$	$-5.14\cdot10^{-7}$	0.003	0.406
$\omega_{tot}u^2$	$-3.63\cdot10^{-7}$	0.003	0.353	$\omega_{tot}u^2$	$-7.04\cdot10^{-7}$	0.002	0.492	$\omega_{tot}u^3$	$3.53\cdot10^{-8}$	0.005	0.383
$\sin(\theta)\omega_{tot}^2$	$5.99\cdot10^{-10}$	0.003	0.300	$\omega_{tot}U_q$	$2.03\cdot10^{-9}$	0.003	0.412	$\omega_{tot}^3 q$	$-2.12\cdot10^{-16}$	0.008	0.363
$\omega_{tot}u^3$	$1.82\cdot10^{-8}$	0.006	0.285	$\omega_{tot}u^4$	$3.52\cdot10^{-9}$	0.004	0.379	$\omega_{tot}\sin(\theta)qw$	$1.15\cdot10^{-6}$	0.005	0.346
$\cos(\theta)U_q$	$5.43\cdot10^{-5}$	0.007	0.276	$\sin(\theta)\omega_{tot}^2$	$3.26\cdot10^{-10}$	0.006	0.361	$\omega_{tot}\sin(\theta)^2 q$	$-5.14\cdot10^{-6}$	0.009	0.340
R^2: 0.946				R^2: 0.916				R^2: 0.621			

Table 16 $F_{z_{a,T}}$ **models for 0** ms^{-1}

$F_{z_{a,T}}$ models 0 ms^{-1}									
Unducted Model				Ducted Model				Residual Model			
Regressor	$\hat{\Theta}$	$s(\hat{\Theta})/\lvert\hat{\Theta}\rvert$	RMSE	Regressor	$\hat{\Theta}$	$s(\hat{\Theta})/\lvert\hat{\Theta}\rvert$	RMSE	Regressor	$\hat{\Theta}$	$s(\hat{\Theta})/\lvert\hat{\Theta}\rvert$	RMSE
$bias$	3.71	0.005	-	$bias$	4.25	0.004	-				
$\mu_x^2+\mu_y^2$	$-1.09\cdot10^{-1}$	0.031	-	$\mu_x^2+\mu_y^2$	$-9.47\cdot10^{-2}$	0.032	-				
μ_z	$-2.45\cdot10^{-1}$	0.042	0.540	μ_z	$-1.65\cdot10^{-1}$	0.034	0.607	$bias$	$2.71\cdot10^{-1}$	0.007	0.428
$\cos(\theta)\omega_{tot}$	$3.70\cdot10^{-5}$	0.004	0.483	$\cos(\theta)\omega_{tot}$	$4.37\cdot10^{-5}$	0.004	0.531	$\sin(\theta)^2$	$-8.89\cdot10^{-1}$	0.008	0.410
ω_{tot}	$-5.61\cdot10^{-5}$	0.010	0.392	ω_{tot}	$-6.63\cdot10^{-5}$	0.008	0.438	$uw\sin(\theta)$	$-8.06\cdot10^{-2}$	0.012	0.398
$\lvert\mu_x\rvert\mu_z$	$-5.38\cdot10^{-1}$	0.017	0.386	ω_{tot}^2	$2.57\cdot10^{-10}$	0.013	0.424	$w^2\mu_z\lvert\mu_x\rvert$	$5.02\cdot10^{-2}$	0.013	0.386
ω_{tot}^2	$2.15\cdot10^{-10}$	0.018	0.379	$\omega_{tot}\lvert u\rvert w^2$	$2.27\cdot10^{-7}$	0.013	0.414	$\sin(\theta)$	$1.97\cdot10^{-1}$	0.016	0.376
$\cos(\theta)w$	$1.66\cdot10^{-1}$	0.020	0.371	w^3	$1.01\cdot10^{-2}$	0.016	0.401	$u\sin(\theta)$	$7.45\cdot10^{-2}$	0.027	0.372
R^2: 0.532				R^2: 0.565				R^2: 0.242			

Table 17 $F_{z_{a,T}}$ **models for 5** ms^{-1}

$F_{z_{a,T}}$ models 5 ms^{-1}									
Unducted Model				Ducted Model				Residual Model			
Regressor	$\hat{\Theta}$	$s(\hat{\Theta})/\lvert\hat{\Theta}\rvert$	RMSE	Regressor	$\hat{\Theta}$	$s(\hat{\Theta})/\lvert\hat{\Theta}\rvert$	RMSE	Regressor	$\hat{\Theta}$	$s(\hat{\Theta})/\lvert\hat{\Theta}\rvert$	RMSE
$bias$	3.03	0.004	-	$bias$	3.48	0.001	-				
$\mu_x^2+\mu_y^2$	-1.38	0.013	-	$\mu_x^2+\mu_y^2$	$-5.52\cdot10^{-3}$	0.176	-				
μ_z	$3.99\cdot10^{-1}$	0.017	0.404	μ_z	$-1.22\cdot10^{-1}$	0.043	0.458				
$\sin(\theta)\mu_z$	$-6.52\cdot10^{-1}$	0.019	0.355	$\sin(\theta)\mu_z$	-2.13	0.008	0.376	$bias$	$-8.68\cdot10^{-2}$	0.021	0.396
$\sin(\theta)\lvert\mu_x\rvert^2$	$-3.40\cdot10^{-1}$	0.016	0.334	ω_{tot}^3	$9.60\cdot10^{-16}$	0.009	0.354	μ_z	$-3.69\cdot10^{-1}$	0.010	0.357
$\cos(\theta)\lvert\mu_x\rvert^2$	1.38	0.013	0.321	$\sin(\theta)\lvert\mu_x\rvert$	$-6.57\cdot10^{-1}$	0.011	0.337	w^2	$-7.27\cdot10^{-2}$	0.010	0.349
$\cos(\theta)\omega_{tot}$	$7.88\cdot10^{-6}$	0.023	0.315	$\omega_{tot}\lvert u\rvert^2w^2$	$-1.84\cdot10^{-8}$	0.016	0.331	$w\mu_z$	$1.94\cdot10^{-1}$	0.016	0.335
$\sin(\theta)\omega_{tot}$	$-5.76\cdot10^{-6}$	0.025	0.310	$\omega_{tot}\mu_z^2$	$6.56\cdot10^{-6}$	0.024	0.326	$\lvert\mu_x\rvert^2\sin(\theta)^2$	$3.90\cdot10^{-1}$	0.013	0.325
R^2: 0.413				R^2: 0.499				R^2: 0.346			

Table 18 $F_{z_{a,T}}$ **models for 8** ms^{-1}

$F_{z_{a,T}}$ models 8 ms^{-1}											
Unducted Model				Ducted Model				Residual Model			
Regressor	$\hat{\Theta}$	$s(\hat{\Theta})/\lvert\hat{\Theta}\rvert$	RMSE	Regressor	$\hat{\Theta}$	$s(\hat{\Theta})/\lvert\hat{\Theta}\rvert$	RMSE	Regressor	$\hat{\Theta}$	$s(\hat{\Theta})/\lvert\hat{\Theta}\rvert$	RMSE
$bias$	1.88	0.005	-	$bias$	3.01	0.002	-				
$\mu_x^2+\mu_y^2$	$-4.96{\cdot}10^{-1}$	0.010	-	$\mu_x^2+\mu_y^2$	$3.55{\cdot}10^{-3}$	0.175	-				
μ_z	$3.89{\cdot}10^{-1}$	0.009	0.448	μ_z	$-1.03{\cdot}10^{-2}$	0.687	0.498	$bias$	$-7.93{\cdot}10^{-2}$	0.032	0.367
$\sin(\theta)\lvert\mu_x\rvert$	$-6.24{\cdot}10^{-1}$	0.020	0.373	$\omega_{tot}\lvert u\rvert$	$1.18{\cdot}10^{-6}$	0.011	0.382	$\lvert\mu_x\rvert\sin(\theta)$	$5.43{\cdot}10^{-1}$	0.020	0.338
$\cos(\theta)\omega_{tot}$	$2.83{\cdot}10^{-5}$	0.006	0.330	$\omega_{tot}\mu_z^2$	$6.15{\cdot}10^{-6}$	0.020	0.347	uw^2	$-1.15{\cdot}10^{-2}$	0.009	0.332
$\cos(\theta)\lvert\mu_x\rvert^2$	$5.53{\cdot}10^{-1}$	0.009	0.311	$\sin(\theta)\omega_{tot}$	$-3.12{\cdot}10^{-5}$	0.008	0.331	$w\lvert\mu_x\rvert\sin(\theta)$	$3.15{\cdot}10^{-1}$	0.010	0.326
$\omega_{tot}\lvert u\rvert$	$-1.29{\cdot}10^{-6}$	0.009	0.297	$\sin(\theta)w$	$-4.60{\cdot}10^{-1}$	0.010	0.314	uw	$-2.95{\cdot}10^{-2}$	0.012	0.316
$\sin(\theta)\lvert u\rvert$	$-1.57{\cdot}10^{-1}$	0.020	0.293	$\cos(\theta)w^3$	$2.48{\cdot}10^{-3}$	0.017	0.308	$w^3\mu_z$	$5.06{\cdot}10^{-4}$	0.031	0.314
R^2: 0.676				R^2: 0.662				R^2: 0.267			

Table 19 $F_{z_{a,T}}$ **models for 10** ms^{-1}

$F_{z_{a,T}}$ models 10 ms^{-1}											
Unducted Model				Ducted Model				Residual Model			
Regressor	$\hat{\Theta}$	$s(\hat{\Theta})/\lvert\hat{\Theta}\rvert$	RMSE	Regressor	$\hat{\Theta}$	$s(\hat{\Theta})/\lvert\hat{\Theta}\rvert$	RMSE	Regressor	$\hat{\Theta}$	$s(\hat{\Theta})/\lvert\hat{\Theta}\rvert$	RMSE
$bias$	1.66	0.006	-	$bias$	2.62	0.002	-				
$\mu_x^2+\mu_y^2$	$2.73{\cdot}10^{-2}$	0.013	-	$\mu_x^2+\mu_y^2$	$-1.01{\cdot}10^{-1}$	0.031	-				
μ_z	$-4.43{\cdot}10^{-2}$	0.119	0.493	μ_z	$5.16{\cdot}10^{-2}$	0.075	0.495	$bias$	$-3.55{\cdot}10^{-1}$	0.009	0.345
$\sin(\theta)\lvert u\rvert$	$-2.84{\cdot}10^{-1}$	0.005	0.406	$\sin(\theta)\lvert u\rvert$	$-3.56{\cdot}10^{-1}$	0.003	0.310	$u^2\sin(\theta)^2$	$6.87{\cdot}10^{-3}$	0.036	0.282
$\cos(\theta)\omega_{tot}$	$2.95{\cdot}10^{-5}$	0.008	0.360	ω_{tot}^3	$1.64{\cdot}10^{-15}$	0.006	0.281	$u^3\mu_x$	$1.43{\cdot}10^{-4}$	0.012	0.275
$\sin(\theta)\lvert u\rvert^3w$	$-1.27{\cdot}10^{-4}$	0.026	0.340	$\omega_{tot}\lvert u\rvert w^2$	$-3.01{\cdot}10^{-8}$	0.009	0.262	$\sin(\theta)^4$	1.93	0.014	0.269
$\cos(\theta)\lvert u\rvert w^3$	$3.09{\cdot}10^{-4}$	0.016	0.333	$\lvert U_q\rvert\lvert u\rvert^3w$	$-1.37{\cdot}10^{-8}$	0.025	0.257	u^2w	$-9.03{\cdot}10^{-4}$	0.019	0.266
$\omega_{tot}\lvert u\rvert$	$-1.09{\cdot}10^{-6}$	0.017	0.325	$\cos(\theta)\lvert\mu_x\rvert^2$	$1.36{\cdot}10^{-1}$	0.027	0.255	$\mu_z\sin(\theta)^3$	$-4.66{\cdot}10^{-1}$	0.024	0.263
R^2: 0.735				R^2: 0.739				R^2: 0.417			

Table 20 Global models for $F_{z_{a,T}}$

Global $F_{z_{a,T}}$ models												
Unducted Model				Ducted Model				Residual Model			
Regressor	$\hat{\Theta}$	$s(\hat{\Theta})/\lvert\hat{\Theta}\rvert$	RMSE	Regressor	$\hat{\Theta}$	$s(\hat{\Theta})/\lvert\hat{\Theta}\rvert$	RMSE	Regressor	$\hat{\Theta}$	$s(\hat{\Theta})/\lvert\hat{\Theta}\rvert$	RMSE
$bias$	4.92	0.003	-	$bias$	4.22	0.003	-				
$\mu_x^2+\mu_y^2$	$-2.52\cdot10^{-2}$	0.010	-	$\mu_x^2+\mu_y^2$	$-2.83\cdot10^{-2}$	0.015	-				
μ_z	$2.19\cdot10^{-2}$	0.091	0.499	μ_z	$-8.88\cdot10^{-1}$	0.009	0.538	$bias$	$1.03\cdot10^{-1}$	0.011	0.435
$\cos(\theta)\omega_{tot}$	$6.47\cdot10^{-5}$	0.004	0.443	$\sin(\theta)\lvert u\rvert^2$	$-3.02\cdot10^{-2}$	0.002	0.447	$uw\sin(\theta)^2$	$-8.24\cdot10^{-2}$	0.004	0.392
$\sin(\theta)\lvert\mu_x\rvert$	$-7.52\cdot10^{-1}$	0.003	0.402	$\cos(\theta)\omega_{tot}$	$3.68\cdot10^{-5}$	0.003	0.409	w^2	$-6.04\cdot10^{-3}$	0.021	0.378
ω_{tot}	$-1.43\cdot10^{-4}$	0.006	0.376	ω_{tot}	$-6.60\cdot10^{-5}$	0.005	0.399	$\sin(\theta)$	$2.92\cdot10^{-1}$	0.008	0.372
ω_{tot}^2	$1.14\cdot10^{-9}$	0.007	0.369	ω_{tot}^2	$3.25\cdot10^{-10}$	0.007	0.387	$\sin(\theta)^2$	$-5.78\cdot10^{-1}$	0.009	0.368
$\cos(\theta)\omega_{tot}^3$	$-4.59\cdot10^{-15}$	0.009	0.361	$\cos(\theta)\mu_z$	1.02	0.010	0.380	uw^3	$3.24\cdot10^{-4}$	0.011	0.363
R^2: 0.579				R^2: 0.581				R^2: 0.304			

Table 21 M_y **models for 0** ms^{-1}

M_y models 0 ms^{-1}											
Unducted Model				Ducted Model				Residual Model			
Regressor	$\hat{\Theta}$	$s(\hat{\Theta})/\lvert\hat{\Theta}\rvert$	RMSE	Regressor	$\hat{\Theta}$	$s(\hat{\Theta})/\lvert\hat{\Theta}\rvert$	RMSE	Regressor	$\hat{\Theta}$	$s(\hat{\Theta})/\lvert\hat{\Theta}\rvert$	RMSE
$bias$	$3.47{\cdot}10^{-3}$	0.008	-	$bias$	$8.23{\cdot}10^{-4}$	0.096	-				
q	$3.27{\cdot}10^{-4}$	0.054	-	q	$1.07{\cdot}10^{-3}$	0.018	-				
U_q	$6.13{\cdot}10^{-6}$	0.004	0.006	U_q	$7.64{\cdot}10^{-6}$	0.002	0.008	$bias$	$2.18{\cdot}10^{-4}$	0.112	0.007
$U_q\mu_z$	$-2.06{\cdot}10^{-6}$	0.021	0.005	u	$-3.07{\cdot}10^{-3}$	0.008	0.007	$\sin(\theta)^2 q$	$5.68{\cdot}10^{-3}$	0.013	0.007
u	$-5.98{\cdot}10^{-4}$	0.026	0.005	$U_q\mu_z^2$	$-1.59{\cdot}10^{-6}$	0.016	0.007	$U_q\mu_z$	$2.44{\cdot}10^{-6}$	0.011	0.007
$\omega_{tot}U_q^3$	$2.45{\cdot}10^{-18}$	0.024	0.005	qu^2	$-1.06{\cdot}10^{-4}$	0.019	0.007	$w\sin(\theta)$	$1.99{\cdot}10^{-3}$	0.017	0.007
μ_z	$-2.31{\cdot}10^{-3}$	0.030	0.005	ω_{tot}^2	$5.41{\cdot}10^{-13}$	0.025	0.007	$U_q w^2$	$-1.28{\cdot}10^{-7}$	0.020	0.006
U_q^3	$-1.28{\cdot}10^{-13}$	0.030	0.005	$U_q\mu_x^2$	$-5.99{\cdot}10^{-7}$	0.025	0.007	$\sin(\theta)q^2$	$-3.56{\cdot}10^{-4}$	0.026	0.006
R^2: 0.764				R^2: 0.802				R^2: 0.236			

Table 22 M_y **models for 5** ms^{-1}

M_y models 5 ms^{-1}											
Unducted Model				Ducted Model				Residual Model			
Regressor	$\hat{\Theta}$	$s(\hat{\Theta})/\lvert\hat{\Theta}\rvert$	RMSE	Regressor	$\hat{\Theta}$	$s(\hat{\Theta})/\lvert\hat{\Theta}\rvert$	RMSE	Regressor	$\hat{\Theta}$	$s(\hat{\Theta})/\lvert\hat{\Theta}\rvert$	RMSE
$bias$	$4.69{\cdot}10^{-3}$	0.042	-	$bias$	$9.55{\cdot}10^{-3}$	0.008	-				
q	$2.18{\cdot}10^{-4}$	0.062	-	q	$2.78{\cdot}10^{-4}$	0.064	-				
U_q	$4.03{\cdot}10^{-6}$	0.026	0.005	U_q	$2.92{\cdot}10^{-6}$	0.037	0.006	$bias$	$2.21{\cdot}10^{-3}$	0.024	0.006
$\cos(\theta)\mu_z^2$	$-5.60{\cdot}10^{-3}$	0.024	0.005	$U_q uw$	$-1.30{\cdot}10^{-7}$	0.011	0.005	$\sin(\theta)$	$1.01{\cdot}10^{-3}$	0.106	0.005
$\cos(\theta)U_q$	$5.73{\cdot}10^{-6}$	0.022	0.005	$\omega_{tot}u$	$1.51{\cdot}10^{-8}$	0.015	0.005	μ_z^3	$-1.22{\cdot}10^{-3}$	0.013	0.005
$U_q\mu_x$	$-1.42{\cdot}10^{-6}$	0.021	0.005	$\sin(\theta)\mu_x^2$	$2.94{\cdot}10^{-3}$	0.014	0.005	U_q	$-1.26{\cdot}10^{-6}$	0.013	0.005
$\sin(\theta)U_q$	$-1.06{\cdot}10^{-6}$	0.028	0.005	w^4	$-1.04{\cdot}10^{-5}$	0.021	0.005	$U_q\mu_z$	$-2.62{\cdot}10^{-6}$	0.014	0.005
$\cos(\theta)\omega_{tot}$	$1.05{\cdot}10^{-7}$	0.028	0.005	$\cos(\theta)U_q$	$4.17{\cdot}10^{-6}$	0.028	0.005	$U_q w^3$	$2.95{\cdot}10^{-8}$	0.022	0.005
R^2: 0.884				R^2: 0.802				R^2: 0.264			

Table 23 M_y **models for 8** ms^{-1}

M_y models 8 ms^{-1}											
Unducted Model				Ducted Model				Residual Model			
Regressor	$\hat{\Theta}$	$s(\hat{\Theta})/\lvert\hat{\Theta}\rvert$	RMSE	Regressor	$\hat{\Theta}$	$s(\hat{\Theta})/\lvert\hat{\Theta}\rvert$	RMSE	Regressor	$\hat{\Theta}$	$s(\hat{\Theta})/\lvert\hat{\Theta}\rvert$	RMSE
$bias$	$6.74{\cdot}10^{-3}$	0.020	-	$bias$	$1.89{\cdot}10^{-2}$	0.003	-				
q	$2.01{\cdot}10^{-4}$	0.060	-	q	$1.30{\cdot}10^{-4}$	0.115	-				
U_q	$6.89{\cdot}10^{-6}$	0.002	0.005	U_q	$7.58{\cdot}10^{-6}$	0.002	0.006	$bias$	$3.95{\cdot}10^{-3}$	0.012	0.005
$\sin(\theta)\mu_x$	$2.54{\cdot}10^{-3}$	0.023	0.005	$\omega_{tot}\mu_x\mu_z$	$6.53{\cdot}10^{-8}$	0.018	0.005	μ_z^4	$2.34{\cdot}10^{-4}$	0.009	0.005
$U_q\mu_z^2$	$-5.00{\cdot}10^{-7}$	0.028	0.005	$\cos(\theta)u^2w^2$	$1.00{\cdot}10^{-5}$	0.012	0.005	w	$3.33{\cdot}10^{-4}$	0.033	0.005
$\sin(\theta)\mu_x\mu_z^2$	$1.75{\cdot}10^{-3}$	0.027	0.005	$\sin(\theta)u^2w^2$	$7.52{\cdot}10^{-6}$	0.024	0.005	U_q^4	$-4.25{\cdot}10^{-18}$	0.015	0.005
$\sin(\theta)U_q$	$-1.31{\cdot}10^{-6}$	0.022	0.005	$\sin(\theta)\mu_x$	$4.42{\cdot}10^{-3}$	0.029	0.005	$U_q^3\sin(\theta)$	$-4.60{\cdot}10^{-14}$	0.020	0.005
$\cos(\theta)\omega_{tot}$	$7.51{\cdot}10^{-8}$	0.027	0.005	$\omega_{tot}\mu_z^4$	$-4.23{\cdot}10^{-9}$	0.038	0.005	U_q^2	$1.67{\cdot}10^{-10}$	0.024	0.004
R^2: 0.830				R^2: 0.828				R^2: 0.200			

Table 24 M_y **models for 10** ms^{-1}

M_y models 10 ms^{-1}											
Unducted Model				Ducted Model				Residual Model			
Regressor	$\hat{\Theta}$	$s(\hat{\Theta})/\lvert\hat{\Theta}\rvert$	RMSE	Regressor	$\hat{\Theta}$	$s(\hat{\Theta})/\lvert\hat{\Theta}\rvert$	RMSE	Regressor	$\hat{\Theta}$	$s(\hat{\Theta})/\lvert\hat{\Theta}\rvert$	RMSE
$bias$	$1.96{\cdot}10^{-2}$	0.005	-	$bias$	$2.60{\cdot}10^{-2}$	0.004	-				
q	$1.74{\cdot}10^{-4}$	0.077	-	q	$-4.96{\cdot}10^{-6}$	3.456	-				
U_q	$1.38{\cdot}10^{-6}$	0.072	0.006	U_q	$5.82{\cdot}10^{-6}$	0.010	0.006	$bias$	$8.83{\cdot}10^{-3}$	0.009	0.005
μ_z	$3.76{\cdot}10^{-3}$	0.014	0.005	$\sin(\theta)\mu_x$	$1.04{\cdot}10^{-2}$	0.010	0.005	$U_q\sin(\theta)^2$	$2.61{\cdot}10^{-6}$	0.013	0.005
μ_x	$-2.58{\cdot}10^{-3}$	0.014	0.005	$\sin(\theta)w^3$	$-1.50{\cdot}10^{-5}$	0.023	0.005	$\sin(\theta)^4$	$-8.95{\cdot}10^{-2}$	0.017	0.005
$\cos(\theta)U_q$	$6.00{\cdot}10^{-6}$	0.018	0.005	$\cos(\theta)uw^3$	$-3.28{\cdot}10^{-6}$	0.024	0.005	w^2	$1.50{\cdot}10^{-4}$	0.013	0.005
$\sin(\theta)u^2w^2$	$4.09{\cdot}10^{-6}$	0.022	0.005	U_qu	$2.72{\cdot}10^{-7}$	0.026	0.005	$\sin(\theta)$	$2.37{\cdot}10^{-2}$	0.015	0.005
U_qw^4	$3.20{\cdot}10^{-10}$	0.028	0.005	$\omega_{tot}\mu_z$	$6.31{\cdot}10^{-8}$	0.031	0.005	$\sin(\theta)^3$	$-8.03{\cdot}10^{-2}$	0.020	0.005
R^2: 0.846				R^2: 0.864				R^2: 0.194			

Table 25 Global models for M_y

Global M_y Models											
Unducted Model				Ducted Model				Residual Model			
Regressor	$\hat{\Theta}$	$s(\hat{\Theta})/\lvert\hat{\Theta}\rvert$	RMSE	Regressor	$\hat{\Theta}$	$s(\hat{\Theta})/\lvert\hat{\Theta}\rvert$	RMSE	Regressor	$\hat{\Theta}$	$s(\hat{\Theta})/\lvert\hat{\Theta}\rvert$	RMSE
$bias$	$5.33{\cdot}10^{-3}$	0.004	-	$bias$	$4.58{\cdot}10^{-3}$	0.005	-				
q	$3.98{\cdot}10^{-4}$	0.017	-	q	$8.43{\cdot}10^{-4}$	0.010	-				
U_q	$6.27{\cdot}10^{-6}$	0.002	0.006	U_q	$4.87{\cdot}10^{-6}$	0.002	0.007	$bias$	$-7.71{\cdot}10^{-4}$	0.024	0.006
$U_q\mu_z$	$-9.47{\cdot}10^{-7}$	0.009	0.006	$U_q\mu_z$	$-1.85{\cdot}10^{-6}$	0.005	0.007	U_q	$-1.62{\cdot}10^{-6}$	0.004	0.006
$\omega_{tot}u$	$9.56{\cdot}10^{-9}$	0.005	0.006	$\cos(\theta)u$	$9.89{\cdot}10^{-4}$	0.006	0.006	$\sin(\theta)q^2$	$-7.64{\cdot}10^{-4}$	0.009	0.006
$\sin(\theta)\mu_x^2$	$1.33{\cdot}10^{-3}$	0.010	0.005	$\omega_{tot}U_q^3$	$4.08{\cdot}10^{-19}$	0.009	0.006	U_qw	$-2.74{\cdot}10^{-7}$	0.007	0.006
$U_q\mu_z^2$	$-4.65{\cdot}10^{-7}$	0.013	0.005	$\sin(\theta)\omega_{tot}$	$-6.22{\cdot}10^{-8}$	0.009	0.006	$\sin(\theta)$	$-3.38{\cdot}10^{-3}$	0.010	0.006
$\cos(\theta)U_q^3$	$2.19{\cdot}10^{-14}$	0.013	0.005	$\sin(\theta)\mu_x^2$	$1.89{\cdot}10^{-3}$	0.010	0.006	$U_q\sin(\theta)q$	$-5.19{\cdot}10^{-7}$	0.014	0.006
R^2: 0.805				R^2: 0.758				R^2: 0.197			

Appendix B: Global quadrotor parameter covariance matrices

This appendix contains the parameter covariance matrices for the global model structures, which was selected to represent the quadrotor in general purposes

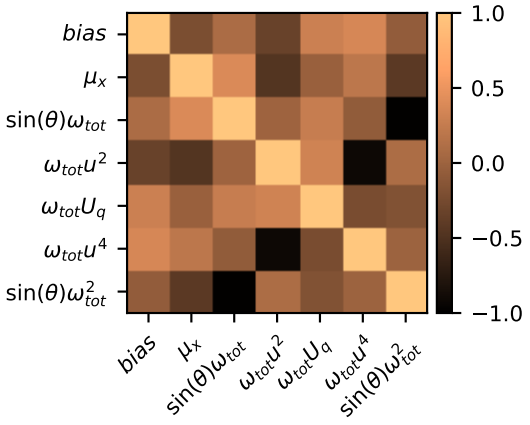

(a) Parameter covariance matrix of the ducted global model identified for F_x

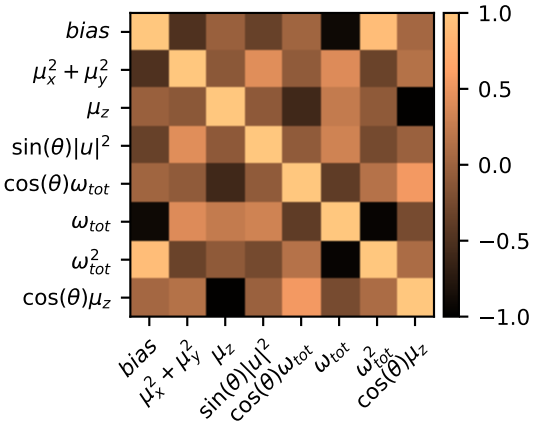

(b) Parameter covariance matrix of the ducted global model identified for $F_{z_{a,T}}$

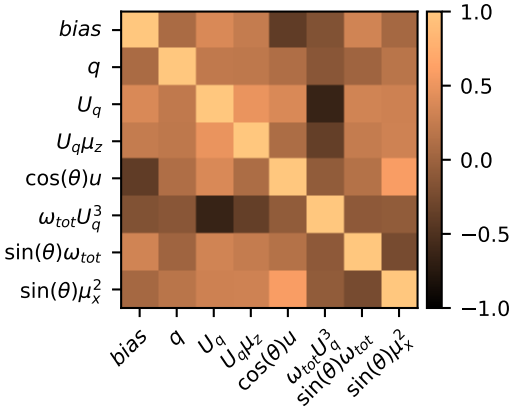

(c) Parameter covariance matrix of the ducted global model identified for M_y

Fig. 17 Parameter covariance matrices for the global ducted models

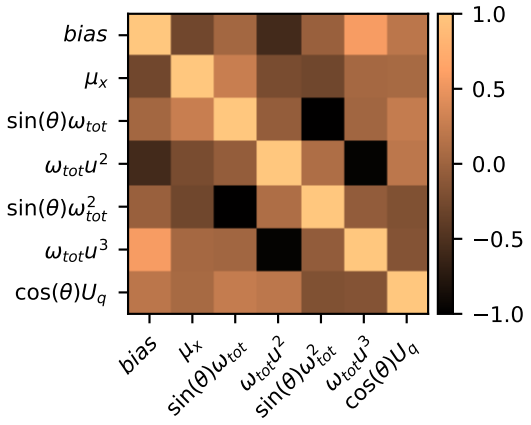

(a) Parameter covariance matrix of the unducted global model identified for F_x

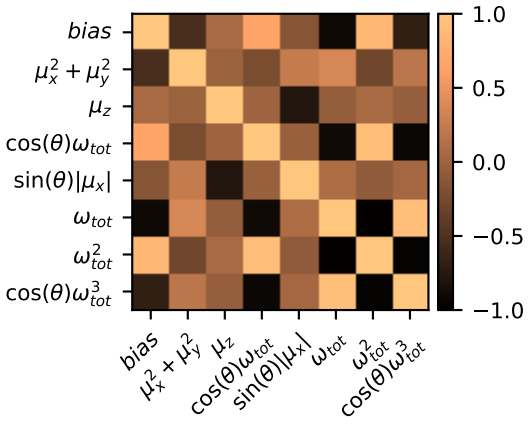

(b) Parameter covariance matrix of the unducted global model identified for $F_{z_{a,T}}$

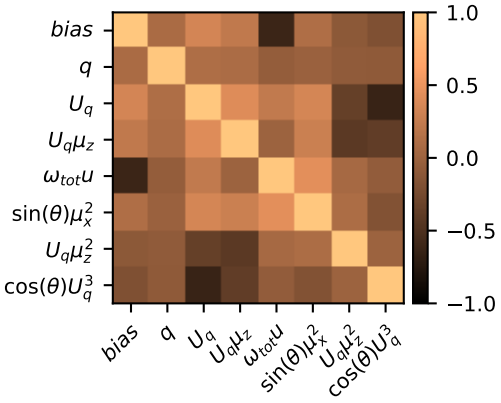

(c) Parameter covariance matrix of the unducted global model identified for M_y

Fig. 18 Parameter covariance matrices for the global unducted models

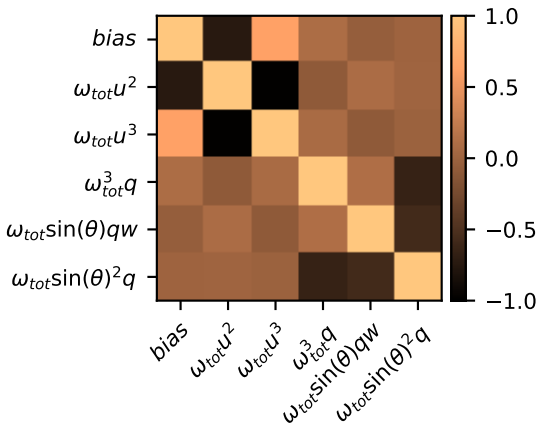

(a) Parameter covariance matrix of the residual global model identified for F_x

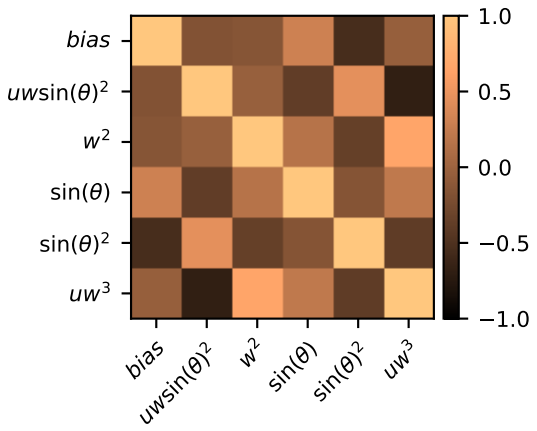

(b) Parameter covariance matrix of the residual global model identified for $F_{z_{a,T}}$

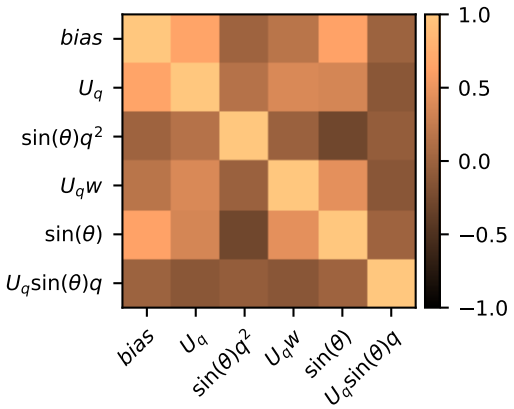

(c) Parameter covariance matrix of the residual global model identified for M_y

Fig. 19 Parameter covariance matrices for the global residual models

Appendix C: Candidate regressors

This appendix includes the candidate regressors for 1 selected regressor. The table indicates how small the differences in correlation are and that there is not a lot separating the choices between different correlations and therefore models

Table 26 Candidate regressors for the first selected regressor, for the F_x model at 5 ms^{-1}

Candidate regressors for F_x at 5 ms^{-1} at the first step	
Regressor	Correlation with ϵ
$\sin(\theta)\omega_{tot}$	0.881
w	0.846
$\omega_{tot}\mu_z$	0.845
$\sin(\theta)\mu_x$	0.836
μ_z	0.832
$\sin(\theta)\omega_{tot}^2$	0.811
$\cos(\theta)w$	0.811
$\omega_{tot}w$	0.803
$\sin(\theta)u$	0.796
$\cos(\theta)\mu_z$	0.790

Appendix D: F_x model responses to other airspeeds

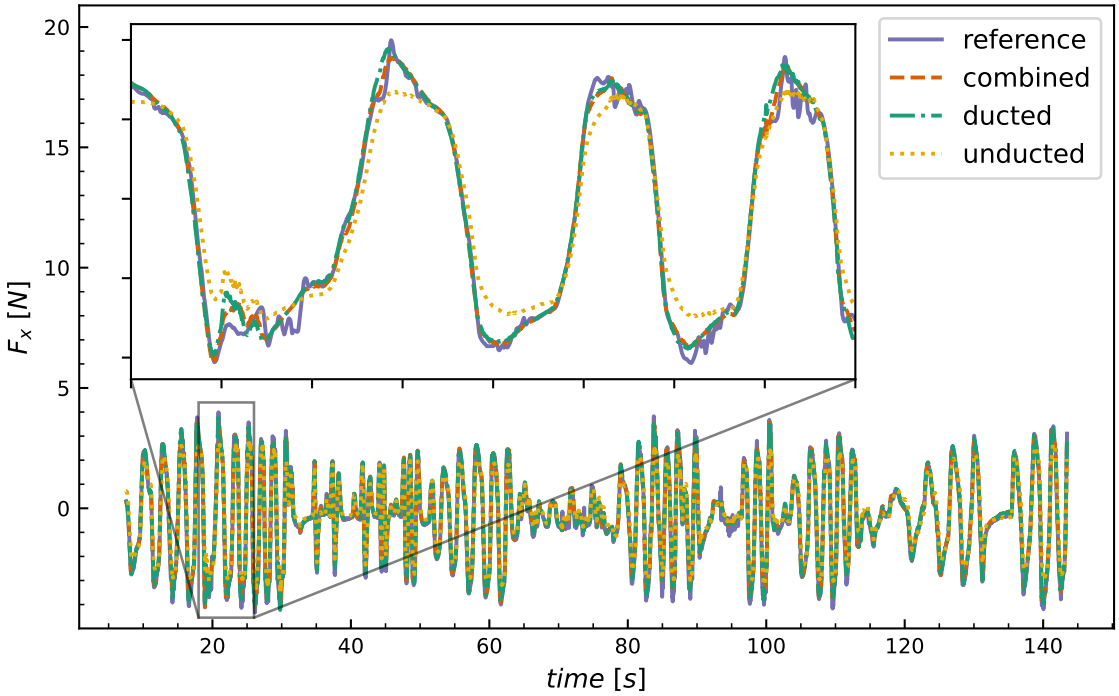

Fig. 20 Model predictions on ducted data of F_x at 0 ms^{-1}

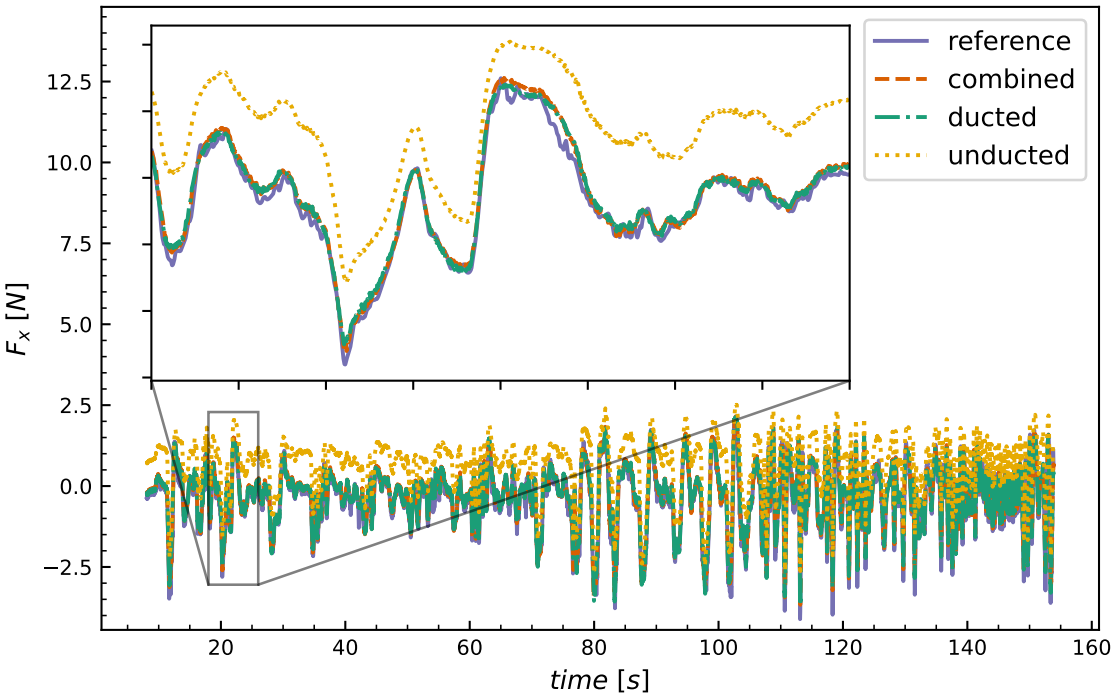

Fig. 21 **Model predictions on ducted data of F_x at 8 ms^{-1}**

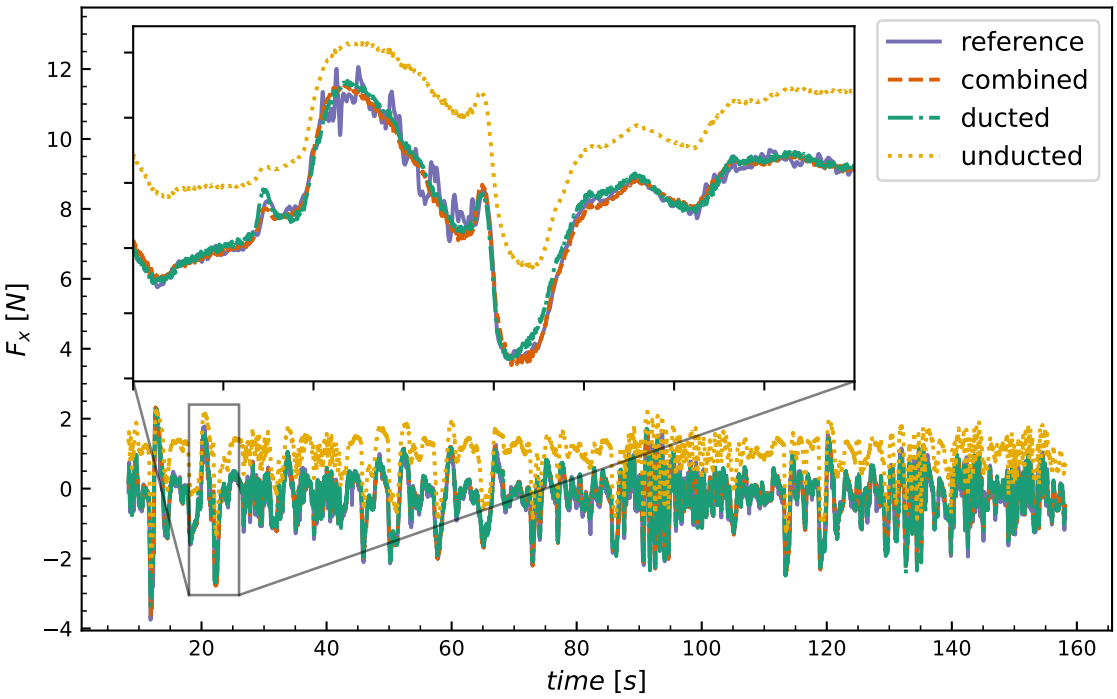

Fig. 22 **Model predictions on ducted data of F_x at 10 ms^{-1}**

Chapter III

Preliminary Report

1 Introduction

The concept of the quadrotor by itself already dates back to 1907 [1], however quadrotors only became popular with the development of smaller and lighter micro electro-mechanical systems (MEMS) [2]. Due to electrical motors becoming smaller and lighter, this allowed for the quadrotor as is now known to be developed. Quadrotors are popular due to their simple design in combination with their agility, and their ability to hover. Because of this quadrotors have a multitude of applications, mainly to do with observation of some sort.

Along with the growing amount of use cases comes the need for the quadrotors to perform more efficiently, and for them to be able to perform more specific and extreme manoeuvres [3]. In order to make more efficient controllers, and to gain more insight into the driving dynamics, a big area of research into quadrotors is the modeling of quadrotors. The basis of most models is the so called hover model [4]. This model is a linearised model which is linearised about the hover state of the quadrotor, and performs well for quadrotors in hover, or at small deviations from the hover state. However for high speed flight the model starts to deviate from reality due to it violating the assumptions made in the hover model, not being in or near hover state. Meaning that the linearisation about the hover state is not valid anymore, causing non-linear effects to become noticable. Therefore different types of models are researched, for control purposes often the so called black box models are used to be applied in for example model predictive control [5, 6]. The models that aim to give more insight into the dynamics of the quadrotor, are of either the gray box type, or white box. Where the white box models are often based on helicopter theory, which includes momentum analysis in combination with the blade element method [7]. Next to this also research is done using wind tunnel tests [8,9] and CFD simulations, in order to measure or visualise aerodynamic effects

This literature review will be structured as follows. First the dynamics of quadrotors are discussed. In this chapter the mathematical representation of quadrotor dynamics are discussed, along with some of the physical phenomena which dominate the dynamics of the quadrotor. After that the dynamics are discussed, the model identification techniques are reviewed, where the focus is put towards the gray box methods due to the ability of these methods to provide insight into what is driving the system dynamics. Then the following chapter discusses both the sensors used to collect data, and the state estimation algorithms used to filter and improve the collected data. Lastly a small summary of the findings in literature is presented, and from the gaps found here a research proposal is presented.

2 Quadrotor dynamics

In order to understand what is driving the motions of quadrotors and to find the effects different quadrotor configurations have on the performance of a quadrotor, it is important to understand the physics driving the dynamics of a quadrotor. Next to understanding what happens it is also important to be able to model these effects such that the effect of different configurations can be quantified, but also such that a prediction can be made of how new configurations will perform. This section will therefore discuss the modeling and aerodynamic effects of a quadrotor. To do so, first the necessary reference frames will be discussed and how to transform between these reference frames. Secondly, the rigid body dynamics are briefly discussed. Then the different ways to model the forces and moments acting on the quadrotor are discussed. Lastly some additional aerodynamic effects are discussed which are also known to be present, but do not have a clear way to model them.

2.1 Reference frames

For the dynamic representation of a quadcopter at least two reference frames are needed. The first one is an inertial reference frame, for this a North East Down (NED) reference frame is used which is fixed at a spot where the testing takes place. Figure III.1 shows two different reference frames, the NED frame, given by the subscript N, and the Earth centred reference frame, given by the subscript E. Technically these reference frames are not inertial reference frames as they are rotating, however especially for short flights this effect is negligible and the reference frames are therefore assumed to be inertial reference frames. The second reference frame is a body fixed reference frame. This reference frame has its origin in the centre of gravity of the drone, its x-axis is pointing in the flight direction (the direction the camera is pointing), the y-axis forms a 90 degree angle with the x axis, and together the axes form a plane parallel to the rotor disk planes. The z-axis is pointing the opposing the thrust completing the right handed reference frame. Figure III.2 also illustrates the way the body reference frame is oriented.

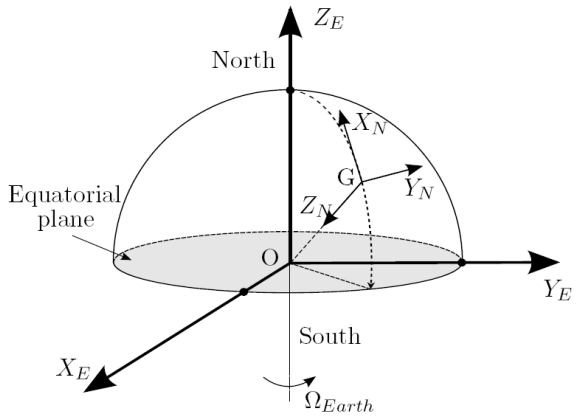

Figure III.1: The Earth reference frame and the North East Down reference frame [10]

2.2 Reference frame transformations

The transformation between these two coordinate frames is usually done in either one of two ways. The first option is to use rotation matrices based on Euler angles, the advantage of this method is that Euler angles give an intuitive insight in what is happening between transformations, with as downside that there are singularities in the transformation matrices at certain Euler angles. The second option is to use quaternions to do the transformation. The advantage of quaternions is that they prevent the singularities in the transformations, however, they do not give an intuitive picture of what is happening in the system.

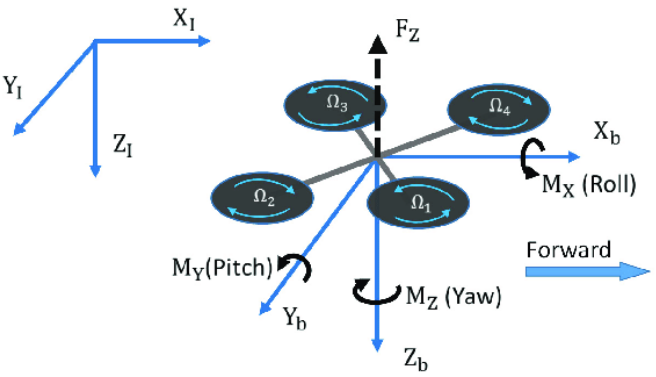

Figure III.2: Body reference frame on the quadrotor [11]

$$R_x(\phi) = \begin{bmatrix} 1 & 0 & 0 \\ 0 & c(\phi) & -s(\phi) \\ 0 & s(\phi) & c(\phi) \end{bmatrix} \tag{III.1}$$

$$R_y(\theta) = \begin{bmatrix} c(\theta) & 0 & s(\theta) \\ 0 & 1 & 0 \\ -s(\theta) & 0 & c(\theta) \end{bmatrix} \tag{III.2}$$

$$R_z(\psi) = \begin{bmatrix} c(\psi) & -s(\psi) & 0 \\ s(\psi) & c(\psi) & 0 \\ 0 & 0 & 1 \end{bmatrix} \tag{III.3}$$

$$R_{EB} = \begin{bmatrix} c(\theta)c(\psi) & c(\psi)s(\theta)s(\phi) - s(\psi)c(\phi) & s(\phi)s(\psi) + c(\phi)c(\psi)s(\theta) \\ s(\psi)c(\theta) & c(\psi)c(\phi) + s(\psi)s(\theta)s(\phi) & s(\psi)s(\theta)c(\phi) - c(\psi)s(\phi) \\ -s(\theta) & c(\theta)s(\phi) & c(\phi)c(\theta) \end{bmatrix} \tag{III.4}$$

In Equation III.1 until Equation III.3 the Euler transformation matrices for transformations about single axis are given, in these equations the $s(\cdot)$ stands for the sine of what is in between brackets, and $c(\cdot)$ stands for the cosine of what is in between the brackets. When applying the 3 transformations in order of transformations about the x, y, z axis then the final transformation matrix given in Equation III.4 is obtained. This is the transformation matrix which is used to transform a vector from the body reference frame to the inertial Earth reference frame [12]. When the transformation matrix from the Earth frame to the body frame is needed the order of transformations is simply reversed, or another option is to take the transpose of the R_{EB} matrix.

$$R_{BE} = R_{EB}^T = \begin{bmatrix} c(\theta)c(\psi) & c(\theta)s(\psi) & -s(\theta) \\ c(\psi)s(\theta)s(\phi) - s(\psi)c(\phi) & c(\psi)c(\phi) + s(\psi)s(\theta)s(\phi) & c(\theta)s(\phi) \\ s(\phi)s(\psi) + c(\phi)c(\psi)s(\theta) & s(\psi)s(\theta)c(\phi) - c(\psi)s(\phi) & c(\phi)c(\theta) \end{bmatrix} \tag{III.5}$$

2.3 Quadrotor rigid body dynamics

The general rigid body dynamics for a quadrotor can be described as in Equation III.6. In this equation $\boldsymbol{V} = \begin{bmatrix} u & v & w \end{bmatrix}^T$ is the vector containing the speeds of the quadrotor in the body reference frame, and $\boldsymbol{\Omega} = \begin{bmatrix} p & q & r \end{bmatrix}^T$ is the vector containing the rotational rates of the drone expressed in the body frame. Then there is m which equals the mass of the drone, and I_v which indicates the inertia matrix of the quadrotor. Lastly there are the F and M terms, which are the force and moment vector which are affecting the quadrotor and will be elaborated upon in the next sections.

$$m\dot{\boldsymbol{V}} + m(\boldsymbol{\Omega} \times \boldsymbol{V}) = \boldsymbol{F} \tag{III.6a}$$

$$I_v\dot{\boldsymbol{\Omega}} + \boldsymbol{\Omega} \times I_v\boldsymbol{\Omega} = \boldsymbol{M} \tag{III.6b}$$

2.4 Modelling Force

The force vector can be modelled in different ways, the simplest way is the form which is used in what is called the hover model, which works for hovering and low speed flight. In this model no drag is modelled in the horizontal plane of the quadrotor resulting in the force vector given in Equation III.7 [4]. It can be seen here that there are two parts to the force vector, first there is the gravity which is transformed from the Earth reference frame to the body frame, and secondly there is the force generated by the propellers of the quadrotors. Which is equal to the sum of the square of the angular speed of the propellers ω which is multiplied by the propeller coefficient κ_0. It should be noted that the thrust produced by the propeller is defined as negative due to the reference frame used.

$$\boldsymbol{F}_h = mR_{EB}\boldsymbol{g_E} + \begin{bmatrix} 0 \\ 0 \\ -\kappa_0 \sum \omega_i^2 \end{bmatrix} \tag{III.7}$$

The thrust generated by the propellers in Equation III.7 comes from the equation for the thrust coefficient C_T which is based on the thrust calculated using the momentum theory analysis for rotorcraft in hovering flight [13], which is given in Equation III.8. When rewriting this equation for T, and using the fact that the rotor parameters A and R, which are the rotor disk area and the rotor radius respectively, stay constant, and assuming the air density ρ stays constant during the flight, all constants can be bundled into one single constant, which is κ_0 in this case.

$$C_T = \frac{T}{\rho A \omega^2 R^2} \tag{III.8}$$

Equation III.7 holds for hover and low speeds due to the fact that there is almost no airflow tangential to the propellers, and due to the negligable inflow speed perpendicular into the propeller disk.. When the quadrotor deviates too much from its hover state both of these speeds cannot be neglected anymore and several aerodynamic phenomena start to occur which make Equation III.7 less and less viable to model the forces acting on the quadrotor. First of all, with increasing speed the friction of the air starts to increase and aerodynamic drag starts to play a bigger role in the force model. Secondly the air inflow into the propeller disk plays a big role in the thrust generated, and when the flight condition changes from hover to vertical climb and/or moving flight, air inflow speed V_∞ and an angle of attack α are introduced changing the the thrust generated by propellers. Lastly the force generated by the propellers is not as straightforward anymore due to effects like blade flapping, and interactions between the different propellers of the quadrotor [7, 13]. The following section discusses these effects.

Forward and Vertical Rotor Flight

The thrust generated by a rotor is depending on the incoming flow velocity entering the rotor disk. Meaning that the speed of the quadrotor, and therefore the speed at which the air enters the rotors matters for the calculation of the thrust generated by the quadrotor propellers. In literature two different methods are used to describe the thrust generated by a propeller in moving flight, momentum theory, and blade element theory. Using momentum theory the following equation for vertical flight can be obtained [13].

$$T = \dot{m}w = 2\rho A(V_\infty + \nu_i)\nu_i \tag{III.9}$$

Equation III.9 describes the thrust generated by a propeller in terms of the airspeed V_∞ the propeller is experiencing and the velocity induced by the propeller ν_i. Further in this equation $\dot{m}$ is the mass flow through the propeller, w is the air speed added by the effects of the propeller, ρ is the air density and A is the rotor disk area. The downside of Equation III.9 is that it does not use any of the propeller properties like its rotational speed. In order to solve for the thrust of the quadrotor [14] adds an equation which was derived using blade element theory. Equation III.10 is derived with the assumption that the propeller is a constant chord, linear twist propeller, which would give the propeller disk in the vertical flight case a uniform inflow which according to momentum theory makes for the smallest induced power loss [15].

$$T = \frac{\rho a b c \omega^2 R^3}{4}\left(\theta_{prop_{tip}} - \frac{V_\infty + \nu_i}{\omega R}\right) \tag{III.10}$$

Equation III.10 gives the thrust for vertical flight of a rotor, and was derived using blade element theory [15]. In this equation a, b, and c are the lift curve slope, number of blades and the blade chord respectively. $\theta_{prop_{tip}}$ is the propeller blade pitch angle at the tip of the propeller blade. In [14] the combination of Equation III.9 and Equation III.10 is then used to calculate ν_i in vertical flight, which is then used to calculate the thrust of the quadrotor in vertical flight.

Now for the forward flight case the situation changes a little, due to the forward speed of the quadrotor, the angle of attack of the air with respect to the rotor disks needs to be taken into account. Figure III.3 gives an example of the definitions for forward flight using a helicopter instead of a quadrotor, but the theory still applies of course. Again momentum theory and blade element theory can be applied to obtain definitions for the thrust for the forward flight case.

$$T = \dot{m}w = 2\rho A\nu_i\sqrt{(V_\infty \cos\alpha)^2 + (V_\infty \sin\alpha + \nu_i)^2} \tag{III.11}$$

Equation III.11 describes the thrust generated by a rotor in forward flight according to momentum theory. Here the α is the angle of attack of the rotor disk, as defined in Figure III.3. Again like in the vertical flight case, this does not relate the thrust generated directly to the parameters of the propeller such as the ω, however it can be used to obtain a definition for the induced velocity in forward flight [13] the relation is shown in Equation III.12. In this equation ν_h is the induced velocity for the hover case. The equation itself can be solved using a numerical recursive solver in order to find ν_i.

$$\nu_i = \frac{\nu_h^2}{\sqrt{(V_\infty \cos\alpha)^2 + (V_\infty \sin\alpha + \nu_i)^2}} \tag{III.12}$$

Again here the equation obtained from momentum theory does not contain any of the parameters of the rotors itself aside from the area of the rotor disk. Here again, by using blade element theory the thrust can be written using more parameters of the propellers of the quadrotor [14, 15].

$$T = \frac{\rho abc\omega^2 R^3}{2}\left(\frac{\theta_{prop}}{3} + \frac{V_\infty^2 \cos^2(\alpha)\theta_{prop}}{2\omega^2 R^2} + \frac{V_\infty \sin(\alpha) + \nu_i}{2\omega R}\right) \tag{III.13}$$

Equation III.13 is the thrust as obtained from the blade element method, here θ_prop is the pitch angle of the rotor blade. In [16, 17] Equation III.13 in combination with Equation III.12 is used in order to obtain the thrust generated by the quadrotor. In this equation it is assumed that the chord of the propeller blades are constant. It should be noted that Equation III.13 is derived for the thrust generated by a single propeller, and does not take into account the interactions between propellers. It also does not include the effects of the propeller airframe interactions. A solution for this can be by using stepwise regression to select extra model terms [16], which will be described in more detail in subsection 3.2.

Other forces acting on the quadrotor

In the above sections only the thrust force acting on the quadrotor was discussed. However there are of course two more axes on which forces can and do act. These forces are due to the forces exerted by the rotors [13, 15, 18], mainly due to blade flapping effects, and the other cause is the aerodynamic body drag [16, 17, 19].

For the forces generated by the rotors there are two ways of modelling this, there is the analytical way as presented in [3, 13, 15] which use BEM to calculate the forces generated by the rotors. The other way is to represent these forces using a polynomial model, and estimating the corresponding coefficients using system identification methods [17, 19]. The leading terms in the polynomial model are the rotor speeds ω_i and the velocity of the quadrotor $\boldsymbol{V}$.

The system identification method can also be applied to find the aerodynamic body drag. In [17] the body speeds of the quadrotor are used as model candidates for which coefficients are estimated. While in [19] a more classical approach was used with a force coefficient per axis which is then multiplied by $\frac{1}{2}\rho V^2$. In this case the force coefficients of the aerodynamic body drag could even be determined from windtunnel tests for example.

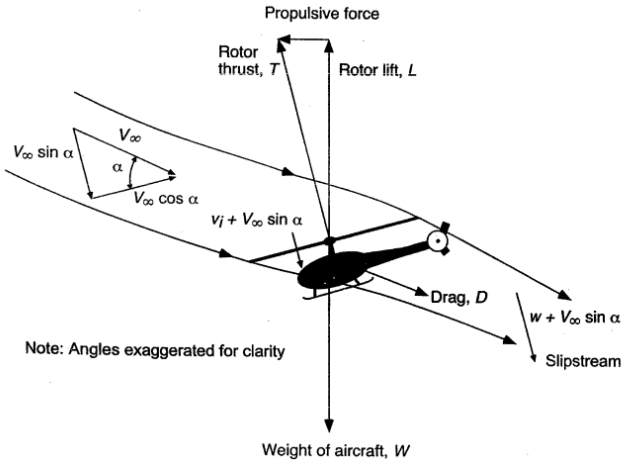

Figure III.3: The definitions of forward flight for a rotorcraft [13]

2.5 Modelling moments

The basics of the models for moments acting on quadrotors are based on the differences in thrust between the four rotors, by applying a higher thrust on the rear or front to rotors, a pitching moment is created. Applying a higher thrust on the left or right two propellers a rolling moment is created. The yawing moments are created by increasing the reactionary torque, meaning that diagonally opposing propellers are increasing their thrust and by the reactionary torques a yawing moment is generated. Equation III.14 shows the relations just described when applied to the quadrotor as depicted in Figure III.4. In this equation κ_0 is the thrust coefficient also applied in Equation III.7, τ_0 is a coefficient like κ_0 but then for the torque the rotors apply to the body, and b and l are the moment arms of the rotors to the centre of gravity, where it is assumed that the quadrotor is both symmetric about its x and y body axes. The downside of this model is that it assumes that the quadrotor is in hover state, meaning that the incoming airflow is stationary before being accelerated by the propellers of the quadrotor. However it is found that already at small values of translational speed this assumption does not hold anymore and the model becomes more and more inaccurate.

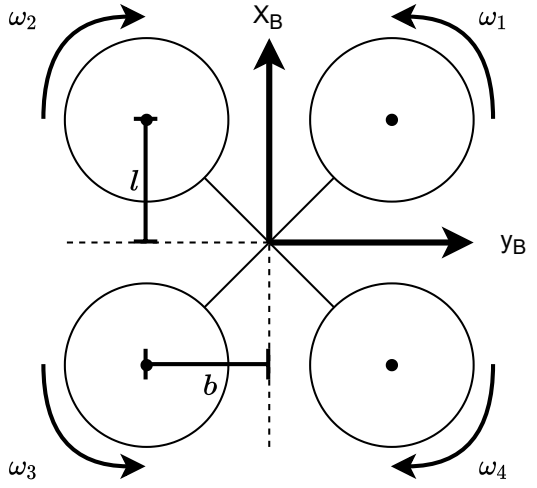

Figure III.4: Schematic top view of a quadrotor with definition for the rotor directions

$$\boldsymbol{M}_h = \begin{bmatrix} b\kappa_0(-\omega_1^2 + \omega_2^2 + \omega_3^2 - \omega_4^2) \\ l\kappa_0(\omega_1^2 + \omega_2^2 - \omega_3^2 - \omega_4^2) \\ \tau_0(\omega_1^2 - \omega_2^2 + \omega_3^2 - \omega_4^2) \end{bmatrix} \tag{III.14}$$

One way to make this model more complete is to include the rotor spin up dynamics as is done

in [20]. Here the Newton-Euler equation for rotational motion is also applied to the propellers resulting in Equation III.15.

$$\boldsymbol{I}_r\dot{\boldsymbol{\omega}} + \boldsymbol{\Omega} \times \boldsymbol{I}_r\boldsymbol{\omega} = \boldsymbol{M}_{r_i} \tag{III.15}$$

Then the assumption is made that due to the relatively light weight propellers and their small moment of inertia, compared to the entire vehicle, only terms with a high rotational velocity are relevant. Because the rotors spin around their z axis this means that $\omega_x \ll \omega_z$ and $\omega_y \ll \omega_z$. This assumption results in Equation III.16. It should be noted here that this assumption was made for a Parrot Bebop Quadrotor, which is of a different size class than for example a Tiny Whoop class drone, meaning that the ratios may differ for tiny quadrotors and make the assumption less relevant.

$$\boldsymbol{M}_{r_i} = \begin{bmatrix} I_{r_z} q\omega_z \\ -I_{r_z} p\omega_z \\ I_{r_z}\dot{\omega}_z \end{bmatrix} \tag{III.16}$$

Equation III.16 can then be extended to include all four rotors which results in Equation III.17. Finally it was found that the moments about the x and y axes had next to no influence on the model so one could reduce it even further down to include only the third row of the $\boldsymbol{M}_r$ vector [20].

$$\boldsymbol{M}_r = \begin{bmatrix} I_{r_z} q(-\omega_1 + \omega_2 - \omega_3 + \omega_4) \\ I_{r_z} p(\omega_1 - \omega_2 + \omega_3 - \omega_4) \\ I_{r_z}(-\dot{\omega}_1 + \dot{\omega}_2 - \dot{\omega}_3 + \dot{\omega}_4) \end{bmatrix} \tag{III.17}$$

Another way of modelling the moments can again be found by the use of BEM, as is done in [3]. The approach here calculates the forces and torques on each propeller and uses these to calculate the total forces and moments on each of the propellers. The advantage of this method is that it takes into account the forward flight effects acting on the quadrotor, however it still neglects the interactions between propellers and the airframe effects. Another downside of this method is that a lot more data about the propellers needs to be known to calculate the moments.

2.6 Aerodynamic effects

Here some other aerodynamic effects are discussed. Of these effects the blade flapping was already taken into account in the modelling of the forces by the BEM representation of the thrust, and in the suggested terms of the polynomial model for the other forces. The effects on the moments were not directly discussed. The propeller interactions are not included in the models given above, but definitely do play a role in the dynamics of quadrotors and thus should not be forgotten.

Blade Flapping

Blade flapping is what occurs when forward flight introduces a translational velocity at the propeller disk. This causes the advancing blade of the propeller to experience an increase in effective velocity meaning that the advancing blade generates extra lift. For the retreating blade the opposite holds, here the translational velocity of the rotorcraft reduces the effective velocity the blade experiences, meaning that the retreating blade produces less lift. As a result the rotor disk is angled, meaning that the thrust will be placed at an angle as well. Next to this the difference in lift also means that at there are some reactionary moments at the rotor hub. As a result of the rotor disk being placed at an angle due to the blade flapping, first of all the thrust generated is reduced because of the thrust vector tilting along with the rotor disk plane. For quadrotors the lateral forces generated by the blade flapping are cancelled as long as the yaw rate of the quadrotor is relatively low compared to the airspeed [21]. What does have an impact is the backwards tilt of the rotor plane which creates a force in the same direction of the incoming airflow. When the rotor hub is not at the same vertical height as the c.g. of the quadrotor this force also induces a moment on the quadrotor. Next to this due to the stiff blades which are often used in quadrotors also a moment is generated at the rotor hub [21].

Propeller interactions

Next to the effects due to an incoming airflow, there are also some aerodynamic effects which occur due to the interactions between the airflow coming off of the propellers. There are multiple studies which show that the rotors in proximity of each other have an effect on the airflow through and behind the rotors [8, 9, 22].

It is shown through the use of windtunnel experiments that the effects of other rotors being in the proximity of a rotor decreases the performance of that rotor. In [8] a couple of different windtunnel tests were done for two rotors operating behind each other, rotating in opposite directions, like adjacent propellers in a quadrotor would as well. The tests were done in a hovering condition for 1280 RPM and 2500 RPM, and with ducted and un-ducted rotors, the results of the tests are shown in Figure III.5 and Figure III.6. From these tests several conclusions could be drawn, first of all the SPIV tests showed that the 2500 RPM test cases show more dominant vortices, and with that also less interaction between the vortices generated by the two propellers. This becomes especially clear in the test cases with the un-ducted propellers. The more dominant vortices are explained by the higher Reynolds number of the 2500 RPM case. This difference is also visible in the figure of merit (FM) of the propellers, which indicates the efficiency of the propellers. The FM clearly increases with the increase of rotor speed. Interesting to see here is that for the ducted 1280 RPM rotor case the FM of the rotors is about the same as the FM of the un-ducted 2500 RPM rotors. Indicating that the efficiency of the propellers in hover goes up as propeller ducts are added.

The same test was also done for a forward flight scenario, with a speed of 3 m/s. Here only the 2500 RPM case was tested for the ducted and un-ducted propellers. For this test no FM values were reported, however the test did show the wake of the duct interacting with the vortices of the propellers causing the vortices of the propellers to break up almost immediately which can be seen in Figure III.8 as compared to the unducted case presented in Figure III.7. Showing that contrary to the hover case the duct does not necessarily aid in the efficiency of the forward flight of a quadrotor. Next to this it should be mentioned that for the forward flight test even at 2500 RPM clear interactions were seen between the vortices of the propellers, contrary to the hover case.

In [9] the effect of the distance between the rotors is investigated, here again the test is performed for two different Reynolds numbers, and in line with the previously described tests the FM of the rotors producing the high Reynolds number flow does not change too much with increasing distance between the rotors. For the lower Reynolds number case this decrease in FM is seen, for this lower Reynolds number the FM of the rotors seems to be lower when the distance between the centres of the rotors is less than 2.3 times the rotor radius. Again this loss in efficiency can be attributed to the interaction of the tip vortices of the two rotors.

Next to the interaction of the rotor tip vortices also the down and upwash of the propellers play a role in the dynamics of the quadrotor. In [7] a potential flow method is used to show the effects of the down and upwash of the lead propellers on the rear propellers of a quadrotor. One of the main effects of the downwash generated in forward flight is that the rear propellers of a quadrotor generate less thrust. This then results in a pitch up moment due to the difference in thrust between the lead and rear propellers. Next to this for angles of attack lower than 5°even the configuration of the rotational directions of the propellers matters where the so called bear-hug configuration generates a slightly bigger pitch up moment [7]

What makes these effects harder to model is that there is no analytical expression for these effects, which is why they are often approached by system identification methods like in [16, 17, 22].

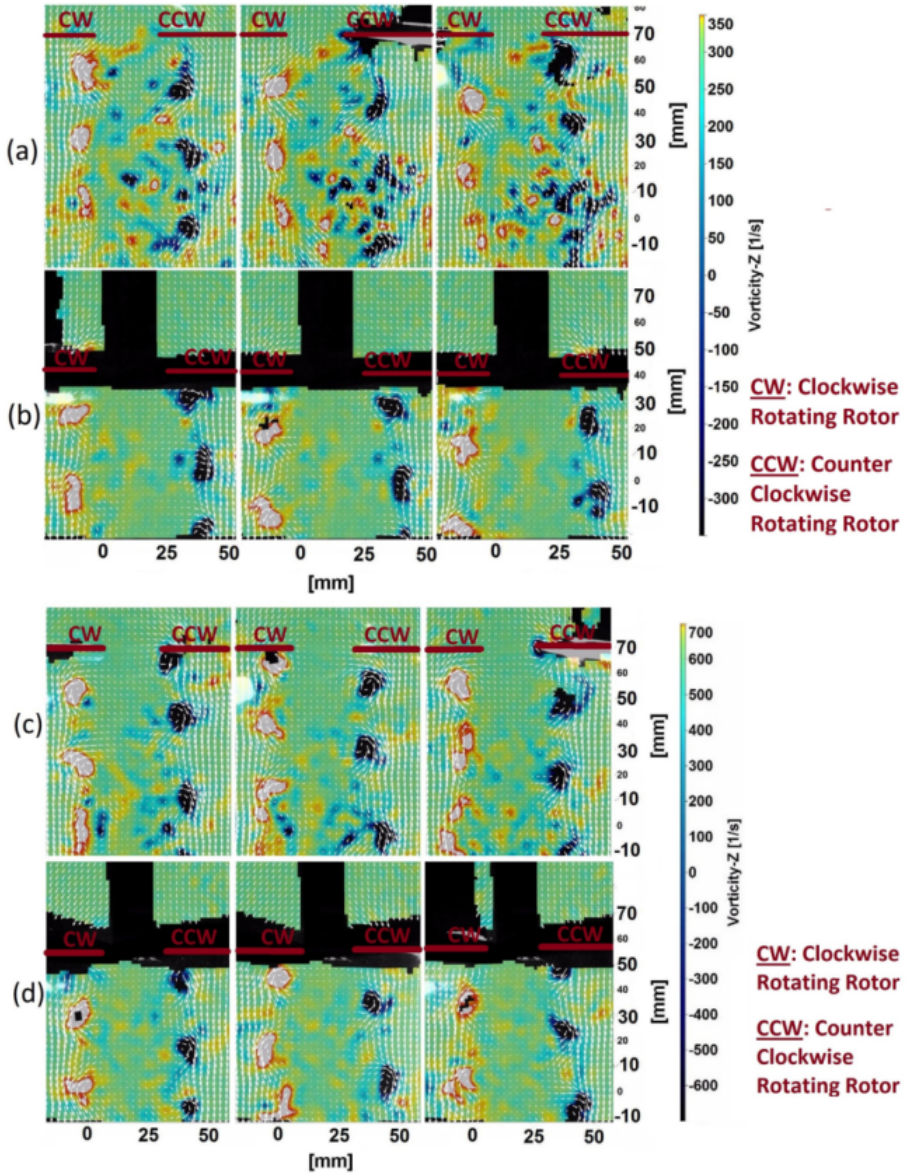

Figure III.5: Instant vorticity plots of: (a) 1208 RPM un-ducted propellers, (b) 1280 RPM ducted propellers, (c) 2500 RPM un-ducted propellers, and (d) 2500 RPM ducted propellers. Taken from Ref. 8.

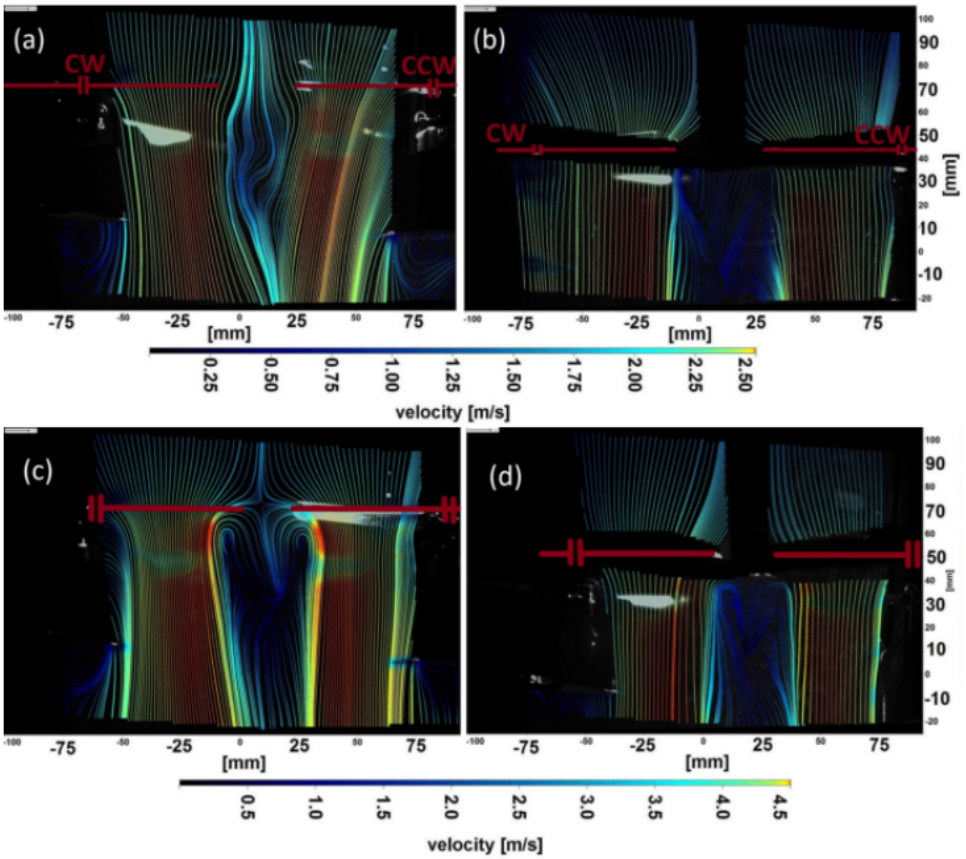

Figure III.6: Average streamline plots of: (a) 1208 RPM un-ducted propellers, (b) 1280 RPM ducted propellers, (c) 2500 RPM un-ducted propellers, and (d) 2500 RPM ducted propellers. Taken from Ref. 8.

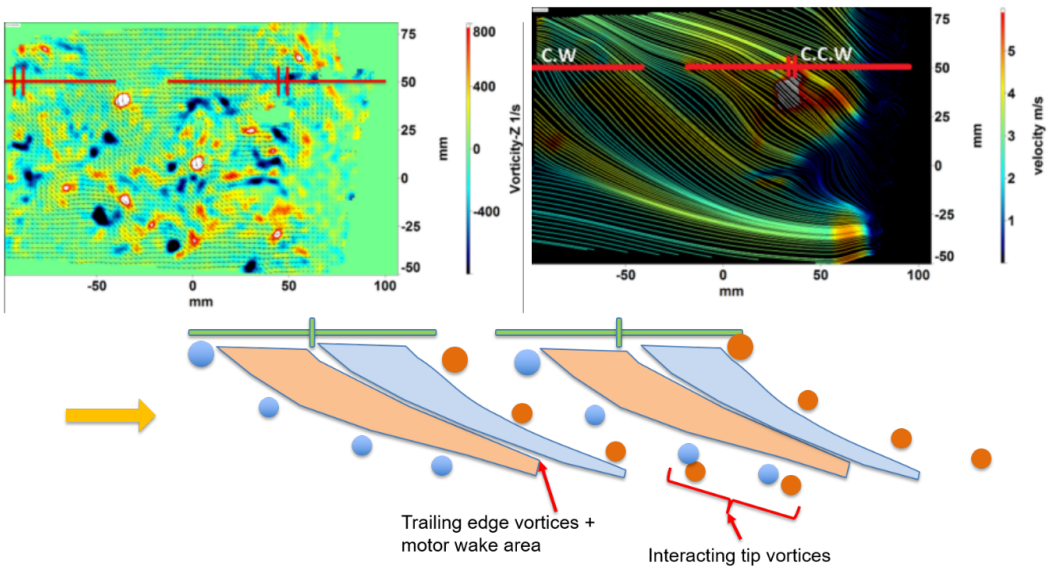

Figure III.7: Instant vorticity plot, average streamline plot, and illustration of the aerodynamics of two un-ducted propellers in forward flight [8].

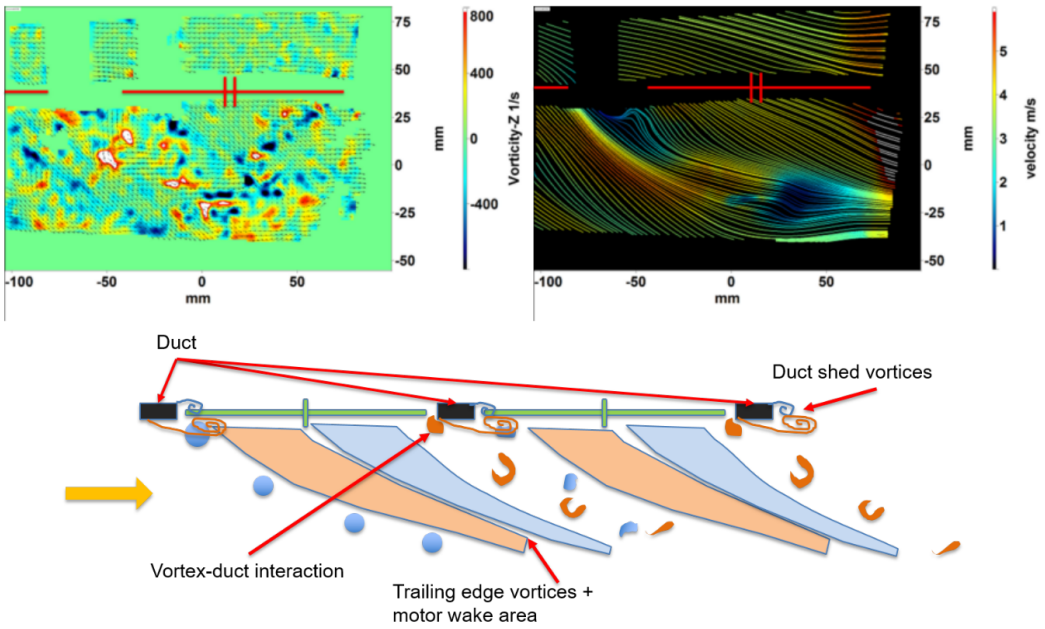

Figure III.8: Instant vorticity plot, average streamline plot, and illustration of the aerodynamics of two ducted propellers in forward flight [8].

3 Model Identification

In order to efficiently model the dynamics of quadrotors an accurate model is required. While the general dynamics of the quadrotor are quite straightforward to model, it is the force and moment terms which are harder to be modelled. In general there are three approaches to the model identification. The first one is the white box modelling approach, which derives the model directly from the known physical principles, this is also known as a first principles model. The other extreme is black box modelling which creates models which are completely based on the data put into the model, this is often done with the use of neural networks. The downside of these models is that they provide few to no insights into what is driving the dynamics of the system. The third approach to the model identification is the gray-box approach. This approach combines the white box and black box approach and by doing this provides a model based on the underlying physics using flight data. The advantage of this approach is that it does not require all the exact physical knowledge of the system but still provides an insight in what is driving the dynamics of the model.

Current research on model identification for quadrotors is being done in all three categories. For this research the important methods of model identification are the ones obtained from flight data. This means that this research will focus on the data driven model identification techniques. Current research on model identification from flight data can generally be put in three categories. There is the gray box models, which can be divided into the linearized models which are usually linearized about the hover state of the quadcopter model, and then use flight data to identify the corresponding parameters, and the non-linear models which are more elaborate models compared to the linearized models. The third category found in literature are the models made using a black-box modelling approach, which often seems to be quite efficient in modelling quadrotor dynamics. The problem of this method is that these models do not give an insight in what is actually driving the dynamics, which is an integral part in the goal of trying to get a better understanding of the high speed dynamics of quadrotors. For these reasons the main part of this chapter will be focused on model identification methods suited to identify non-linear models for quadrotors.

This chapter will first review data collinearity, after which stepwise regression algorithm for determining model structure, and finding the corresponding parameters is discussed. Followed by an explanation of the selection of regressor pools. After which a review of data collinearity is done. Lastly finding the inertia of the quadrotor is discussed.

3.1 Data Collinearity

Data collinearity is when a regressor is a linear combination of the other regressors in the data set [23]. This is a problem because this prevents the estimation method from assigning specific values to the parameters because there are infinite combinations which provide the best fit. An example of high data collinearity in real life is between the rate of change of the angle of attack and the pitch rate. It is therefore important to identify potential data collinearity to improve the parameter estimates. Various ways of detecting data collinearity are described in [23], such as examination of the regressor correlation matrix, eigensystem analysis and singular value decomposition (SVD), and parameter variance decomposition. In order to prevent data collinearity from influencing the parameter estimation several approaches can be taken. The first one is to adjust the experiment done to gather the data, and alter it in such a way that the different regressors are excited separately from each other. For the stepwise regression Equation III.30 is applied, where the effect of the regressor minus the terms already in the model is checked. By doing this when two regressors are highly correlated, only one is included due to its effect on the model. Another option is to create a set of orthogonal multivariate regressors, which is discussed below.

Orthogonal Regressors

or a set of orthogonal regressors the following property holds:

$$\boldsymbol{p}_i^T \boldsymbol{p}_j = 0 \qquad i \neq j, \quad i, j = 1, 2, \ldots, n \tag{III.18}$$

A set of ordinary regressors can be transformed into an orthogonal set of regressors using Gram-Schmidt orthogonalisation [23]. The process takes one regressor vector as a start and uses this to

create an orthogonal basis of regressors. Where it is common to take the bias regressor as the first orthogonal regressor.

$$\boldsymbol{p}_1 = \boldsymbol{\xi}_1 = \mathbf{1} \tag{III.19}$$

Then using this first vector in the orthogonal basis the Gram-Schmidt orthogonalisation can be applied as described in Equation III.20. Here $\boldsymbol{p}_j$ is the j$^{\text{th}}$ vector in the orthogonal basis, $\boldsymbol{\xi}_j$ is the j$^{\text{th}}$ vector in the original regressor basis, and γ_{kj} is the Gram-Schmidt coefficient.

$$\boldsymbol{p}_j = \boldsymbol{\xi}_j - \sum_{k=1}^{j-1} \gamma_{kj} \boldsymbol{p}_k \qquad j = 2, 3, \ldots, n \tag{III.20}$$

$$\gamma_{kj} = \frac{\boldsymbol{p}_k^T \boldsymbol{\xi}_j}{\boldsymbol{p}_k^T \boldsymbol{p}_k} \tag{III.21}$$

The relation between the orthogonal regressor basis P and the original regressor basis X can also be described using the following equation:

$$X = PG \tag{III.22}$$

$$G = \begin{bmatrix} 1 & \gamma_{12} & \gamma_{13} & \cdots & \gamma_{1n} \\ 0 & 1 & \gamma_{23} & \cdots & \gamma_{2n} \\ 0 & 0 & 1 & \cdots & \gamma_{3n} \\ \vdots & \vdots & \vdots & \ddots & \vdots \\ 0 & 0 & 0 & \cdots & 1 \end{bmatrix} \tag{III.23}$$

Due to the orthogonal basis the ordinary least squares is simplified to where the parameters $\hat{a}_j$ of the model made out of the orthogonal regressors, can be estimated separate from the other parameters. As is shown in Equation III.24.

$$\hat{a}_j = \frac{\boldsymbol{p}_j^T \boldsymbol{y}}{\boldsymbol{p}_j^T \boldsymbol{p}_j} \tag{III.24}$$

This separation from the other regressors also goes for calculation the reduction of the cost function, which only depends on $\boldsymbol{p}_j$ and $\boldsymbol{y}$ as is shown in Equation III.25.

$$J(\hat{\boldsymbol{a}}) = \frac{1}{2} \left[\boldsymbol{y}^T \boldsymbol{y} - \sum_{j=1}^{n} \frac{(\boldsymbol{p}_j^T \boldsymbol{y})^2}{\boldsymbol{p}_j^T \boldsymbol{p}_j} \right] \tag{III.25}$$

Due to the ability to calculate the reduction in the cost function separately orthogonal data sets and orthogonal least squares are also good candidates for stepwise regression algorithms [24]. The resulting parameters from the parameter estimation can be converted back to the parameters $\hat{\boldsymbol{\theta}}$ for the original regression by the following relation.

$$\hat{\boldsymbol{\theta}} = G^{-1} \hat{\boldsymbol{a}} \tag{III.26}$$

3.2 Stepwise Regression Algorithm

One way of modeling is presented in Ref. 16. In this paper a method is applied which not only identifies the parameters for the model, but it also constructs the model from a set of selected regressors. The way the model selects the regressors is that it finds the regressor term from the pool of regressors which reduces the error of the model the most. The algorithm described in Ref. 16, 23 chooses the regressor from a pool of candidate regressors not necessarily orthogonal to each other. It should be noted here that when the candidate regressor pool is not a set of orthogonal regressors, the order of the selected regressors matters.

General stepwise regression algorithms work on orthogonal data sets and generally only make use of a forward or backward selection step Ref. 24, this is due to the fact that per definition orthogonal regressors have no influence on eachother meaning that there is no need to take out regressors after they've been added or the other way around.

Orthogonolizing a dataset according to Gram-Schmidt as described in 3.1 however does also depend on the order in which the data set is orthogonalised meaning that unless an orthogonal dataset can be created this issue will always persist.

The model as described in Ref. 16, 23 is initiated in its simplest form possible, where the regressor matrix only contains a constant term. This is the initialisation step where the initial error is calculated which is used as base line.

$$\boldsymbol{y} = A\boldsymbol{\theta_0} + \epsilon, \quad A = \begin{bmatrix} 1 \\ \vdots \\ 1 \end{bmatrix} \tag{III.27}$$

After this the iteration starts, first the parameters for the current model are estimated according to Equation III.28.

$$\hat{\boldsymbol{\theta}} = (A^T A)^{-1} A^T \boldsymbol{y} \tag{III.28}$$

This estimation of the parameters can then be used to calculate the residual vector of the current model according to Equation III.29.

$$\boldsymbol{\epsilon} = \boldsymbol{y} - A\boldsymbol{\theta} \tag{III.29}$$

The next step is to calculate the rest value of each regressor which is left in the regressor pool. The rest value is described in Equation III.30. In this equation λ_i is the rest value, ξ_i is the i$^{\text{th}}$ regressor taken from the pool and A is the old regressor matrix from the previous step, or in case of the first iteration the regressor matrix A described in the initialisation step.

$$\boldsymbol{\lambda}_i = \boldsymbol{\xi}_i - A\hat{\boldsymbol{\theta}} \tag{III.30}$$

The regressor which is then to be added is selected by checking which λ_i has the highest correlation with the error calculated in the previous step. If j is taken as the selected regressor this can be expressed as in Equation III.31

$$j = argmax_i(corr(\lambda_i, \epsilon)) \tag{III.31}$$

The next step is to create the new regressor matrix by adding the newly found regressor, which is shown in Equation III.32, where the subscript k and k+1 indicate the steps taken. Then for the updated regressor matrix the corresponding parameter vector $\hat{\boldsymbol{\theta}}$ is calculated according to Equation III.28.

$$A_{k+1} = \begin{bmatrix} A_k & \xi_j \end{bmatrix} \tag{III.32}$$

This ends what is called the forwards selection part of the algorithm. Which is the part which selects the terms to include. To make sure that the generality of the model is kept and thereby prevent the model from overfitting the data such that it also starts modeling the noise present in the data the following step is added. Next the backwards elimination starts which checks the regressors currently present in the regressor matrix.

The first step in the backwards elimination process is to calculate the F-ratio of each regressor in the current regressor matrix. This is done according to Equation III.33. In this equation SS_R is the regression sum of squares as calculated in Equation III.34, $\hat{\theta}_p$ indicates that the regression sum of squares is taken from the full model, and $\hat{\theta}_{p-i}$ indicates the model with the i$^{\text{th}}$ regressor removed. s^2 is the variance of the residuals corresponding to the estimation of $\hat{\theta}_p$ and is calculated according to Equation III.35.

$$F_{0,i} = \frac{SS_R(\hat{\theta}_p) - SS_R(\hat{\theta}_{p-i})}{s^2} \tag{III.33}$$

$$SS_R = \hat{\theta}^T A^T y - N\bar{y} \tag{III.34}$$

$$s^2 = \frac{\epsilon^T \epsilon}{N - p - 1} \tag{III.35}$$

In the above equations N is the amount of datapoints, and $\bar{y}$ is the mean of all the measurements. After calculating the F-ratio for all regressors currently in the model the minimum F-ratio is selected and tested against the predetermined F_{out}. Which in this case is set to be 4. When the regressor with the minimal F-ratio is smaller than F_{out} that regressor is removed from the current regressor matrix. After this step the process can be carried out again from the beginning of the forward selection part of the algorithm. To exit the loop there are some exit conditions. The first one is the predict square error (PSE). The PSE consists out of two parts, one part which is made up of the errors from the estimated model, and one term which punishes model redundancy. The calculation of the PSE is described in Equation III.36.

$$PSE = \frac{1}{N}\epsilon^T\epsilon + \sigma^2_{max}\frac{P}{N} \tag{III.36}$$

$$\sigma^2_{max} = \frac{1}{N}\sum_{i=1}^{N}[y(i) - \bar{y}]^2 \tag{III.37}$$

The PSE can exit the algorithm in one of two ways, either when the calculated PSE is bigger then the PSE calculated in the last step, or when the PSE is lower than a certain tolerance set at the beginning of the algorithm. The last way the algorithm can exit is when the algorithm has reached a certain amount of iterations set at the beginning of the algorithm.

The stepwise regression algorithm is not the only one out there [24] lists some other methods for stepwise regression as well, however the model described above as taken from [16, 17] was the only version which was applied to a quadrotor system in recent literature. Other algorithms which could be applied are for example the SINDyc algorithm [25]. This algorithm is however made for low data and aims at sparsity of the model, which is not necessarily the aim of this model identification experiment.

3.3 Choosing a regressor pool

The previously described stepwise regression algorithm still needs a suitable pool of regressors. Preferably a pool which is limited in some way in order to reduce the computational effort of the stepwise regression algorithm. Often a set of polynomials is chosen for the regressor pool. In [17] theoretical knowledge on the thrust production of rotors in combination with the knowledge of drag terms present is used to formulate the polynomial regressor pool. To create a polynomial regressor pool it is important to define two things, the order of the polynomial and the variables which should be included. Following the notation from [17] a set of polynomial regressor candidates can be written as follows $P^2(x_1, x_2)$. Here the 2 denotes the degree of the polynomial, and x_1 and x_2 are the variables for the polynomial. The resulting set is also shown in Equation III.38

$$P^2(x_1, x_2) = \{x_1, x_2, x_1^2, x_2^2, x_1x_2\} \tag{III.38}$$

The set following from $P^d(\boldsymbol{x})$ does not include a bias term, it is assumed that this term is already included in the regressor pool. Using this representation the amount of resulting regressors can be calculated using Equation III.39 [26].

$$N = \frac{(n+d)!}{n!d!} - 1 \tag{III.39}$$

By using these models and parameterising the equations obtained from theory a polynomial representation can be created. Using Equation III.13 and lumping all terms related to the propeller properties into separate parameters the equation can be simplified into Equation III.40.

$$T = \sum T_i = \kappa_1 \sum \omega_i^2 + \kappa_2(u^2 + v^2) + \kappa_3(w + v_i)\sum \omega_i \tag{III.40}$$

Then the thrust needed for hover is subtracted from this model resulting in the thrust variance effect T_a.

$$T_a = T - T_h = \kappa_2(u^2 + v^2) + \kappa_3(w + v_a)\sum \omega_i \tag{III.41}$$

This thrust variance effect is then combined with the aerodynamic drag D_z. Then the terms related to the airspeed of the quadrotor, and the D_z term are replaced by 3rd order polynomial expansions as follows [17].

$$F_{a,z} = P_1^3(u, |v|, w) + P_2^3(u, |v|, w) \sum \omega_1 \tag{III.42}$$

The representation as given in Equation III.42 can then be used with a stepwise regression algorithm in order to see which terms of the polynomials should be included.

3.4 Finding the inertia of the Quadrotor

In order to accurately estimate the paremeters of the quadrotor model it is important to have accurate values of the properties of the quadrotor, meaning the mass and inertia of the quadrotor. The mass of the quadrotor can simply be measured using a scale. However the inertia of the quadrotor is not as straightforward.

In literature several methods have already been presented, including measuring the Inertia by applying torques to the different body axis [27], augmenting the state vector of a linear model and using a Kalman Filter, an Unscented Kalman Filter [28], or by calculating it through geometric approximations of the shapes of the quadrotor [27]. If the tools are available for the experimental testing [27] proved that this method works, however the same research also showed that the geometrical approach delivers about the same results. The downside of the experimental method presented in [27], is that an expensive setup is needed for the determination of the moment of inertia. The setup consists of a two axis motion simulator and a force and torque sensor. The motion simulator is connected to the torque and force sensor, which in turn is connected to the quadrotor, such that the z-axis of the quadrotor is aligned with the centre of the motion simulator. The motion simulator is then used to excite the rotations about the principal axes of the quadrotor, the torque and force sensor then measures the torques and forces applied to the quadrotor. With the angular rates of the motion simulator known and using the force sensor to account for the misallignment of the centre of gravity of the quadrotor the moments of inertia of the quadrotor can be calculated. However as mentioned before this setup is quite expensive, and takes time to setup and use, which may not be worth it when a theoretical approach using geometrical shapes representing the quadrotor can also be used.

Another method of experimentally determining the moment of inertia of the quadrotor is by using a bifilar [29] or trifilar pendulum [30]. Especially the bifilar pendulum is a easy to make test setup due to the fact that the quadrotor which is suspended from the pendulum can also be used to measure the rotational rates using the on board gyroscope.

4 State Estimation

In order to estimate a model of the quadrotor it is important to get a good estimation of the states of the quadrotor. For this the sensors gathering the data and the filtering of this data needs to be discussed. First the typical sensors used to gather data are discussed, and after that filters used to so the state estimation are discussed.

4.1 Sensors

The sensors to measure the states of the quadrotor can be divided into two different sections, the sensors on board of the quadrotor itself usually an IMU consisting out of an accelerometer and a gyroscope. The IMUs on board of quadrotors are MEMS. The other sensors are systems which are used to measure the states of the quadrotors which are not onboard, such as the optitrack system. The systems which are not carried on board of the quadrotor usually have the ability to be much more precise than the onboard equipment, with as downside of course that the system should be present in the room where the quadrotor flies.

Accelerometer

Accelerometers are used in quadrotors to measure the specific acceleration in the body frame of the quadrotor. The specific acceleration means that the acceleration due to gravity is subtracted from the total acceleration of the quadrotor [31]. In Equation III.43 the measurement of the specific acceleration is shown, in this equation $\boldsymbol{F}$ represents the sum of all external forces acting on the quadrotor, as specified in the earth reference system, m is the mass of the quadrotor, $\boldsymbol{g}$ is the gravity vector expressed in the earth reference system, and $\boldsymbol{a}_s^b$ is the specific acceleration in the body frame.

$$\boldsymbol{a}_s^B = \frac{1}{m} R_{BE}(\boldsymbol{F} - m\boldsymbol{g}) \tag{III.43}$$

The downside of the MEMS IMU is that as with all sensors noise is present in the measurements [32,33]. The measured acceleration by the accelerometer is therefore represented by Equation III.44.

$$\boldsymbol{a}_m^B = \boldsymbol{a}_s^B + \boldsymbol{\epsilon}_a + \boldsymbol{\delta}_a \tag{III.44}$$

Here $\boldsymbol{a}_m^B$ is the measured acceleration in the body fixed frame, $\boldsymbol{\epsilon}_a$ is the noise measured by the accelerometer which is assumed to be Gaussian white noise with no cross correlation between the accelerometer axis. $\boldsymbol{\delta}_a$ is the bias of the accelerometer.

Rate Gyroscope

The rate gyroscope, or just gyroscope, measures the rotation of the quadrotor in the body frame with respect to the inertial frame, or Earth frame [34]. Known problems with gyroscopes are the the drift of the gyroscope over the flight duration, and again like in the accelerometer the noise on the measurements [34, 35]. The rotational rates as measured by the gyroscope can then be modelled by Equation III.45

$$\boldsymbol{\Omega}_m^B = \boldsymbol{\Omega}^B + \boldsymbol{\epsilon}_\Omega + \boldsymbol{\delta}_\Omega \tag{III.45}$$

Here $\boldsymbol{\Omega}^B$ is the quadrotor rotational rate in the body frame with respect to the earth frame, and the subscript m indicates the measured rotational rate by the gyroscope. ϵ_Ω is the measurement noise of the gyroscope, which is assumed to be Gaussian white noise, with no cross correlation between the axes of the gyroscope.

Magnetometer

The magnetometer is a sensor which is used to measure the magnetic field of the Earth. This data is then predominantly used to determine the heading angle of the quadrotor [36]. It should be noted that unlike the accelerometer and the rate gyroscope magnetometers are not always included in small quadrotors of the tinywhoop size, the F4 flightcomputer included in the emax tinyhawk for example does not have one. The magnetic field of the Earth depends on the location of where

the test takes place, however for small testing areas the magnetic field of the earth can be taken as constant, there can however be disturbances from the environment. Often because of these disturbances it is important to calibrate the magnetometer before testing [34]. The measurement of the magnetometer can then be written as follows.

$$\boldsymbol{B}_m^B = R_{BE}\boldsymbol{B} + \boldsymbol{\epsilon}_B + \boldsymbol{\delta}_B \tag{III.46}$$

Here $\boldsymbol{B}$ is the magnetic field, R_{BE} is the rotation matrix from the inertial frame to the body frame of the quadrotor, $\boldsymbol{\epsilon}_B$ is the sensor noise measured, which is assumed to be Gaussian white noise, with no cross correlation between the axis, and $\boldsymbol{\delta}_B$ is the bias of the magnetometer.

Motion Caption Systems

Motion caption systems are external systems which as the name suggests caption the motion of objects. At the TU-Delft in the Cyberzoo an Optitrack motion caption system is installed. This system can precisely measure the position and attitude of an object using an array of infra red cameras. The cameras measure the reflections of the infra red signals send out by the LED's of the cameras which are reflected by reflective markers on the vehicles. This data is then used to calculate the position of the vehicle within the volume encompassed by the camera setup, and at the same time also the orientation of the vehicle is calculated. This data can then in turn also be used to calculate the other states of the quadrotor. The advantage of the Optitrack system is that it delivers very precise data, with as downside that the testing space is limited to the cyberzoo. Meaning that reaching high speeds for gathering data is harder to do, or even impossible.

Other Onboard Sensors

The accelerometer, gyroscope and the magnetometer mentioned above, are the onboard sensors most commonly used to gather data and estimate the states. However some other onboard sensors are also used in the data gathering and state estimation process. The first one to be discussed is the camera, which is already included in most commercial quadrotors. The camera can be used to obtain the position of the quadrotor using a SLAM algorithm for example, or to obtain the speed of the quadrotor using optical flow [36, 37]. Other sensors contain GPS sensors to aid in position measurements, mass-flow sensors [36] to determine velocities, barometers to determine altitude, and there are more others.

4.2 State Estimation methods

As already shown in the previous subsection the measurements from the onboard sensors of the quadrotor contain noise and biases. When this data is then used to calculate the states as is done in inertial navigation systems, these errors due to the noise and bias in the data get integrated and the error in the attitude and velocity grow over time [32]. In order to reduce the noise present in these measurements and obtain better estimates of the states, some state estimation methods will be discussed. First the extended Kalman filter (EKF) will be discussed which is an adapted version of the Kalman Filter suited for non-linear problems [38], after that the Mahony Filter is discussed, and last the Madgwick Filter is discussed.

Extended Kalman Filter

The Kalman filter is a well known filter applied to get a state estimation of a stochastic system [23]. It does this by making a weighted average between the state predicted by the system and the measured state.

$$\hat{\boldsymbol{x}} = \boldsymbol{x}_p + K(\boldsymbol{z}_m - H\boldsymbol{x}_p) \tag{III.47}$$

Here $\hat{\boldsymbol{x}}$ is the estimated state, $\boldsymbol{x}_p$ is the state predicted by the system, K is the Kalman gain, $\boldsymbol{z}_m$ is the measured state, and H is the observation matrix. For linear systems the original Kalman filter is an optimal filter. The original Kalman filter does however only work on linear systems. Therefore several extensions have been made on the original Kalman filter such as the EKF, which linearises the non-linear state and observation equations about the current state in order to apply the filter. A general version of the EKF which is applied for state estimation is the 15 state EKF

as used in [38]. Which uses the accelerometer and the gyroscope as inputs of the system, and has GPS data to provide position and velocity measurements of the states. In [37] they used the basis of this EKF however the GPS measurements were replaced by a position obtained from the camera of the quadrotor. The advantages of the EKF are that it is easy to add extra sensors if they are available, its proven reliability, and also its ability to estimate parameters or for example the biases of sensors used as input to the system while performing the state estimation [38, 39].

Mahony Filter

The Mahony filter is actually a set of three different filters which were designed on the SO3 group (the special orthogonal group) [40]. The filters are complementary filters, which means that the filter combines two signals which complement eachother. Usually one of these signals has accurate data for low frequencies, but has a lot of high frequency noise, and the other signal is the opposite of that. The idea of the complementary filter is to low-pass filter the first signal, and to high-pass filter the other, and combining the two to optimise the resulting signal. In this case the signals are generated by the accelerometer and the magnetometer, and the gyroscope. The filters Mahony describes assume that there are two vectors which are non-collinear which describe the orientation of the system. This rotation can then be used to correct the orientation obtained by integrating the gyroscope data, resulting in an improved attitude estimation.

Madgwick Filter

The Madgwick filter is an attitude filter which can be applied to IMU and MARG sensor data, and makes use of a quaternion representation for the attitude of the system. The filter makes use of the accelerometer data to estimate the attitude of the systems, and combines this data with the integrated angular velocities of the system to get a better estimate for the orientation of the system [41].

The simple version of the filter, which uses only the data from the IMU applies a gradient descent method on the orientation data found from the accelerometer. It uses this method in order to correct for the gyroscope bias. Then the corrected angular rates from the gyroscope can be numerically integrated to obtain the attitude estimate for the system. The downside of not using magnetometer data is that the system cannot resolve the heading angle from the accelerometer values by itself. Another influence on the system is that obtaining attitude measurements from an accelerometer is based on measuring the gravity vector. This means that when the system is accelerating that the attitude measurement will be off. In the end the filter can be seen as the numerical integration of the angular rates, as is shown in Equation III.48, where $\boldsymbol{q}$ is the quaternion representation of the attitude of the system, $\dot{\boldsymbol{q}}$ is the rate of change of the attitude, or also the angular rates of the system, and $\hat{\boldsymbol{q}}$ denotes a normalised quaternion vector. Equation III.49 shows the correction of the gyroscope measurement with the gradient descent method, where the term following the β is the correction term coming from the accelerometer, and the $\dot{\boldsymbol{q}}_{\omega,t}$ term is the measurement from the gyroscope.

$$ {}^{S}_{E}\boldsymbol{q}_{est,t} = {}^{S}_{E}\hat{\boldsymbol{q}}_{est,t-1} + {}^{S}_{E}\dot{\boldsymbol{q}}_{est,t}\Delta t \tag{III.48} $$

$$ {}^{S}_{E}\dot{\boldsymbol{q}}_{est,t} = {}^{S}_{E}\dot{\boldsymbol{q}}_{\omega,t} - \beta\frac{\nabla \boldsymbol{f}}{\|\nabla \boldsymbol{f}\|} \tag{III.49} $$

The previous description of the filter assumed that only the accelerometer was used in the gradient descent method, however the data from the magnetometer can also be added to the $\nabla \boldsymbol{f}$ term. With the data from the magnetometer, and knowing the local magnetic field direction, also the yaw angle of the system can be estimated.

5 Research Proposal

From the literature review a few gaps in the current research became apparent, which all tie into each other. The first gap is the models and understanding of the governing aerodynamics for (high-speed) aerodynamics, while there definitely are more and more papers researching this topic most models for quadrotors still tend to go for either simple models, or models which provide next to no insight into the dynamics of the system. In research where more detailed polynomial models are used such as Ref. 16, 17, 19 this is often done on drones which are a size or two bigger than the small quadrotors that fly around, such as tinywhoop frames or the emax tinyhawk, and even still a size bigger than 3 inch propeller drones often used for consumers. Which leads to the second gap which is that in general the modelling for the above mentioned classes of quadrotors is lacking. And seeing that the difference in Reynolds number makes such a difference in the rotor interactions it may be interesting to see how much it plays a role for the general quadrotor dynamics. The last gap is that not a lot is known about the effect of propeller ducts in quadrotors, Ref. 8 shows that the duct is beneficial for the efficiency of the rotor in hover conditions, but does not mention whether this gain in efficiency offsets the added weight of the duct, next to this no specifications of the duct are given which also may have an influence. Lastly Ref. 8 already mentions that the duct is not performing as well in forward flight conditions. Aside from the analysis of the SPIV visuals not a lot of other information is given about the effects of the duct in forward flight. Combining these gaps in research the following research topic came forward:

To determine the effects of propeller ducts on quadrotors in forward flight, using system identification techniques and flight data.

The research topic is particularly interesting due to the small Reynolds numbers these tiny quadrotors operate in. Current rotor wake models were designed for helicopters which generally operate in Reynolds numbers around 10^7, while micro aerial vehicles generally operate in the Reynolds number range of 10^3 to 10^5. Besides this most CFD models are not verified for these small Reynolds numbers, however in [42] it is shown that it is possible to get accurate numbers from CFD methods, however like with most CFD methods it is computationally expensive. The time needed in the article was 48-72 hours [42], this was to simulate a full quadrotor with the simulation containing 30 revolutions of the rotors.

From this topic a couple of questions arose relevant to the problem and are listed below:

1. What manoeuvres should be flown to identify the effect of the duct?
   (a) How does the effect differ with flight speed, and when does the effect become unwanted?
   (b) Is there a noticeable difference between manoeuvres?
   (c) How much space is needed to perform the tests?
2. Is it possible to isolate the effect of the ducts on the quadrotor dynamics?
   (a) Can the same model be used between ducted and un-ducted, and does for example a stepwise regression yield the same model terms?
   (b) What regressors dominate the duct related aerodynamics?
3. Which sensors are necessary to gather the data needed?
   (a) Do onboard sensors suffice?
4. How does the duct affect the efficiency or flight time of the quadrotor?

6 Research Plan

To research the research questions the following steps are decided to be taken. First a test platform has to build and tested to make sure it is the right platform to test on. Afterwards there are two big steps for the research, gathering flight data of forward flight, and the modelling using that data.

6.1 Testing the base setup

The first part of the research is to test the base setup of the quadrotor, check whether everything works, but more importantly to identify the effects of the ducts in hovering flight to make sure the positive effect of the ducts is actually present. Besides this it is also important in this phase to gather data about the test platform itself, its mass, inertia, centre of gravity location. This for both the ducted and unducted configuration, such that the mass and inertia can be compensated for in the tests.

6.2 Flight testing

Flight tests are needed to gather the flight data necessary to model the quadrotor. Next to this analysis on the data itself can also give extra information on what happening in the quadrotor, think about rotor speeds for example. The first flight tests are to be performed in the cyberzoo, both due to the fact that it is easily accessible and due to the optitrack system providing accurate speed measurements. Should the speeds achieved in the cyberzoo not be high enough it is possible to look at flights outside, with as downside that wind may influence the models, and that GPS readings are happening at a much lower frequency than the optitrack measurements. The other option is to do flight tests in a windtunnel, with as downside that the windtunnel has to be available for the experiment, and that less space is available for the flight tests.

6.3 Modelling

For the modelling the stepwise regression algorithm described in subsection 3.2 will be used to identify the model structure and its parameters. The idea is that in the best case scenario the stepwise regression will yield similar model structures for both the ducted and unducted data. When these structures differ from each other other methods of comparing these models will have to be found.

6.4 Iteration

In order to know what manoeuvres to fly for effective identification of the models the modelling and flight testing process will have to be iterated, and by doing this improve the flight data gathered and thereby also the models resulting from this flight data.

Bibliography

[1] AbuAssi, L., "The breguet-richet quad-rotor helicopter of 1907," *Vertiflite*, 2002.

[2] Bouabdallah, S., Murrieri, P., and Siegwart, R., "Design and control of an Indoor micro quadrotor," Vol. 2004, Institute of Electrical and Electronics Engineers Inc., 2004, pp. 4393–4398.

[3] Bauersfeld, L., Kaufmann, E., Foehn, P., Sun, S., and Scaramuzza, D., "NeuroBEM: Hybrid Aerodynamic Quadrotor Model," 6 2021.

[4] Six, D., Briot, S., Erskine, J., and Chriette, A., "Identification of the Propeller Coefficients and Dynamic Parameters of a Hovering Quadrotor from Flight Data," *IEEE Robotics and Automation Letters*, Vol. 5, 4 2020, pp. 1063–1070.

[5] Torrente, G., Kaufmann, E., Fohn, P., and Scaramuzza, D., "Data-Driven MPC for Quadrotors," *IEEE Robotics and Automation Letters*, Vol. 6, 4 2021, pp. 3769–3776.

[6] Ferdaus, M. M., Pratama, M., Anavatti, S. G., and Garratt, M. A., "Online identification of a rotary wing Unmanned Aerial Vehicle from data streams," *Applied Soft Computing Journal*, Vol. 76, 3 2019, pp. 313–325.

[7] Barcelos, D., Kolaei, A., and Bramesfeld, G., "Aerodynamic interactions of quadrotor configurations," *Journal of Aircraft*, Vol. 57, 7 2020, pp. 1074–1090.

[8] Shukla, D., Hiremath, N., and Komerath, N., "Low reynolds number aerodynamics study on coaxial and quadrotor," American Institute of Aeronautics and Astronautics Inc, AIAA, 2018.

[9] Shukla, D. and Komerath, N., "Multirotor Drone Aerodynamic Interaction Investigation," *Drones 2018, Vol. 2, Page 43*, Vol. 2, 12 2018, pp. 43.

[10] Silva, P., Lopes, H., and Silva, J., "On the Evaluation of Galileo E5 AltBOC Signals for GNSS-INS Integration," 09 2012.

[11] He, X., Guo, D., and Leang, K., "Repetitive Control Design and Implementation for Periodic Motion Tracking in Aerial Vehicles," 05 2017.

[12] R, C. A. C., Morales, C. A. C., Ospina, J. P., Sánchez, J. F., Caro-Ruiz, C., Grisales, V. H., Ariza-Colpas, P., la Hoz-Franco, E. D., and González, R. E., "Mathematical Modelling and Identification of a Quadrotor," Vol. 12249 LNCS, Springer Science and Business Media Deutschland GmbH, 2020, pp. 261–275.

[13] Leishman, J. G., *Principles of helicopter aerodynamics*, Camebridge University Press, 2nd ed., 2005.

[14] Powers, C., Mellinger, D., Kushleyev, A., Kothmann, B., and Kumar, V., *Influence of Aerodynamics and Proximity Effects in Quadrotor Flight*, Springer International Publishing, Heidelberg, 2013, pp. 289–302.

[15] Johnson, W., *Helicopter theory*, Princeton, N.J.: Princeton University Press, 1980, Includes index.

[16] Sun, S., de Visser, C. C., and Chu, Q., "Quadrotor Gray-Box Model Identification from High-Speed Flight Data," *Journal of Aircraft*, Vol. 56, 3 2019, pp. 645–661.

[17] Sun, S., Schilder, R., and de Visser, C. C., "Identification of Quadrotor Aerodynamic Model from High Speed Flight Data," American Institute of Aeronautics and Astronautics, 1 2018.

[18] Kantue, P. and Pedro, J. O., "Grey-box modelling of an Unmanned Quadcopter during Aggressive Maneuvers," Institute of Electrical and Electronics Engineers Inc., 11 2018, pp. 640–645.

[19] Kaya, D. and KUTAY, A. T., "Aerodynamic Modeling and Parameter Estimation of a Quadrotor Helicopter AIAA Atmospheric Flight Mechanics Conference," .

[20] Smeur, E. J., Chu, Q., and de Croon, G. C., "Adaptive incremental nonlinear dynamic inversion for attitude control of micro aerial vehicles," *2016 AIAA Guidance, Navigation, and Control Conference*, 2016.

[21] Hoffmann, G. M., Huang, H., Waslander, S. L., and Tomlin, C. J., "Precision flight control for a multi-vehicle quadrotor helicopter testbed," *Control Engineering Practice*, Vol. 19, 9 2011, pp. 1023–1036.

[22] Altamirano, G. V. and McCrink, M. H., "Investigation of longitudinal aero-propulsive interactions of a small quadrotor unmanned aircraft system," *AIAA Scitech 2021 Forum*, 2021, pp. 1–18.

[23] Klein, V. and Morelli, E. A., *Aircraft system identification: theory and practice*, American Institute of Aeronautics and Astronautics, 2006.

[24] Hong, X., Mitchell, R. J., Chen, S., Harris, C. J., Li, K., and Irwin, G. W., "Model selection approaches for non-linear system identification: A review," *International Journal of Systems Science*, Vol. 39, 10 2008, pp. 925–946.

[25] Kaiser, E., Kutz, J. N., and Brunton, S. L., "Sparse identification of nonlinear dynamics for model predictive control in the low-data limit," *Proceedings of the Royal Society A: Mathematical, Physical and Engineering Sciences*, Vol. 474, 11 2017.

[26] Visser, C. D., "Global Nonlinear Model Identification with Multivariate Splines," 2011.

[27] Mendes, A. S., van Kampen, E., Remes, B. D., and Chu, Q. P., "Determining moments of inertia of small UAVs: A comparative analysis of an experimental method versus theoretical approaches," *AIAA Guidance, Navigation, and Control Conference 2012*, 2012.

[28] Li, Q., "Grey-Box System Identification of a Quadrotor Unmanned Aerial Vehicle," 2014.

[29] Jardin, M. R. and Mueller, E. R., "Optimized Measurements of Unmanned-Air-Vehicle Mass Moment of Inertia with a Bifilar Pendulum," 2008.

[30] Fum, W. Z., "Implementation of Simulink controller design on Iris+ quadrotor," 2015.

[31] Leishman, R. C., MacDonald, J. C., Beard, R. W., and McLain, T. W., "Quadrotors and accelerometers: State estimation with an improved dynamic model," *IEEE Control Systems*, Vol. 34, 2 2014, pp. 28–41.

[32] Zhang, J., Feng, J., and Zhou, B., "Sensor-Fusion-Based Trajectory Reconstruction for Quadrotor Drones," *Communications in Computer and Information Science*, Vol. 997, 1 2018, pp. 3–24.

[33] Mishra, J. P., Singh, K., and Chaudhary, H., "A hybrid noise removal algorithm for MEMS sensors," *Materials Today: Proceedings*, Vol. 46, 1 2021, pp. 5791–5796.

[34] Solanki, P., "Attitude Estimation of a Quadcopter with one fully damaged rotor using onboard MARG Sensors," 2020.

[35] Hegazy, S. A. E. H., Kamel, A. M., Arafa, I. I., and Elhalwagy, Y. Z., "MEMS gyro noise estimation and modeling for precise navigation simulation," *Proceedings of the 8th International Japan-Africa Conference on Electronics, Communications and Computations, JAC-ECC 2020*, 12 2020, pp. 84–89.

[36] Li, Y., Zahran, S., Zhuang, Y., Gao, Z., Luo, Y., He, Z., Pei, L., Chen, R., and El-Sheimy, N., "IMU/Magnetometer/Barometer/Mass-Flow Sensor Integrated Indoor Quadrotor UAV Localization with Robust Velocity Updates," *Remote Sensing 2019, Vol. 11, Page 838*, Vol. 11, 4 2019, pp. 838.

[37] Li, S., de Wagter, C., de Visser, C., Chu, Q. P., and de Croon, G., "In-flight model parameter and state estimation using gradient descent for high-speed flight," *International Journal of Micro Air Vehicles*, Vol. 11, 3 2019.

[38] Gross, J. N., Gu, Y., Rhudy, M. B., Gururajan, S., and Napolitano, M. R., "Flight-test evaluation of sensor fusion algorithms for attitude estimation," *IEEE Transactions on Aerospace and Electronic Systems*, Vol. 48, 2012, pp. 2128–2139.

[39] Cavallo, A., Cirillo, A., Cirillo, P., Maria, G. D., Falco, P., Natale, C., and Pirozzi, S., "Experimental Comparison of Sensor Fusion Algorithms for Attitude Estimation," *IFAC Proceedings Volumes*, Vol. 47, 1 2014, pp. 7585–7591.

[40] Mahony, R., Hamel, T., and Pflimlin, J. M., "Nonlinear complementary filters on the special orthogonal group," *IEEE Transactions on Automatic Control*, Vol. 53, 2008, pp. 1203–1218.

[41] Madgwick, S. O., Harrison, A. J., and Vaidyanathan, R., "Estimation of IMU and MARG orientation using a gradient descent algorithm," *IEEE International Conference on Rehabilitation Robotics*, 2011.

[42] Yoon, S., Nasa, Diaz, P. V., Boyd, D. D., Chan, W., and Theodore, C., "Computational Aerodynamic Modeling of Small Quadcopter Vehicles," *AHS Forum 73*, 2017.

Chapter IV

Conclusions and Recommendations

Conclusions

Having seen the results of the paper and linking those back to the research question in the introduction of the paper we can conclude the following. First of all the effects of propeller ducts in forward flight can definitely be seen in the flight data, and also the stepwise regression algorithm did prove viable for attributing these effects to certain regressors, noting however that the stepwise regression method proved more efficient for specific models, especially the model of F_x.

Looping back to the subquestions, the first topic is regarding the manoeuvres necessary to identify the differences. The steady flight data used for pure flight data analysis did seem to give insight in the steady state performance of the ducts and how this varied with airspeed, and can definitely be taken as a good baseline test. Looking at the the other two questions they can be better related to the active tests. For these tests the manoeuvres necessary have been experimented with. As result, certain manoeuvres did seem more effective for model identification than others. For moment models small oscillations in pitch about a trim point seemed really effective seeing that otherwise a simple pitch forwards or backwards provides little excitation of the pitching moment. However, specific differences between configurations for the same manoeuvre or between manoeuvres with the same configuration have not been found. As for the space required to perform the tests, it has been found that for tests planned to be performed at speeds higher than 5 ms^{-1} the Cyberzoo is not sufficient in space, and the windtunnel could be a solution. In terms of the actual gathered data, the combination of onboard sensors and the Optitrack system seemed sufficient for the goals set. The only lack in information is in the calculation of the induced velocity ν_i.

As aforementioned the flight data and stepwise regression did definitely indicate a difference between the ducted and unducted configurations in flight. However the isolation of these effects remains a challenge. The stepwise regression algorithm showed that the general models identified for the ducted and unducted configurations differed from each other. Also, due to relations between different regressors, the models where hard to use for the isolation of the differences due to the propeller ducts. The residual stepwise regression method did provide some extra insight here, but was only clearly applicable for the F_x model. In the end only one regressor was found which seemed to be definitely influential in the duct related dynamics, which was the $\omega_{tot}u$ regressor. This regressor could be representing effects like a difference in blade flapping or potentially more complex dynamics.

Lastly the effects of ducts do actually seem to change with the speed of the quadrotor. Looking at the results of the forward flight it can be seen that the ducts affect the efficiency of the quadrotor. For lower speeds the ducts do improve the efficiency of the quadrotor. A crossover in efficiency between configurations for the CineGo platform occurs at around 6 ms^{-1}. However, looking at the added mass, when protection of the quadrotor is not important then the unducted case is most likely still more efficient even in the lower speed regimes.

Recommendations

Looking at the conclusions of the entire research given above, a couple of areas are interesting for future research endeavours.

To start off with, it has been shown that the stepwise regression method has great modelling power. There are, however, also some shortcomings here. The regressors selected by the model, are not too consistent and depend a lot on available data and available candidate regressors. Therefore it is recommended to improve on both. As mentioned in the conclusions, the manoeuvres flown have been experimented with, but no proven conclusion has been drawn as to which flight manoeuvres are most effective for system identification routines. On top of this, for this research all manoeuvres were flown manually meaning that the reproducebility of the data becomes hard. Therefore a recommendation is made to explore system identification flights, which are reproducible and provide the necessary information for a consistent model identification routine. The other recommendation is aimed at the candidate regressor selection for the stepwise regression. For this research the candidate regressor pool has been kept relatively open seeing as not a lot was known regarding the effects at play with quadrotor ducts. This did result in high collinearity between regressors, often not giving a clear picture on what is actually driving the underlying dynamics. Restricting the regressor pool could provide more clarity when trying to analyse the selected regressors and their parameters.

Next to this the current research has taken a very practical approach of analysing the effects of propeller ducts, by using actual flight data, which is only applicable to the corresponding flight condition. Such flight conditions are not able to isolate the exact effects the ducts have. When trying to understand the underlying aerodynamic effects it is recommended to perform controlled experiments where the flight condition is the same but the ducts are the only difference. Examples could include flying with smaller diameter propellers which should reduce the extra thrust generated by the ducts but would keep the drag introduced by them, this way the effect of drag can be isolated better.

Other research can include flow visualisation of the quadrotor in free flight, this can aid in obtaining a better understanding on the airflow in and around the ducts. This can then be used to evaluate the hypotheses drawn in the paper, such as why $\omega_{tot}u$ seems to be an important term in the difference between the ducted and unducted configuration. Additionally, these insights can also be used in order to restrict the polynomial structures used in identification, and whether the disregarded ν_{in} can be used, or whether there are better ways of calculating this variable.

The current research has been performed only in forward flight direction, and using only one test platform. Further research could also look into generalising the results obtained in this research. This means research can be done into what the effects are for 6-DOF flight compared to the 3-DOF flight studied here. The other generalization that can be done is regarding different quadrotors. Are the effects found in this study present in all quadrotors, and what about a quadrotor and its ducts influences the position of the crossover point where ducts become less effective compared to the unducted counterpart. For example, what effects does varying parameters like propeller size, pitch, distance between the propeller and the ducts, shape of the ducts, have.